AN INVESTIGATION OF EARLY DISTURBANCES FOUND
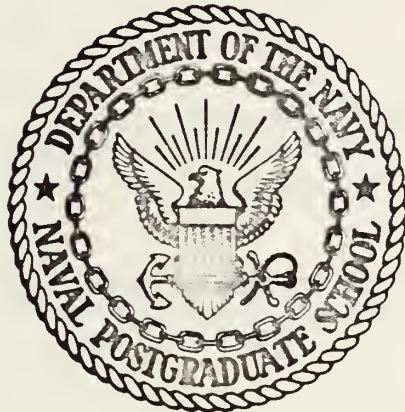# IN ASSOCIATION WITH LASER-PRODUCED PLASMAS

Kenneth Montgomery Brooks

NAVAL POSTGRADUATE SCHOOL
Monterey, California

THESIS

An Investigation of Early Disturbances Found In

Association with Laser-Produced Plasmas

by

Kenneth Montgomery Brooks, Sr.

Thesis Advisor: A. W. Cooper and F. Schwirzke

DEC 1973

An Investigation of Early Disturbances Found in

Association with Laser-Produced Plasmas

by

Kenneth Montgomery Brooks, Sr.
Lieutenant Commander, United States Navy
B. S. Naval Postgraduate School, 1973

Submitted in partial fulfillment of the
requirements for the degree of

MASTER OF SCIENCE IN PHYSICS

from the

NAVAL POSTGRADUATE SCHOOL
December 1973

ABSTRACT

A plasma was produced by the interaction of a 300 MW, 25 nsec, Nd
laser pulse with an aluminum target. The resulting plasma expanded into
an ambient background of 2.5×10^{-5} torr and was analyzed using floating
double probes, magnetic probes and a quartz pressure probe. An early
disturbance was noted before arrival of the main plasma.

Further experiments separate this early signal into photoelectric
response and two fast plasma pulses traveling with constant speeds of
1.1×10^8 cm/sec and 5.9×10^7 cm/sec.

Mapping of the plasma density indicates that the early plasma pulse
is not symmetric with respect to the target normal but expands along a
line defining the reflected laser pulse. This same mapping indicates
that the main plasma expands anisotropically for the first 60 nsec
resulting in an early time asymmetry with respect to the target normal.
At times greater than 120 nsec, the asymmetry of the main plasma is no
longer evident and its density distribution is symmetric with respect
to the target normal.

TABLE OF CONTENTS

3

4

LIST OF FIGURES

8

9

I. INTRODUCTION

Early investigations concerning laser induced electron emission by William I. Linlor [Ref. 36] in 1962 were followed by a multitude of papers dealing with laser produced plasmas. Lichtman and Ready [Ref. 34] were among the first to detect an early signal preceding the main plasma body. They ascribed the signal to reverse photoelectric effect [Ref. 34] from the electrostatic probes being used. This hypothesis received immediate criticism from Honig [Ref. 23] who ascribed the early signal to a fast thermal effect. Since then, several new hypotheses including ionizing potential waves [Refs. 2 and 31] and detonation or blast waves [Refs. 9 and 22] have been forwarded to explain this early disturbance. However, a review of the literature does not reveal a conclusive report on the behavior or content of this signal.

The separate discovery of spontaneously generated magnetic fields by Korobkin and Serov [Ref. 29] and by Stamper [Ref. 43] further stimulated interest in this area. Computer simulations have indicated the presence of megagauss magnetic fields early in the plasma expansion. Fields of this magnitude will influence plasma containment schemes generated in the controlled fusion effort.

In response to an obvious need for complete understanding of the laser produced plasma and its induced magnetic fields McKee [Ref. 38] and Bird [Ref. 8] undertook extensive surveys of the self-induced magnetic fields and attempted to relate them to the expanding plasma. During Bird's investigation he noted the presence of an early magnetic

signal. This revelation led to renewed interest in the early electro-static probe signals. There are four possible sources for this early signal. They are:

1. Laser induced electron emission.

2. Fast plasma blowoff.

3. Electromagnetic disturbances.

4. Ionization of the background gas by plasma produced photons or ionizing potential waves.

This investigation has been conducted in an effort to determine which of these causes is responsible for the observed signal and to provide a more detailed understanding of the behavior of the phenomenon producing the signal.

The thesis is divided into six more sections and two appendixes. Section II is a description of the general experimental arrangement. Section III describes the experiments conducted to solve the problem and discusses the results. Section IV attempts to relate two of the observations made in Section III to theory. Section V presents a summary with conclusions. Section VI provides recommendations for further investigation. Appendixes A and B describe the construction and theory behind two of the diagnostic tools used during this research.

II.   EXPERIMENTAL ARRANGEMENT

A.   LASER

The laser used was a Korad K-1500, Q-switched neodymium-in-glass system. The system consists of an oscillator which generates the initial 25 nsec (full width at half power) pulse through Q-switching by Pockels Cell. The oscillator pulse is expanded and passes through an amplifier which increases the energy of the pulse. The arrangement is shown in Figure 1. A detailed description is provided by Davis [Ref. 7].
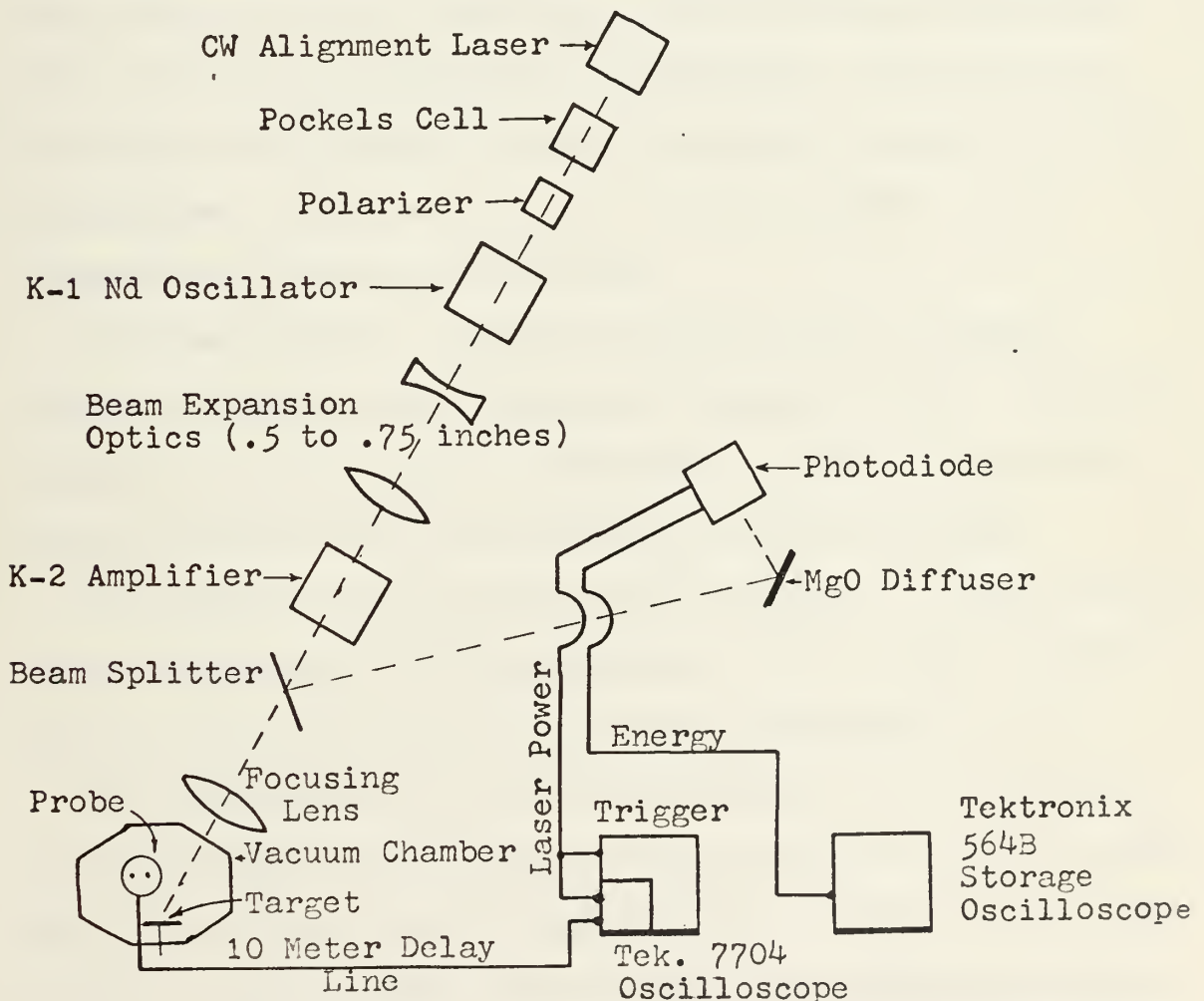
Figure 1. Block Diagram of the General Experimental Layout

The output of the laser was controlled by varying the voltage applied to the K-1 and K-2 flashlamps. The range of energies obtainable is 2.5 to 12 Joules. The duration of the pulse is 25 nsec giving a power range of 100 to 480 MW. The laser focal spot size is approximately 0.15 cm in diameter after focusing. This gives a typical (5 Joules) power density of 2.8 X 10^9 watts/cm^2.

$$\frac{5}{25 \times 10^{-9}} \left[\left(\frac{.15}{2} \right)^2 \pi \right]^{-1} = \boxed{1.1 \times 10^{10} \frac{watts}{cm^2}} \quad ?$$

area = distribution

B. LASER MONITORING TECHNIQUES

Approximately one percent of the laser pulse energy was reflected by a beam splitter onto an MgO block. The laser output was monitored from this block with a Korad K-D1 photodiode after passing through a 0.1 percent neutral density filter. This photodiode provides one signal proportional to the pulse power and a second, integrated, signal proportional to the laser pulse energy.

As shown in Figure 1, the power signal was used to trigger a Tektronix 7704 oscilloscope and was also displayed on that oscilloscope through the positive input in a differential amplifier. The energy signal was displayed on a Tektronix 564B storage oscilloscope.

The photodiode energy signal was calibrated by L. L. McKee [Ref. 38] using a Westinghouse RN-1 Laser Radiometer. The radiometer was used to provide an absolute measure of the incident pulse energy.

The energy output of the laser was monitored on every shot and the power was displayed on the same oscilloscope used to take probe response data. For successive shots during the mapping procedure the energy was allowed to vary by $\pm$ 10%. Shots with energy variations exceeding this were excluded from the data base. When properly aligned the laser produced very consistent pulses. It should be noted that if shots were

14

repeated at intervals of less than one minute, the laser energy tended to increase slightly from shot to shot. A one minute cooling period between shots resulted in excellent reproducibility.

C. TEMPORAL REFERENCE FRAME

The temporal relation between the diagnostic probe response and the leading edge of the laser pulse was determined by taking into account the various cable delays and laser beam optical path lengths. The geometry is depicted in Figure 1. A long (10 meter) delay line was used from the diagnostic probe to the oscilloscope in order to separate the laser pulse input and early diagnostic responses which would otherwise be superimposed by the differential amplifier. The computed delay was 33 nsec assuming the signal to travel at 1.98×10^{10} cm/sec in the RG-174/U coaxial cable.

To experimentally verify this delay, the 100 volt calibration signal from a Tektronix 555 Dual Beam Oscilloscope was fed into a Tektronix Tunnel Diode Pulser. The pulser output was fed into a "T." One side of the T went to the positive side of a Tektronix 7A-13 differential vertical plug-in on a Tektronix 7704 oscilloscope through the photo-diode power signal cable. The other side of the T went to the negative side of the same amplifier through the delay cable. A reproduction of the oscilloscopic trace obtained in this manner is given in Figure 2.
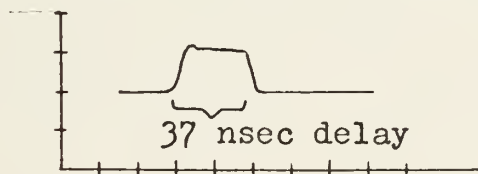
37 nsec delay

Figure 2. Ten meter cable time delay measurement. The horizontal scale is 20 nsec per division. The measured delay is 37 nsec.

15

When the measured 37 nsec delay is corrected for the difference in optical path length from the beam splitter to the target and the MgO diffuser block the delay is found to be 35 nsec. This experimentally measured delay agrees very well with that calculated earlier and is the delay used throughout this thesis in correlating diagnostic probe response with the laser pulse. Zero time is arbitrarily established as that time at which the leading edge of the laser pulse strikes the target. This is depicted in Figure 3.
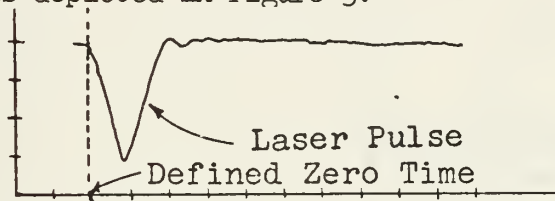
Figure 3. Definition of Zero Time. The horizontal scale is 20 nsec per division.

D. PLASMA CHAMBER

The target was located inside a chamber specifically designed by McKee [Ref. 38] to facilitate diagnosis of the laser plasma by probes or optical means. A horizontal cross section of this chamber is depicted in Figure 4.
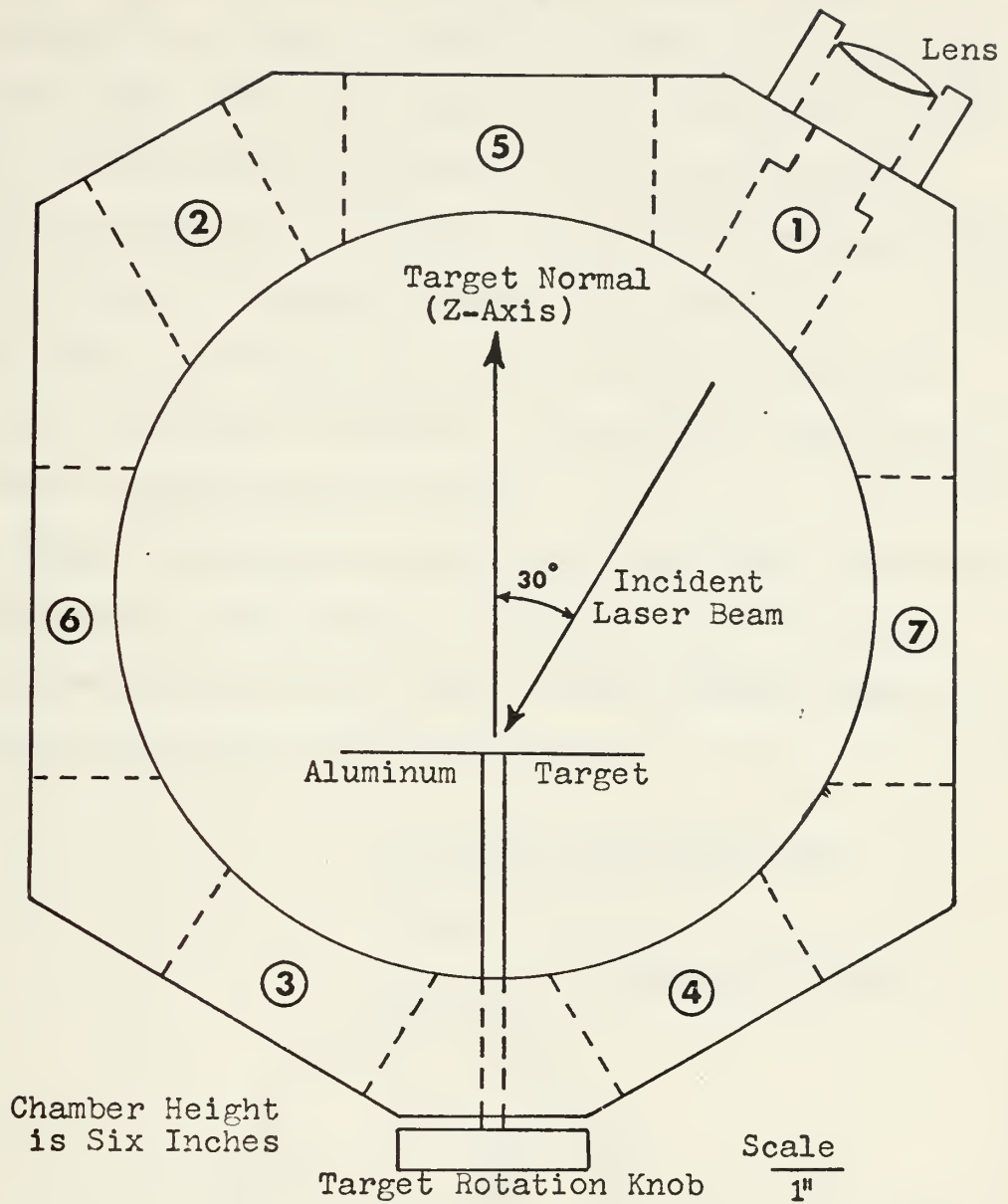
Figure 4. Top view of vacuum chamber. Port #1 is the laser beam entry
port, #2 is the reflected laser beam observation port, #3 is
the transmitted laser beam observation port, ports numbered
4, 5, 6, and 7 are optical/probe observation ports. There is
also an optical/probe port in the top of the chamber.

17

The laser pulse enters the chamber after passing through a converging lens and strikes the target at an angle of 30 degrees with the target normal. This thirty-degree incident angle permits probing along the target normal which appears to be the axis of greatest symmetry in relation to the expanding plasma. The converging lens was normally defocused to minimize cratering of the target.

The target is a flat disk of one-half inch 6061 aluminum alloy plate. It is two inches in diameter. The target was rotated every 25 to 35 shots to prevent severe cratering.

The chamber was pumped to a vacuum of 2.5 X 10^{-5} torr (air) by an oil diffusion pump. This pressure was measured with an ionization gauge attached directly to the chamber. Unless otherwise stated, all measurements were made at this chamber pressure.
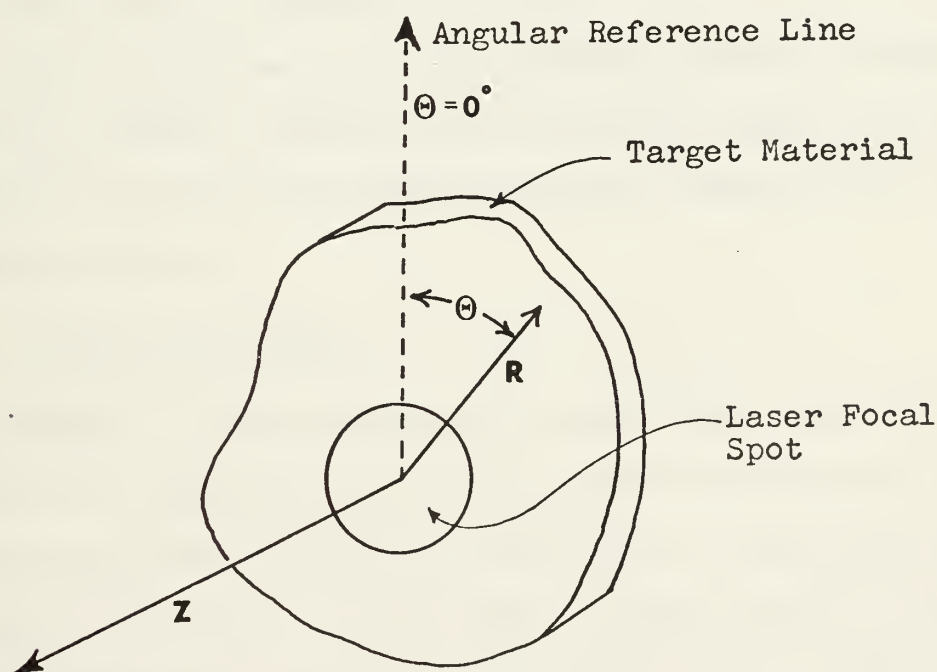
Figure 5. Cylindrical polar coordinate system used in this thesis.

The chamber coordinate system is polar with its center at the focal spot of the laser pulse. This is illustrated in Figure 5. Throughout the text reference positions refer to cylindrical polar coordinates. Distances will be in centimeters unless otherwise specified. As an example, $(0.5, \pi/2, 1.0)$ refers to the position $r = 0.5$ cm, $\theta = \pi/2$ and $z = 1.0$ cm.

E. MAGNETIC PROBES

Probe construction and calibration is covered by McLaughlin [Ref. 39]. During this work a single magnetic probe consisting of five turns of #40 Formvar copper wire with a diameter of one millimeter was used. Using the procedures outlined by McLaughlin, an effective area of $nA = 3.1 \times 10^{-6}$ m^2 was measured for the coil. The coil proved to have a linear frequency response up to 12 MHz.

Since the probe was used only to determine temporal relations and to verify azimuthal symmetry of the self-induced magnetic fields, no integrator was used and the data was recorded simply as the voltage induced in the coil.

F. FLOATING DOUBLE PROBES

Appendix A contains details of the double probe construction and theory. The primary use of these probes was to determine the time at which disturbances arrived at the probe and to determine the relative density of the plasma at a given time in a given position. Probes were biased sufficiently negative to collect saturation ion currents.

Probes used in this investigation have been numbered one through four. Probe number three has larger electrodes and was used extensively due to its higher signal to noise ratio. The characteristic

19

for the peak density of the main plasma pulse is reproduced as Figure 6. The characteristic was measured in a background of 2.5×10^{-5} torr with a nominal laser energy of 5 ± 0.5 joules. The characteristic is symmetric and appears to partially saturate at $\pm$ 10 volts. However, there is another, smaller, break in the curve at 20 to 25 volts. Therefore, the probe was biased at −20 volts to collect a saturated ion current. A large secondary emission coefficient of $\epsilon = 0.5$ was used in obtaining a quantitative idea of plasma density to compensate for this large biasing voltage.

By carefully isolating the entire system from ground, recorded probe response voltages at zero bias were reduced to less than 300 mV. For most probes the response was zero at zero bias indicating that the probe was in fact floating with the plasma potential.

To obtain an estimate of the plasma density, equation (29) of Appendix A is solved for n_i and evaluated with $\overline{Ze} = 1.5$, $\epsilon = 0.5$, $R = 3.8\Omega$, $A = 4.6 \times 10^{-3}$ cm^2 and V_{LP} given a variety of significant stream speeds:

$$(1) \quad n_i \ (cm^{-3}) = 1.59 \times 10^{20} \ \frac{V \ (volts)}{V_{LP} \ (cm/sec)} \qquad .$$
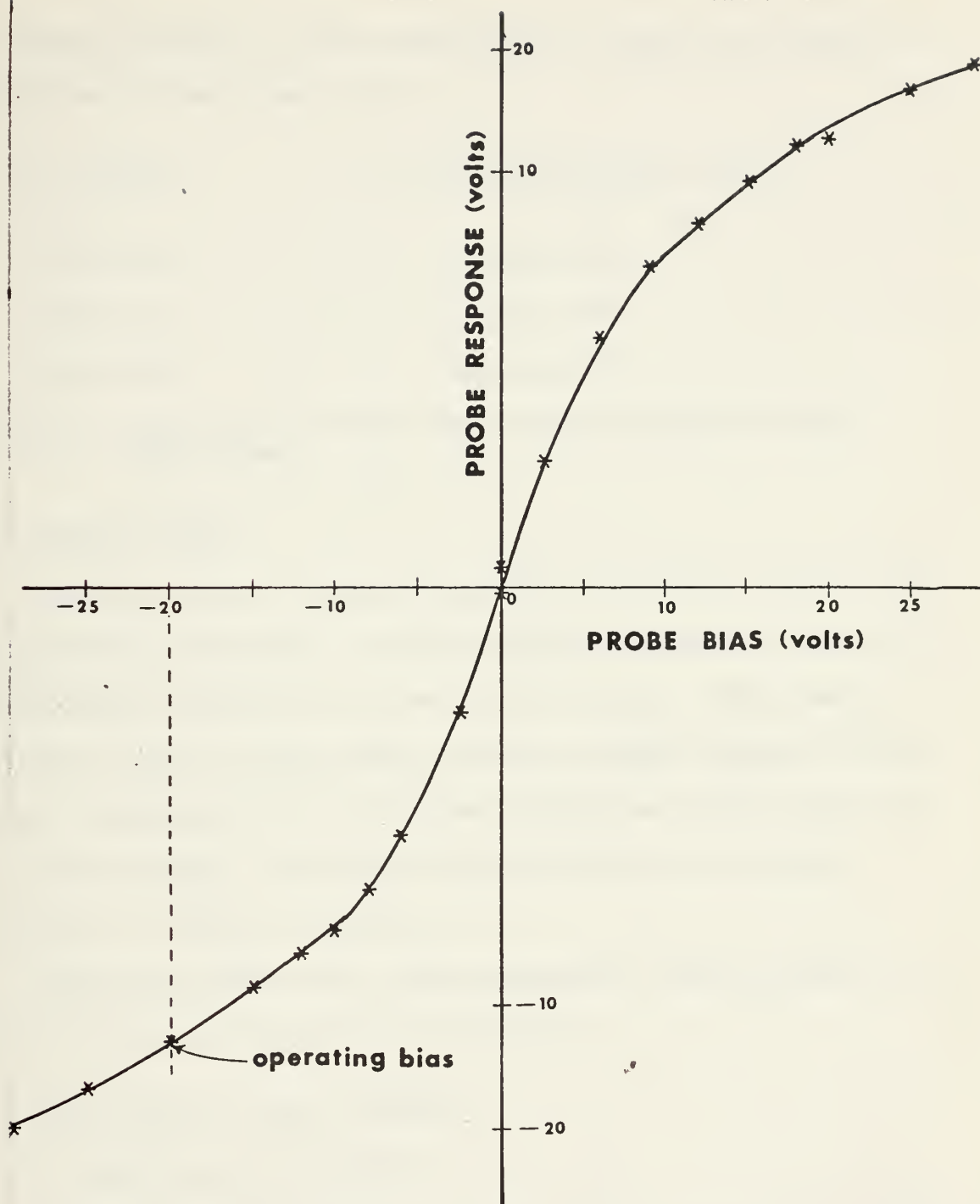
Figure 6.   Probe Number 3 Characteristic at the Peak of the Main Plasma
Pulse.

Table (1) gives n_i versus probe response voltage for a number of significant plasma stream speeds.

V_{LP} (cm/sec)	n_i (cm^{-3})/Probe Response (volts)
1.0×10^7	1.59×10^{13}
5.0×10^7	3.18×10^{12}
1.0×10^8	9.75×10^{11}

Table (1)   Plasma Density Versus Probe Response Voltage for Probe
Number Three

G.   PRESSURE PROBES

Pressure probes are useful in measuring the momentum per unit area transported by the plasma. In this investigation use was made of the piezoelectric properties of an X-cut quartz crystal. The momentum transfer caused by plasma impact with such a crystal creates a stress wave. Propagation of this stress wave through the crystal results in an induced voltage. Theoretical details describing this induced voltage are included in Appendix B.

The pressure probe used in this investigation was constructed and provided by the Stanford Research Institute.

H.   DATA COLLECTION ERROR ESTIMATES

1.   Probe Positioning Errors

The diagnostic probes were inserted into a brass collet system which was welded onto a brass base plate. The base plate could be moved about on an "O" ring seal located on the top of the chamber without breaking the vacuum seal. The base plate was scribed with reference lines. These lines allowed positioning of the plate over a

one millimeter grid attached to the top of the chamber. A new origin was determined at the start of each data session and marked on the grid. The probe was then moved to new positions using the grid as a reference. The position of the probe relative to the target was measured internally at the beginning of each data session and again at the end of the session to insure that the probe had not moved in its holder. While not very sophisticated, this method did allow positioning of the probe to within $\pm$ 1/2 mm of the stated position in relation to the target.

2. Absolute Plasma Density Errors

The relative measure of plasma density from point to point is considered good due to the high reproducibility of the laser and plasma pulses. It is estimated that these relative values are accurate to within $\pm$ 10 percent.

Absolute plasma density calculations are subject to several errors.

a. High Probe Bias

A double probe bias higher than that at which initial saturation occurs may have generated errors as large as 100 percent in the recorded probe response due to secondary emissions and plasma perturbations. This error is consistent for all probe responses and can be ignored in the relative density plots. To help reduce the possibility of introducing a significant error in the absolute density determinations, a large secondary emission coefficient of $\epsilon = 0.5$ was used.

b.   Deviations In the Laser Pulse Energy

While the laser was very reliable and gave very reproducible
pulses, the output energy was allowed to vary by as much as ± 10 percent.
The early signal probe response to the laser's energy content was found
to vary linearly. The slope of the line describing this relation is
such that the allowed deviation in laser energy could result in a
deviation of ± 7 percent in the amplitude of the early signal response.

c.   Error in Probe Tip Measurement

The area of the probe tips is considered accurate to within
ten percent.

d.   The plasma stream speeds are considered accurate to within
ten percent.

In view of these many deviations plus subtle factors [Ref. 48]
in interpretation of double probe signals the absolute plasma densities
are not considered accurate to better than a factor of two.

3.   Errors In Temporal Resolution

The time resolution in these experiments is considered very good.
At this background density, the plasma expansion speed is nearly
constant within the allowed range of energies. The temporal resolution
on individual photographs is enhanced by inclusion of the laser pulse
which serves as a positive indication of zero time. Temporal
correlations and measurements are made with a horizontal scale of less
than 40 nsec per cm. This allows interpretation of the results to with-
in 4 nsec. For two double probes 1.75 cm apart, 4 nsec represents 46
percent of the transit time for the fast pulses travelling at 2×10^8
cm/sec and represents only 4 percent of the time involved in passage of
the main plasma front at 2×10^7 cm/sec. When probe spacing and laser

energy errors are considered, the fast signal speeds should be good to within 47 percent and the main signal speeds to within six percent for single data points. In each case the speed has been averaged from more than 25 data points so that the respective limits are ± 10 percent for the early signal speed and ± 2 percent for the main plasma speed.

III. INDIVIDUAL EXPERIMENTS AND THEIR INTERPRETATION

The thesis problem was attacked through a series of experiments designed to reveal the behavior and make-up of the early disturbance.

A. DISTURBANCE SPEED MEASUREMENTS

The first set of experiments was made in an effort to accurately determine the speed of component parts of the laser produced plasma. These speed measurements were accomplished in two different ways.

1. Pulse Arrival Time at a Geographical Position

In this experiment, a series of oscilloscopic photographs were taken at points along the z-axis. The series starts at 0.5 cm and consists of data points at one millimeter intervals to 3.0 cm, at two millimeter intervals from 3.0 to 4.0 centimeters and a final data point at 5 cm. This series was repeated three times.

a. The first series was taken with the oscilloscope set at 100 nsec and 2 volts per cm. These settings are designed to enhance determination of the speed of the main plasma pulse. A typical probe response is traced as Figure 7 with the pertinent features labeled. Main plasma front passage times were measured for all data points. These times are plotted against the probe position in Figure 8. The slope of the line connecting the data points represents the speed of the main plasma front at any point. As can be seen the velocity is nearly consistent at 1.1×10^7 cm/sec within the limits of this survey.
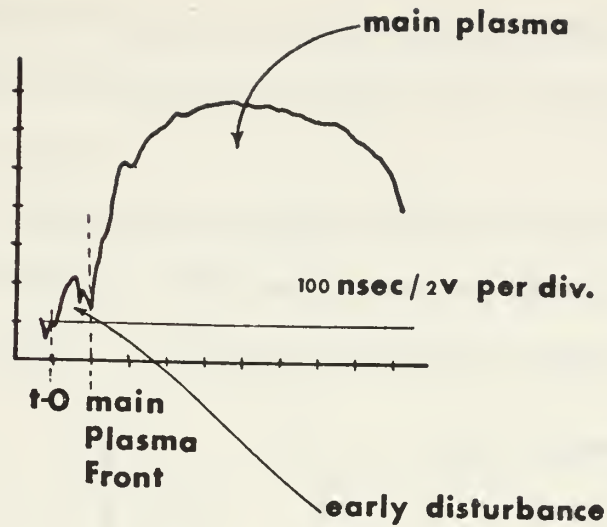
Figure 7. Double Probe Response at (0, 0, 1.0). The dashed line
indicates the time at which the main plasma front passed
the probe position.
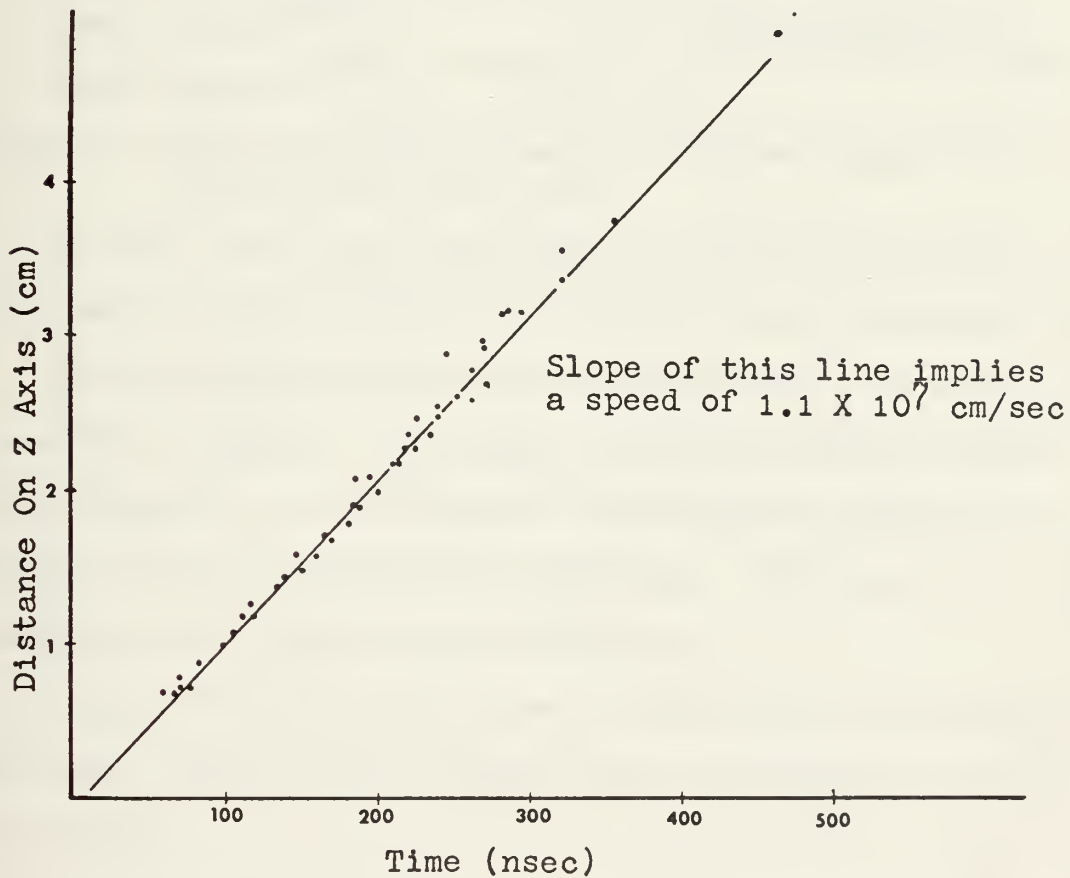
Figure 8. Time of Passage of the Main Plasma Front Versus Probe
Position.

Assuming a constant speed and extrapolating backward indicates that the main pulse left the target very early after laser pulse impact (approximately 10 nsec).

b. The second series was taken with oscilloscope scales of 20 nsec and 500 mV per cm. This scale enhances direct measurement of the early disturbances. A typical oscilloscopic trace is copied as Figure 9.
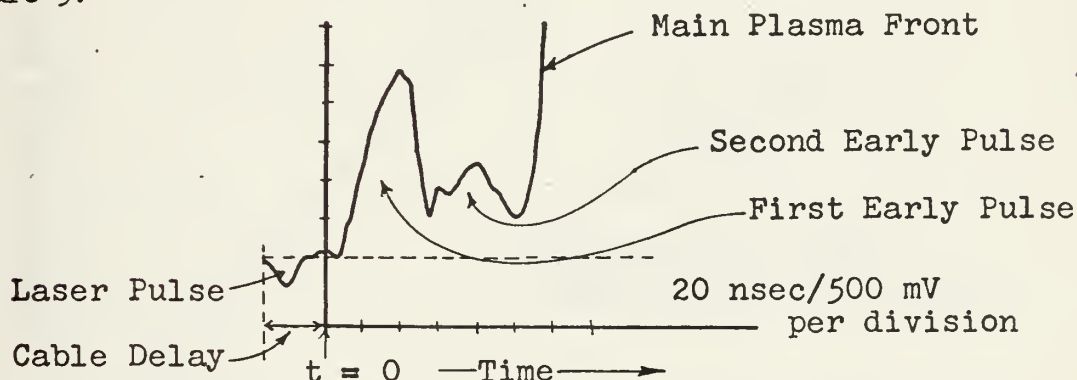
Figure 9. Early Laser Plasma Produced Disturbances Recorded by a Double Probe at (0, 0, 1.25).

The exact front of the early signal is often difficult to fix. This results in the large data scatter seen in early disturbance data.

A plot of early disturbance front passage versus probe position is reproduced as Figure 10. The slope of this plot indicates a fairly constant speed of 1.1×10^8 cm/sec. Also included in Figure 10 is a similar plot for the second early disturbance. The slope of this line indicates a front speed of 5.9×10^7 cm/sec.

It should be noted that the speed of these early disturbances is reasonably constant even to the point where the signals are lost in system noise.

By extrapolating backward assuming a constant speed we find that the various disturbances left the target at the following times; main

28

plasma at t = 0 to 10 nsec, first early disturbance at about 3 nsec and
the second early disturbance at t = 12 nsec.
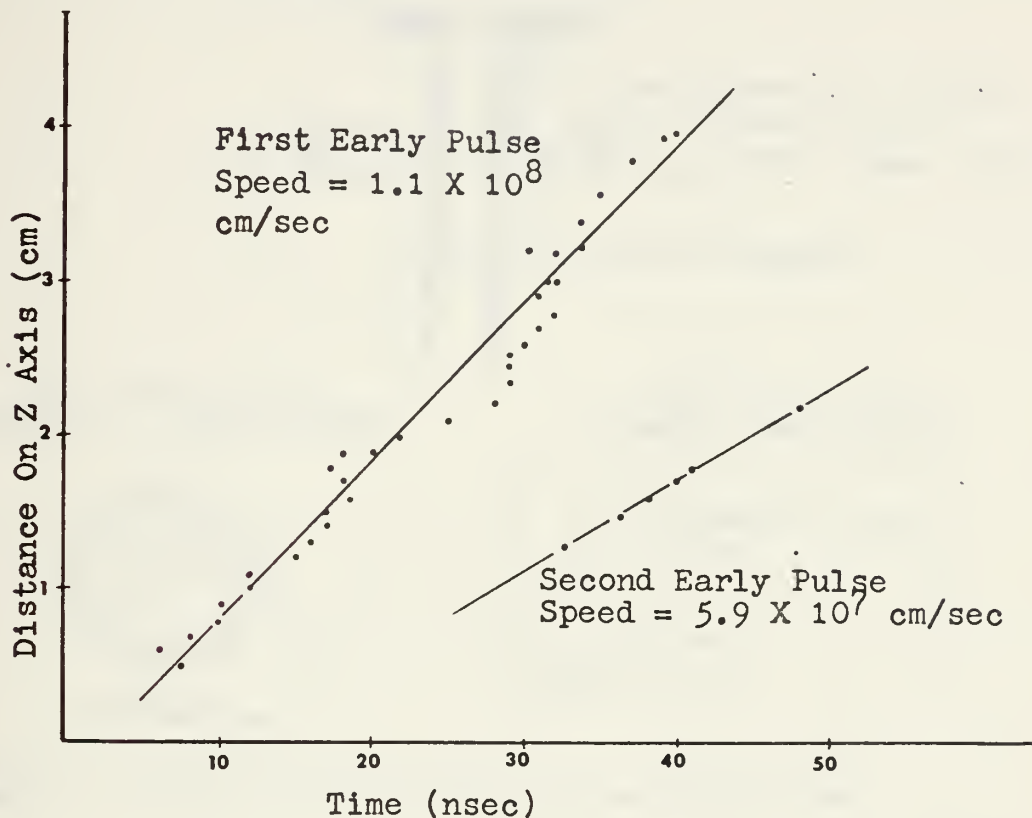
Figure 10.   Plot of the Time of Passage of the Early Disturbance Versus
Probe Position

2.   Two Double Probes

        To obtain more accurate speed information, a two probe holder
was constructed to allow simultaneous sampling of the same plasma by
two tandem probes.   The holder is illustrated in Figure 11.

        The probes used were very fine to minimize perturbation of the
streaming plasma.   The probes were placed in the holder 1.75 cm apart.
They were positioned in the chamber so that one probe was one millimeter
to the right of the target normal and the other was one millimeter to
the left of the target normal.   Each probe was biased at -20 volts and
the chamber pressure was reduced to 1.8 X 10^{-5} torr.   A series of 32
pictures were taken on a Tektronix 555 Dual Beam Oscilloscope.   The

29

Two Double Probes

Brass Insertion Collets
Holddown flange
3/8" Brass Plate

Bakelite Spacer

**Top View of the
Insertion Collet System**

**Top View of the
Movable Brass Plate**

4" Diameter Hole

3/8" × 8" × 14"

5" diameter
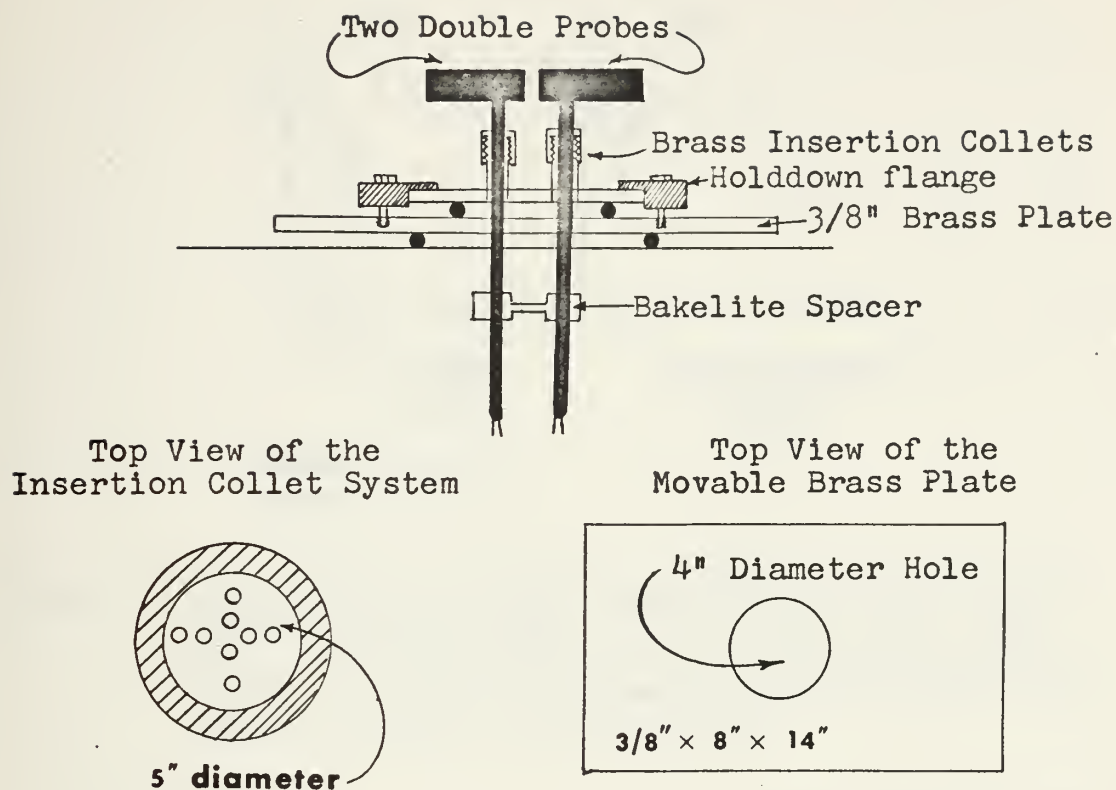
Figure 11. Device for the Insertion of Two Double Probes

scope was set at 500 mV and 40 nsec per cm. A typical oscilloscopic trace of the probe response is depicted in Figure 12. At ten of the data points, the probe cables were reversed. In each instance, the same separation between arrival times was noted. The reversed cable trace is also included in Figure 12.
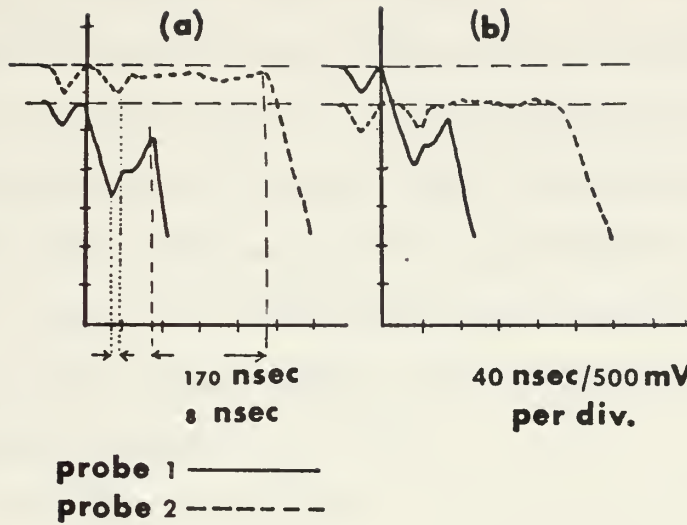
Figure 12. Simultaneously recorded tracings from two double probes sampling the same plasma. (a) The first probe is at (0.1, $\pi/2$, 1.1) and the second probe is at (0.1, $3\pi/2$, 2.85). (b) Taken at the same data points but with the cables reversed at the oscilloscope.

The average speed of the early signal as computed from this data base is 1.0×10^8 cm/sec. The average speed of the main plasma signal is found to be 1.1×10^7 cm/sec. These results agree very well with those found by the first method. A summary of these speeds is given in Table 2.

Plasma Feature	Speed
First Early Disturbance	1.1×10^8 cm/sec
Second Early Disturbance	5.9×10^7 cm/sec
Main Plasma Front	1.1×10^7 cm/sec

Table 2. Summary of Significant Speeds

31

B. EFFECT OF A TRANSVERSE ELECTRIC FIELD

A variable transverse electric field of up to 13,000 volts/cm was applied to a collimated plasma to determine whether the field would deflect the plasma beam. This will reveal information on the charge to mass ratio of the disturbance if it is particulate in nature.

Figure 13 depicts the device constructed to provide a collimating effect on the laser produced plasma. The devise was designed with several purposes in mind:

1. To collimate the plasma.

2. To help shield the electrodes from the plasma and thereby reduce the possibility of discharge across the conductive plasma.

3. To reduce the total number of plasma particles subject to the field in order to reduce the effects of shielding the plasma.
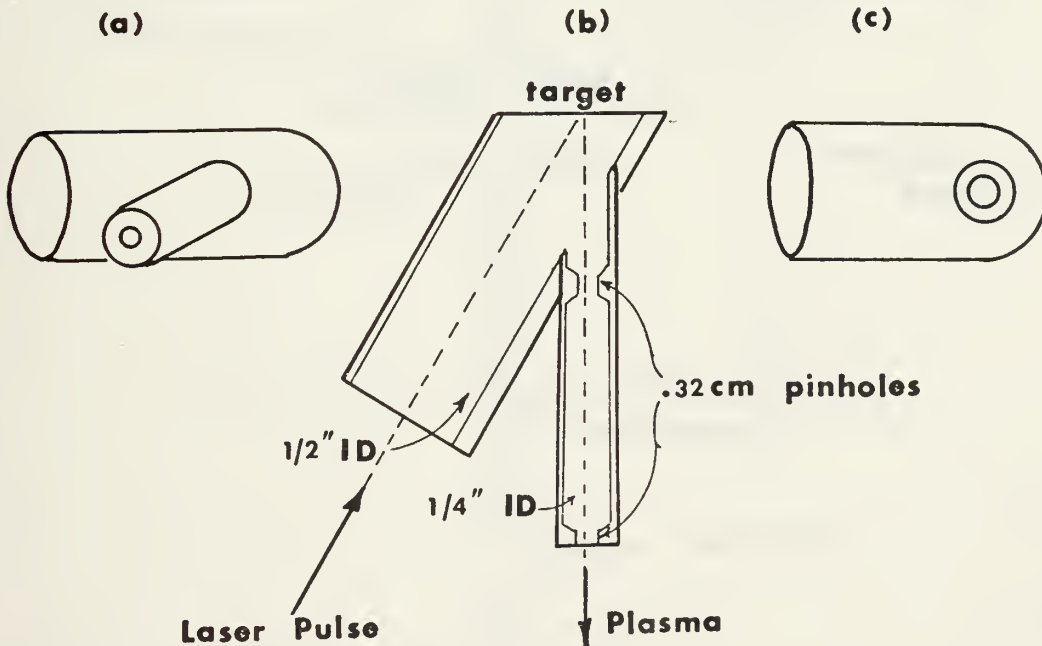
Figure 13. Collimating Device (a) General View, (b) Top View, and (c) Front View

Figure 14 depicts the probe response at (0, 0, 5.8) with and without the plexiglass collimating device in place. As can be seen, the probe response has been altered; however the early disturbance and main plasma pulses remain distinguishable features of the response and therefore the pinhole collimating device is usable.
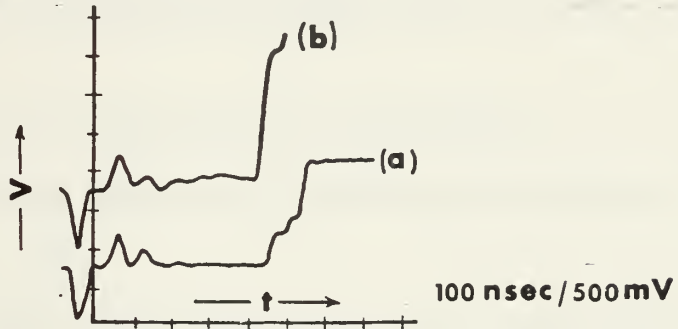
Figure 14.   Effect on the plasma produced by the presence of the collimating device. (a) Double probe response without the device. (b) Double probe response with the device in place.
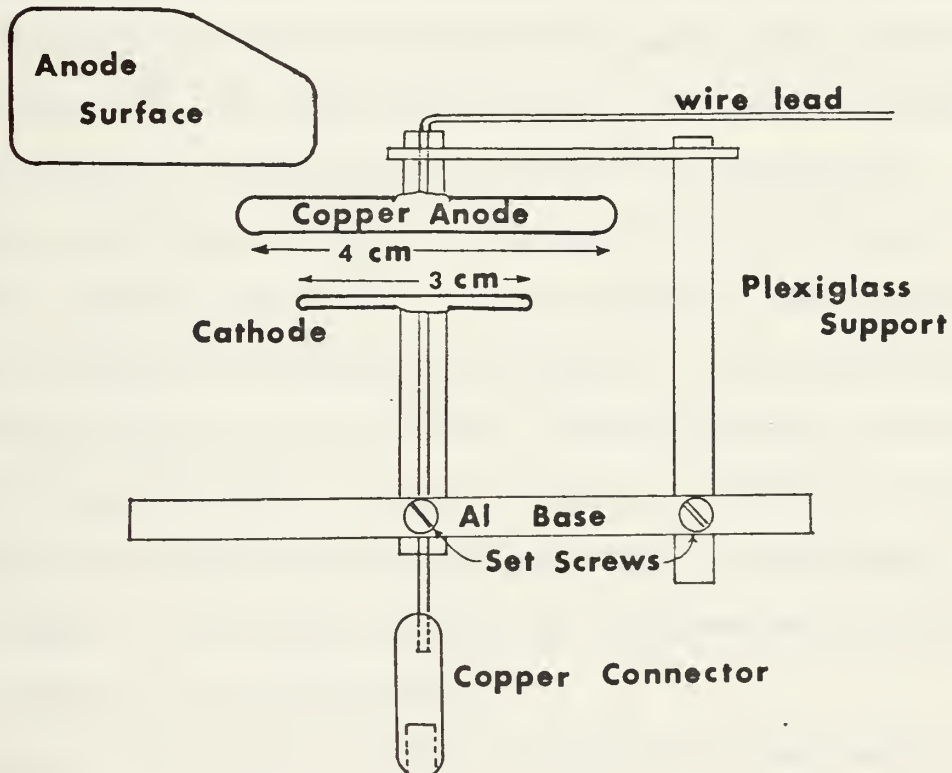
Figure 15.   Electrodes and Their Mounting

Figure 15 depicts the electrodes used in this experiment and the mounting equipment. All surfaces of the entire structure are heavily coated with General Electric "RTV" to eliminate corona formation.

Assuming that the electrodes form a pair of infinite parallel plates (ignore fringing), the stored charge on these electrodes is found to be:

(2) $q = EA$ Where (A) is the plate area

(3) $V = Ed$ Where (d) is the electrode spacing

(4) $q = VA/d$

With V/d = 13,000 volts/cm and (A) = one cm^2 the stored charge is 1.5×10^{-9} coulombs or 7.2×10^9 electrons.

Plasma densities greater than this will be able to completely shield themselves. Typical electron densities in the main plasma pulse are approximately 10^{14} cm^{-3} while probe response to the early disturbance indicates a density of approximately 2.4×10^{12} ion charges/cm^3. Assuming a nearly neutral plasma in each case it is obvious that both pulses are capable of completely shielding themselves. The collimating device has pinholes 3.2 millimeters in diameter. This reduces the early pulse charge density to 2.5×10^{11} cm^{-3}. The early plasma is still capable of shielding itself. However, in doing so, nearly all of the particles would be lost from the beam resulting in a significantly reduced signal. This argument assumes that the plasma particles have time to respond to the applied field.

Because of the shielding problem a large capacitor was used in the electrode charging circuit. This circuit is shown in Figure 16.
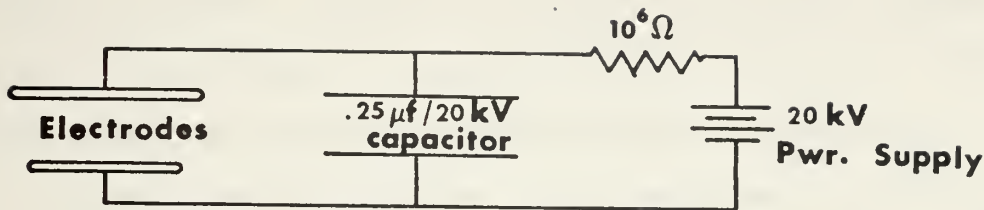
Figure 16. Electrode Charging Circuit

The RC time for this circuit is approximately 2 nsec between the storage capacitor and the electrodes. The capacitor stores 4.5×10^{-3} coulombs of charge at 18,000 volts. Therefore the electrodes will receive a significant amount of additional charge from the power supply during the 27 nsec in which the early disturbance is traversing the field. The charge available in the storage capacitor should be sufficient to overcome any shielding in the early signal.

Deflection of singly ionized aluminum atoms assuming no shielding of the field by the early disturbance will be:

(5) $D = at^2/2$ Where (D) is the lateral displacement

(6) $a = F/m = eE/m = eV/md$

If V/d = 13,000 volts/cm then the acceleration is 4.6×10^{14} cm/sec^2 for aluminum ions and 8.5×10^{17} cm/sec^2 for electrons.

The early disturbance travels with a speed of approximately 1.1×10^8 cm/sec. Therefore, it will be within the 3 cm field for t = 27 nsec. Substituting these values into equation (5) we find that the ions incur a transverse displacement of 0.9 mm during transit while the electron lateral displacement is 170 cm (ignoring space charge effects).

These values indicate that if the early disturbance was composed entirely of electrons, it should be completely deflected and no signal

35

would be received. However, if the early disturbance included ions,
then these ions would not achieve sufficient deflection to miss the
exit pinhole and any signal attenuation would be very small.

An unforeseen problem arose in this experiment either because of
the large distance at which the probe samples the plasma or because of
the pinhole collimator. The plasma sampled by the probe was not
reproducible. Major features were always identifiable but their
amplitudes differed by as much as a factor of three from shot to shot.
This unresolved problem has greatly complicated the analysis by causing
a large deviation in the data.

Results of this experiment are reproduced in Figure 17. The straight
line is a least squares fit to the data. Its slope is 0.19 mV/kV
indicating that there is little dependence of the early disturbance on
the applied transverse field. These results suggest that the early
signal is not composed entirely of electrons but that there are heavier
particles present.
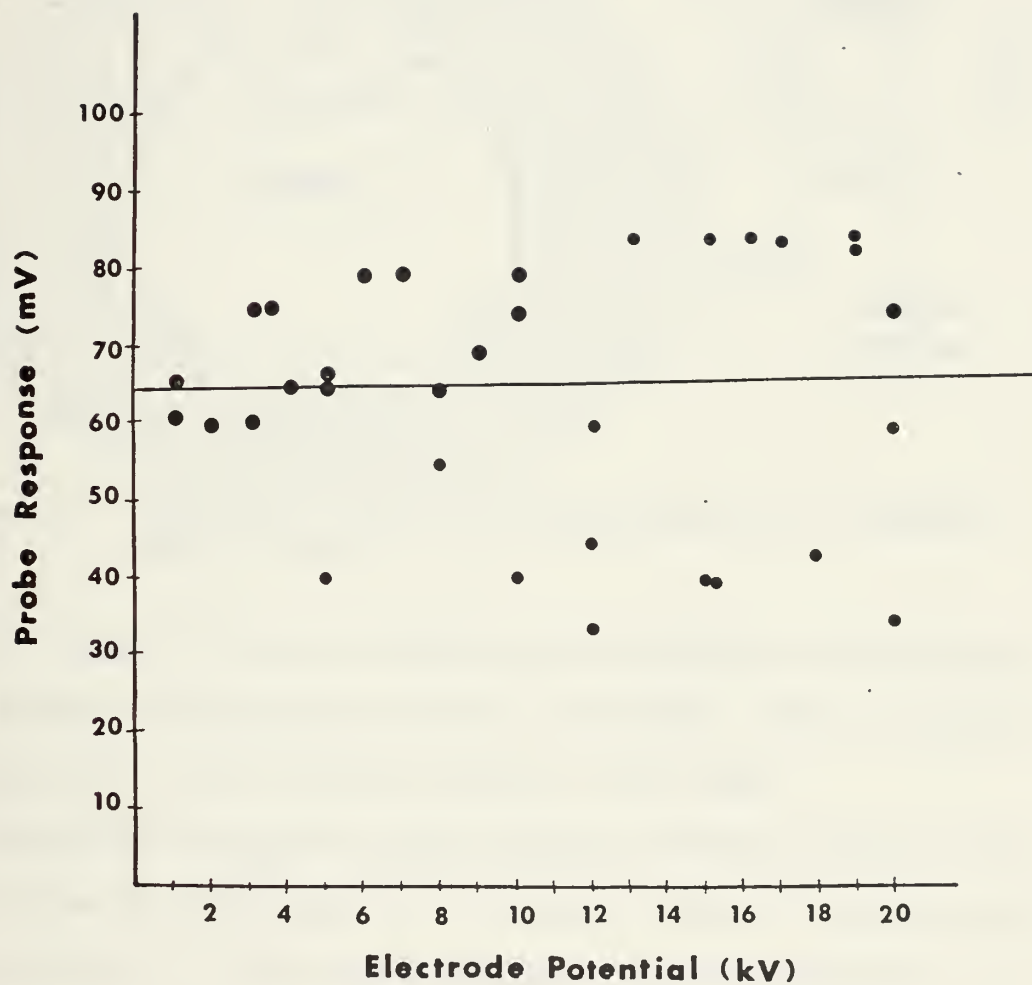
Figure 17. Early Disturbance Peak Amplitude Versus Transverse Electric Field Strength.

C. EFFECT OF A TRANSVERSE MAGNETIC FIELD

Because of the complications inherent in the production and inter-
pretation of data taken with a large transverse electric field, a
transverse magnetic field was applied to the streaming disturbances.
The experimental arrangement is depicted in Figure 18.
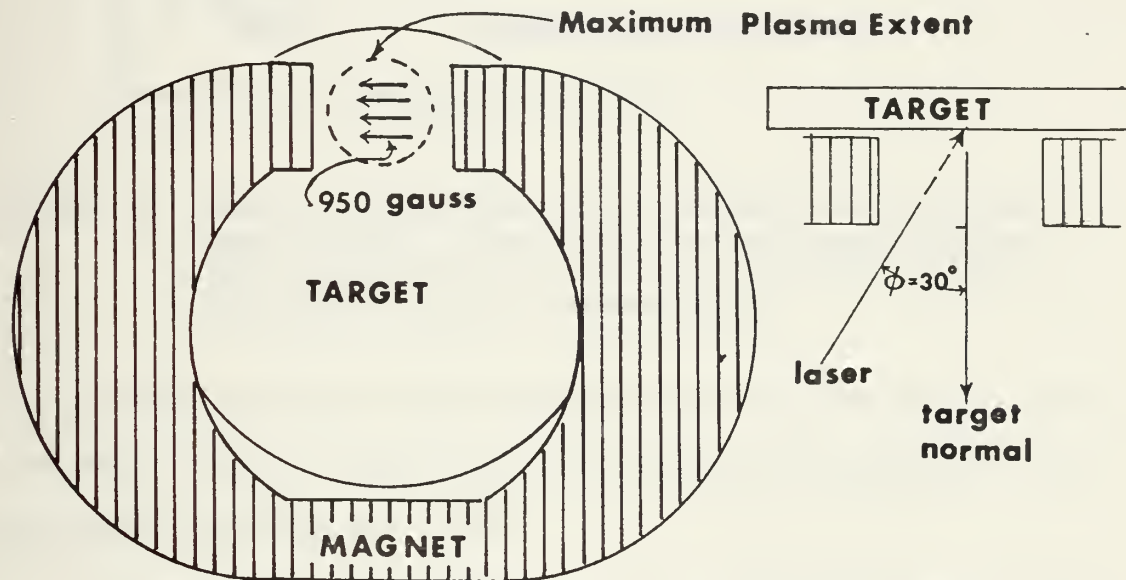
Figure 18. Experimental setup for the application of a transverse
magnetic field.

The magnetic field was measured with a gaussmeter. The field in
the center of the magnetic pole area is 950 gauss. Near the surface of
the poles the field strength increases to 1325 gauss.

Great care was taken to insure that the incoming laser pulse did
not strike the target and that the distance between the magnetic poles
was sufficient to allow plasma expansion without perturbation. In
order to determine if the magnetic field was inducing currents in the
probe a number of pictures were taken with the target removed allowing
the laser pulse to transit the chamber and exit through port number
three. Figure 19 shows the oscilloscope response in this situation.

Double Probe No. 3 @ (0, 0, 1.25)

laser pulse

20 nsec/500 mV per div.
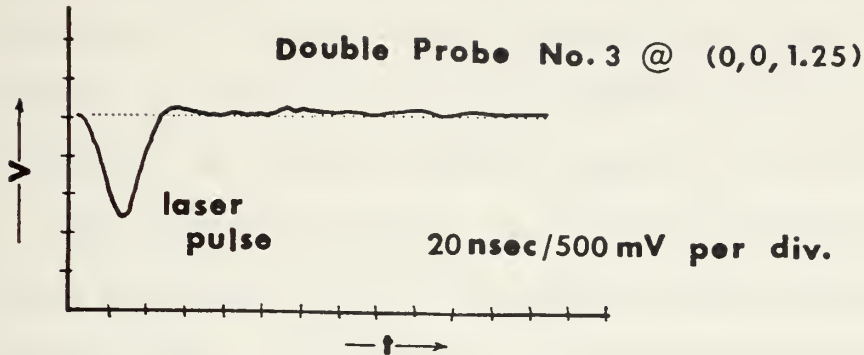
Figure 19. Double probe response in the presence of a 950 gauss magnetic field. The target has been removed and the laser pulse transits the chamber and exits through a glass cover over port number three.

These tracings indicate that no probe response is generated by either the magnetic field or laser pulse interaction with components of the apparatus other than the target.

Gyrofrequencies for electrons and ions are given by equation (7):

(7) ω_c = eB/mc (radians/sec)

The field in this case is 950 gauss so that the ion gyrofrequency is 3.35×10^5 rad/sec and the electron gyrofrequency is 1.67×10^{10} rad/sec.

The Larmor radii are given by equation (8)

(8) $R_L = V_\perp / \omega_c$

From this expression we find that for electrons the Larmor radius is 9.75×10^{-3} cm and for aluminum ions it is 484 cm. From this it is obvious that if the early disturbance is composed essentially of electrons, the signal should be greatly diminished at distances greater than a few gyro radii or 0.5 cm. However, if the early disturbance is

essentially a neutral plasma then there should be little change in the amplitude. The ions with their much larger gyro radius will hardly be deflected by the field. As soon as sufficient space charge separation is created, the ions will drag the electrons out of the magnetic field.

Other researches [Refs. 1, 6, 25, 28 and 33] have reported that plasma fronts tend to be rich in electrons while the main body is ionically rich. In this case, the front will be changed from electron rich to ion rich by the magnetic field. If we consider the plasma on a microscopic, interparticle, basis and set the Lorentz force equal to zero we can obtain a measure of the space charge separation necessary to pull the electrons out of the magnetic field

$$(9) \quad \vec{V}_{LP} \times \vec{B} = \vec{E} = V_{LP}B \quad \text{since } \vec{V}_{LP} \perp \vec{B}$$

$$(10) \quad V_{LP} B = ke/r^2 \text{ which on solving for r gives:}$$

$$(11) \quad r = (ke/VB)^{1/2} \quad \text{where } k = 1/4\pi\epsilon$$

If we substitute $V_{LP} = 1.1 \times 10^7$ cm/sec and B = 950 gauss into equation (11) we find that the separation is 0.1 mm.

Figure 20 duplicates photographs of the oscilloscopic record of the double probe response with and without the transverse magnetic field. There is no discernible change in the early signal when the magnetic field is introduced.
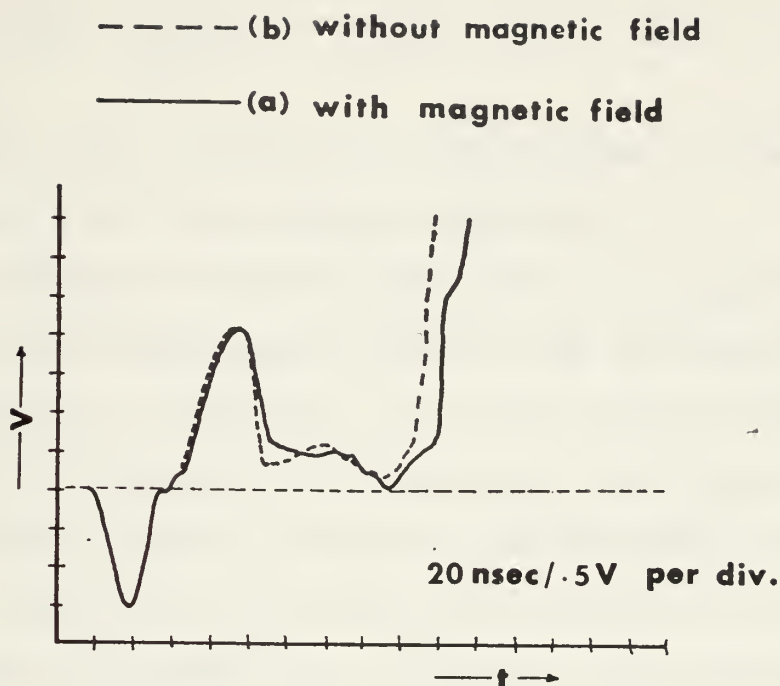
Figure 20. Double probe response at (0, 0, 1.25) to the streaming plasma with (a) and without (b) a transverse 950 gauss magnetic field.

It is interesting to observe that the main plasma is delayed by about 10 nsec and the early plasma by about one or two nsec. For the main plasma traveling at 10^7 cm/sec this delay represents a change in plasma front position of one millimeter. This compares with the prediction obtained from equation (11) if the electron rich area originally extends 0.9 mm in front of the neutral boundary of the plasma.

It might be argued that since the direction of this transverse magnetic field is horizontal there is a drift velocity due to the gravitational force. Depending on the direction of the fields this drift could be either back into the target or away from the target toward the probe. The magnitude of this drift is given by:

(12) $\vec{V}_{DG} = \dfrac{mc\,\vec{g}}{qB^2} \times \vec{B} = mcg/qB$

For the values under consideration in this experiment the magnitude of V_{DG} is 5.9×10^{-8} cm/sec which is insignificant.

Since the magnetic field has little effect on the early disturbance this experiment strongly suggests that the early disturbance is not purely electronic in composition. If it were, then the magnetic field would deflect the electrons into a gyro radius with diameter much smaller than the distances at which the probe measurements were made. This would result in the loss of the early disturbance and the probe's response would drop significantly. Therefore, if the early disturbance is particulate in nature, it must contain heavier ions.

D. SEPARATION OF THE PHOTOELECTRIC RESPONSE

During the density contour mapping a disturbance of small half width (4 nsec) was observed to occur at approximately t = 16 nsec, i.e. near the peak of the laser pulse. The time of occurrence was constant for all points on the mapping grid indicating a very high propagation speed. Several authors [Refs. 16 and 33] have reported strong X-ray and UV radiation emanating from the target area of a laser produced plasma. Ready [Ref. 40] has ascribed the early disturbance noted on his Langmuir probes to reverse photoelectric effect. His measurements were made at 30 cm from the target in near vacuum. As will be noted later, the early plasma decays rapidly between 0.75 and 2.0 cm. Therefore at 30 cm it is most probable that all he saw in terms of early probe response was the reverse photoelectric response. At distances less than one centimeter from the target the photoelectric response is masked

by the much larger response due to the early plasma pulse. Figure 21 illustrates this masking and shows the appearance of the photoelectric signal at 1.7 and 3.0 cm.
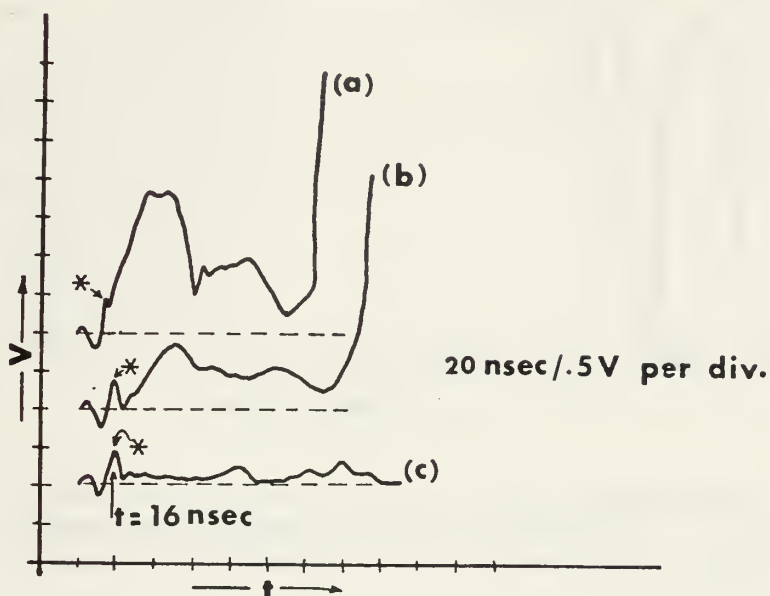
Figure 21. Double probe response to a streaming laser produced plasma at (a) (0, 0, 1.3), (b) (0, 0, 1.7) and (c) at (0, 0, 3.0). Asterisks mark the suspected photoelectric response

In order to verify that this signal was photoelectric in origin, a fused quartz (SiO_2) plate was obtained. The plate is 2.54 cm square and and has a thickness of 0.02 cm. The transmissivity of this plate is greater than ten percent for wavelengths longer than 0.12 microns. Figure 22 depicts the transmissivity as a function of wavelength for a one-half inch plate of the same material. The work function for tungsten is approximately 4.55 eV. Therefore, the maximum wavelength for single photon photoelectric emission from the probe tips is 0.267 microns. This wavelength is marked on Figure 22. The hashed area denotes the transmitted wavelengths capable of producing the observed photoionization.

43
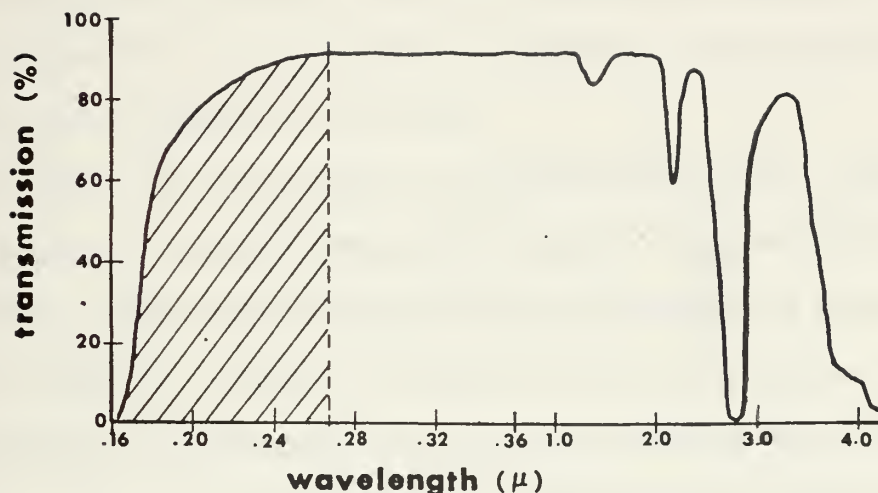
Figure 22. Transmissivity of a 1/2 inch fused quartz plate. The hashed area represents those wavelengths that are transmitted and are capable of ionizing tungsten.

In this experiment, the quartz plate was placed between the probe and the target. Probe response with and without the quartz was recorded and a comparison made. These oscilloscopic traces are reproduced in Figure 23.
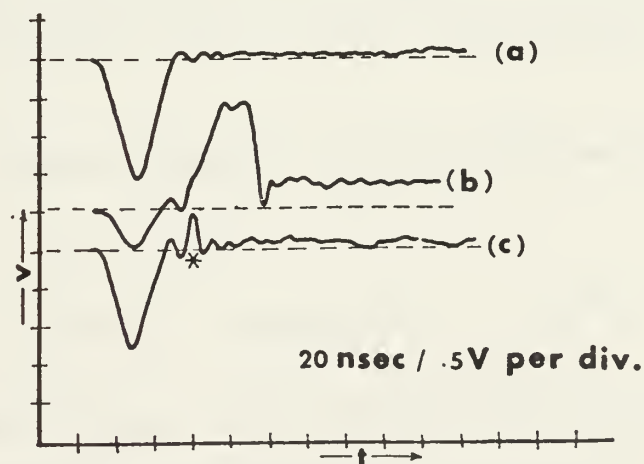
Figure 23. Oscilloscopic record of a double probe response at (0, 0, 1.75) with (a) the laser beam passing through the chamber but no target in place, (b) without the quartz plate screen and (c) with the quartz plate screen in place between the target and the probe. An asterisk marks the verified photoelectric response

This experiment was repeated ten times at different locations in the chamber with identical results. As seen, the quartz plate stops all physical particles but passes UV radiation which produces the photoelectric response at the probe.

The height of the response is approximately 300 mV. Assuming that ten percent of the electrons ejected from the negative electrode are collected at the positive electrode this corresponds to a current flow of 0.079 amps for 4 nsec or a total of 1.97×10^9 electrons. Assuming an average photon energy of six eV and also assuming that ten percent of the incident photons result in the ejection of an electron from the negative electrode we have an energy deposition on the probe tip of 1.9×10^{-8} joules. The cross sectional area of this tip is 4.6×10^{-3} cm^2. Assuming that the electromagnetic radiation is transmitted equally in all directions through a hemisphere whose center is the focal spot on the plane target, this corresponds to a total energy of 7.9×10^{-5} joules transmitted at wavelengths between 0.12 and 0.27 microns. This represents about 1.3×10^{-5} of the incident energy in the laser pulse.

Equation (25) predicts that for a static plasma the ion density is [Ref. 45]:

$$(25) \quad n_i = 1.67 \ I_+ \ (m_i/kT_e)^{1/2}/eA_p \quad (cm^{-3})$$

If the 300 mV probe response is due to photoionization of the background this would correspond to a background gas ion density of 1.79×10^{14} cm^{-3} assuming $kT_e = 3$ eV, $m_i = 28.96$ AMU and that the total surface area of the probe electrode is 1.4×10^{-2} cm^2. Since the background gas density is only 8.85×10^{11} cm^{-3} this response must be due to the reverse photoelectric effect described by Ready.

E. DENSITY MAPPING OF THE EARLY PLASMA

The expanding plasma density has been mapped using a double probe. The mapping grid is shown in Figure 24.
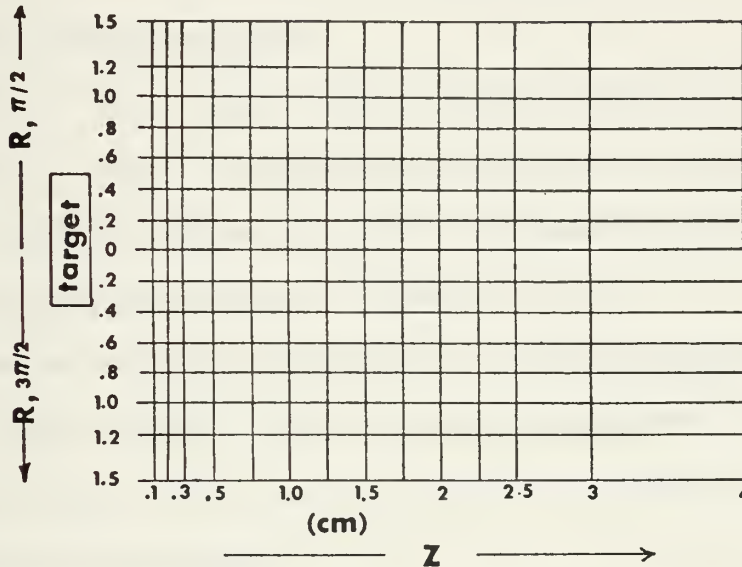
Figure 24. Density Mapping Grid

The general method used was to acquire an oscilloscopic record of the probe response at each grid point. A zero time was marked on each photograph and corrected for the 35 nsec cable delay. Probe response voltages were then read from the photograph corresponding to the desired time intervals for the contour maps. These voltages are readable to within $\pm$ 0.2 volts. The voltage from each grid point corresponding to a specific time is then plotted on the grid depicted in Figure 24. Contours were drawn by hand. All of the data and contour mappings were analyzed manually. However, because these are only relative density contour maps and because of the many data points involved in each map, any errors introduced should be minimal.

The area excluded from each map is the corridor through which the laser pulse travels in reaching the target. Since plasma density is proportional to probe response voltage, these contour maps give relative density contours.

For the early plasma pulse, the probe response was mapped at 10 nsec, 20 nsec, 30 nsec, 40 nsec and then at 20 nsec intervals to 160 nsec. This allows a detailed analysis of the expanding plasma pulse. These contour maps are included as Figures 26 to 35.

The maps indicate that the early disturbance expands rapidly (10^8 cm/sec) along a line inclined at approximately 30 degrees with the target normal. This line also describes the path followed by the reflected laser pulse.

It should be noted that typical densities measured throughout these maps are on the order of 10^{12} cm^{-3}. This is nine orders of magnitude below the critical density so that the plasma being examined here is essentially transparent to the incoming laser radiation.

The focal spot size of this laser pulse is 1.5 mm in diameter. It should be noted that the early disturbance expands very rapidly to a full radius of approximately 1.0 cm by z = 0.2 cm. At z = 0.2 cm the plasma radial expansion stops and all further expansion occurs along the axis of symmetry. This behavior is strongly suggestive of a force acting on the plasma to pinch the radial development. Since no external fields other than the small probe potential were applied, it is evident that this force must be produced internally within the plasma. The self-induced magnetic fields mapped by McKee and Bird [Refs. 8 and 38] would provide a pinching effect on the plasma. The $\vec{J} \times \vec{B}$ force was

neglected by McKee as too small to be significant. However, further investigation of this force seems warranted and is included in Section IV. B.

It should also be noted that the plasma density gradients are higher in the radial direction than in the direction of pulse propagation. This is also strongly suggestive of a radial confining force. These gradients are plotted in Figure 25.

Maximum densities noted in the early pulse are approximately 4×10^{12} cm^{-3}. This corresponds to the 2.5 volt contour in each of Figures 26 to 29. In Figure 30 the early plasma pulse has separated from the main plasma pulse. Subsequent figures contain only main plasma contours. The maximum early plasma densities are greater than the background gas density by a factor of five.

It should be noted that as early as t = 10 nsec there is evidence of plasma at distances as great as 0.8 cm. This plasma may partially be the result of intense background gas photoionization. However, the magnitude of the response indicates ion densities three orders of magnitude higher than the background gas density (assuming a macroscopically quiescent plasma).

These topographical density maps also show that after flooding into the chamber, this early disturbance decays rapidly so that at 100 nsec there is little remaining evidence of the early plasma pulse. Another interesting feature is that the decay appears to proceed more slowly along the target normal than along the axis of propagation of the early disturbance (see Figures 30 and 31).
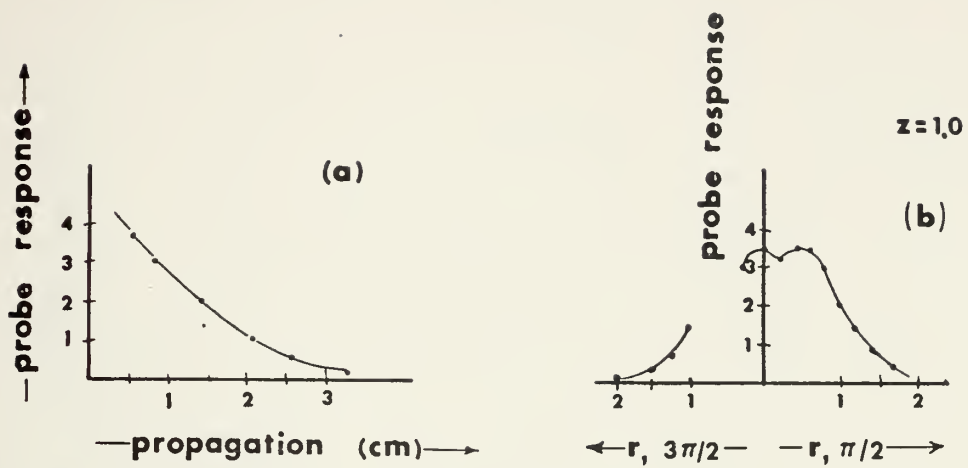
Figure 25. Early plasma pulse density gradients in (a) the direction of propagation and (b) in the radial direction
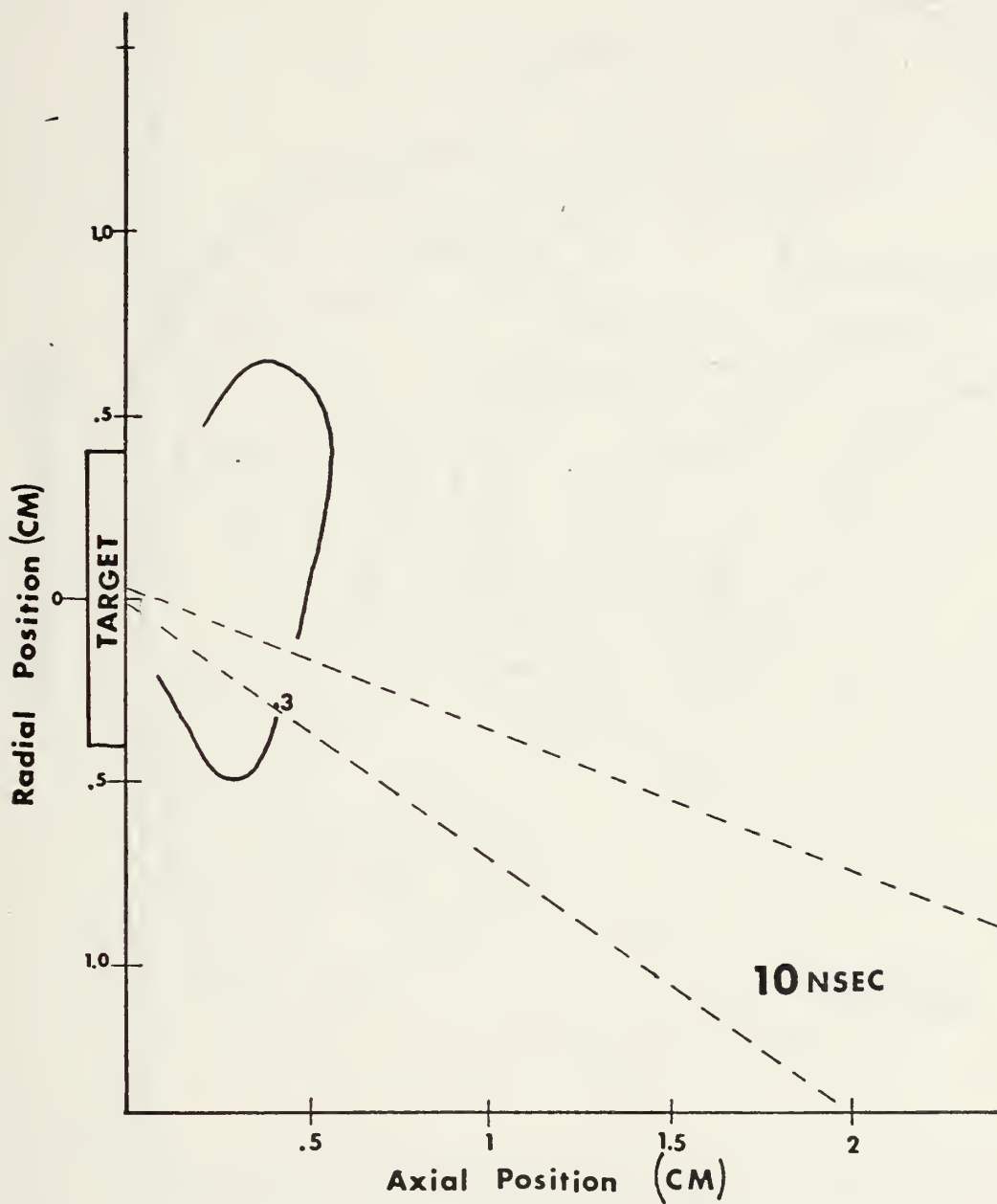
Figure 26. Laser-produced plasma relative density contours at t = 10 nsec.
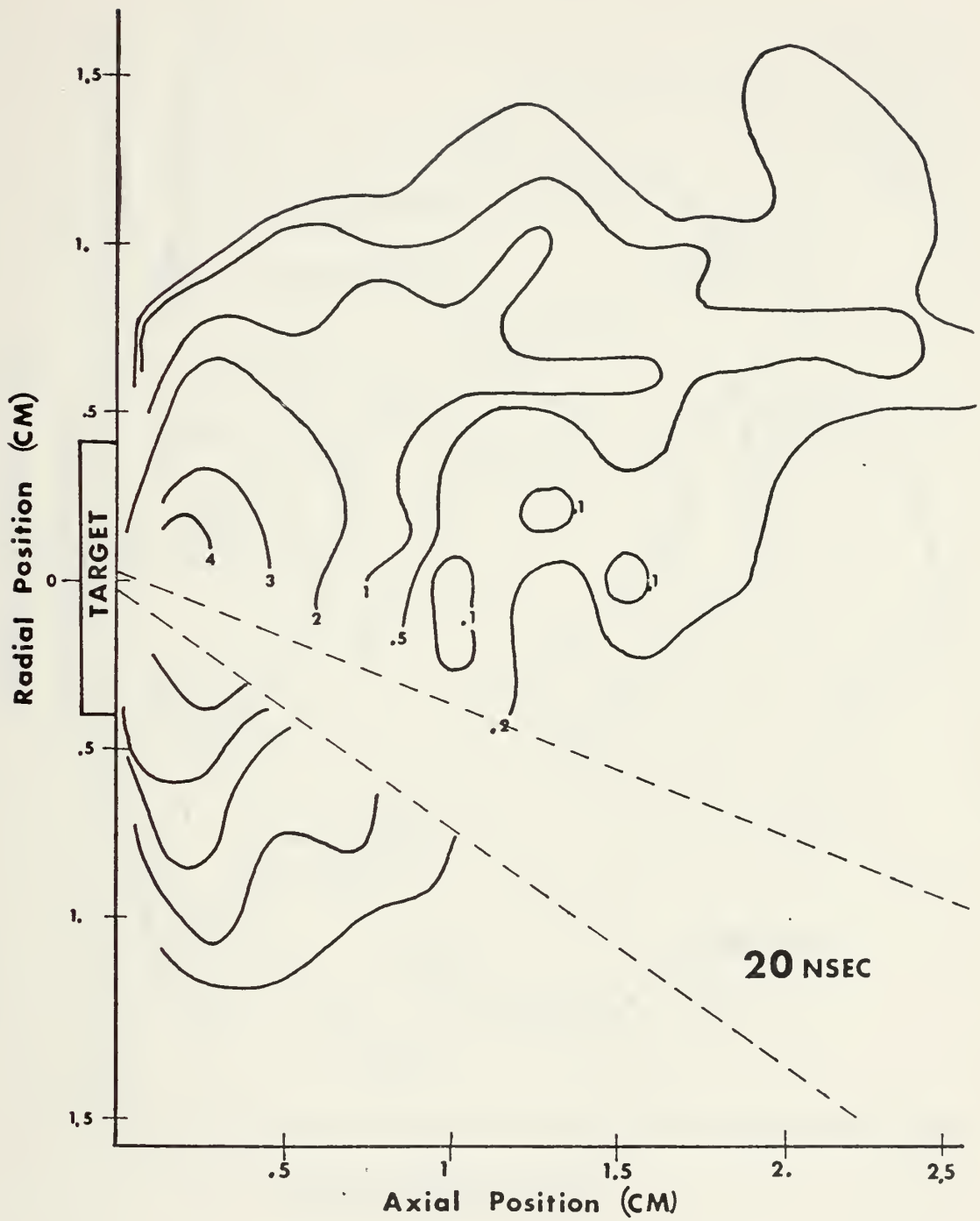
Figure 27. Laser-produced plasma relative density contours at
t = 20 nsec.
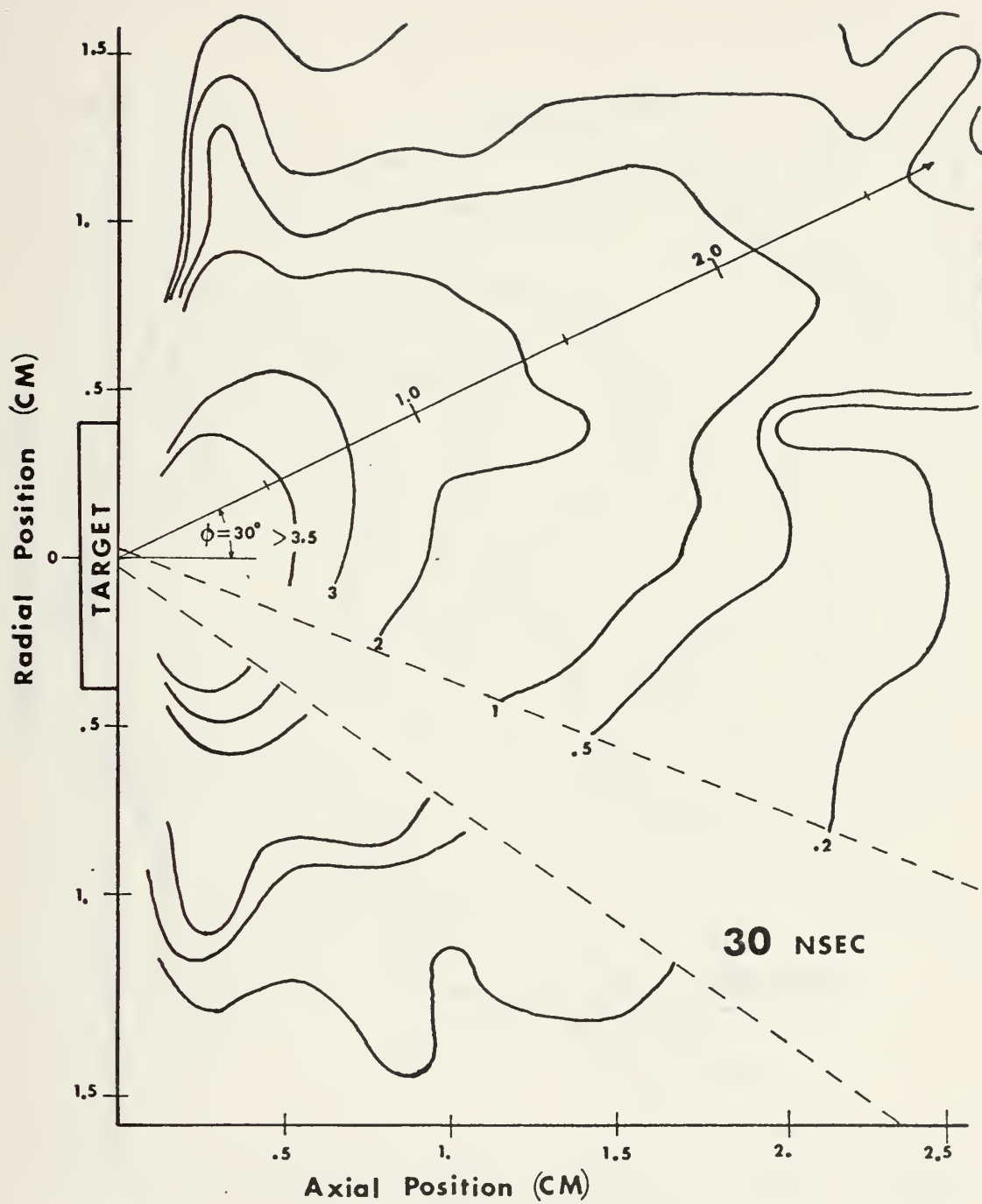
Figure 28. Laser-produced plasma relative density contours at
t = 30 nsec.
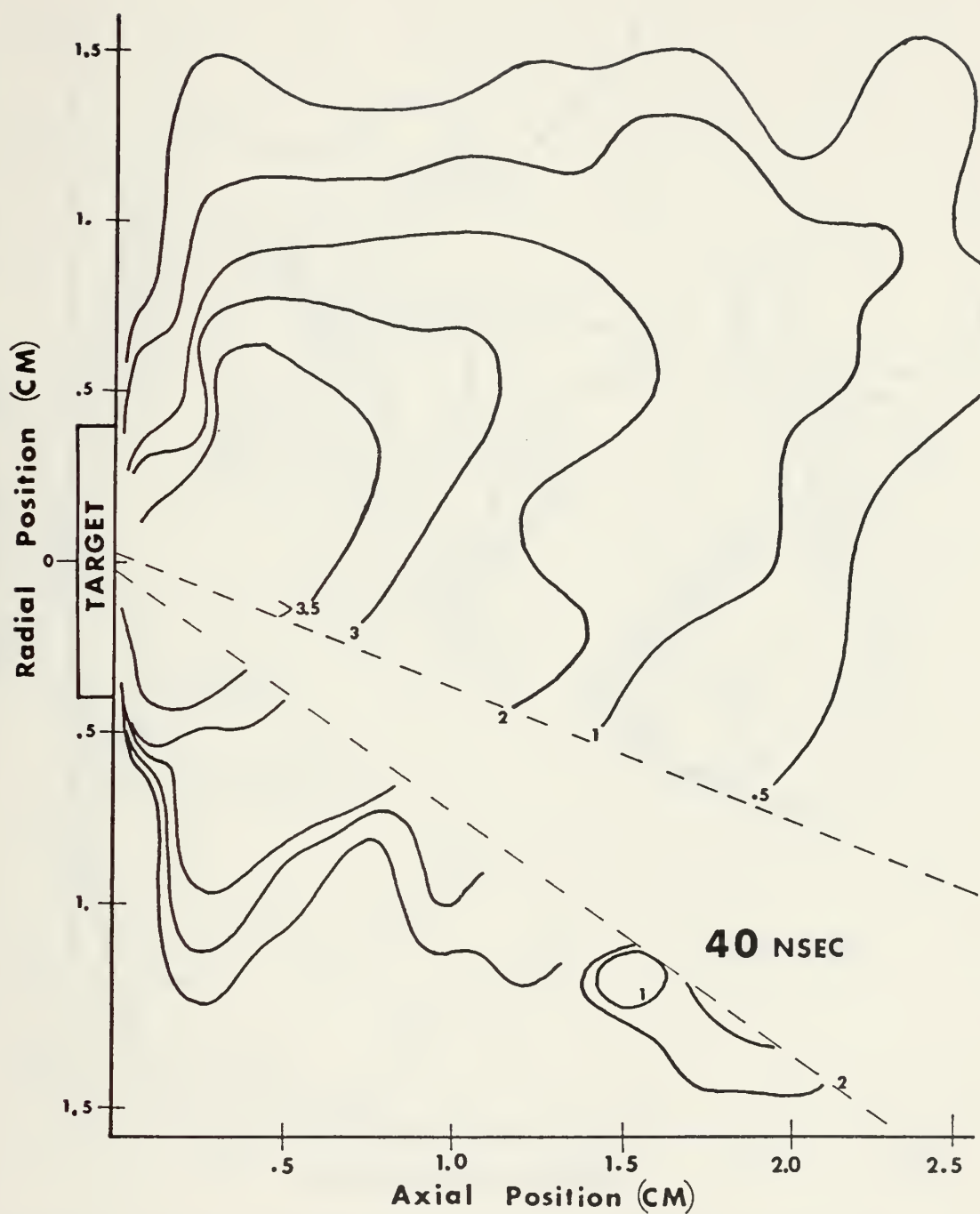
Figure 29. Laser-produced plasma relative density contours at
t = 40 nsec.

Figure 30. Laser-produced plasma relative density contours at
t = 60 nsec.
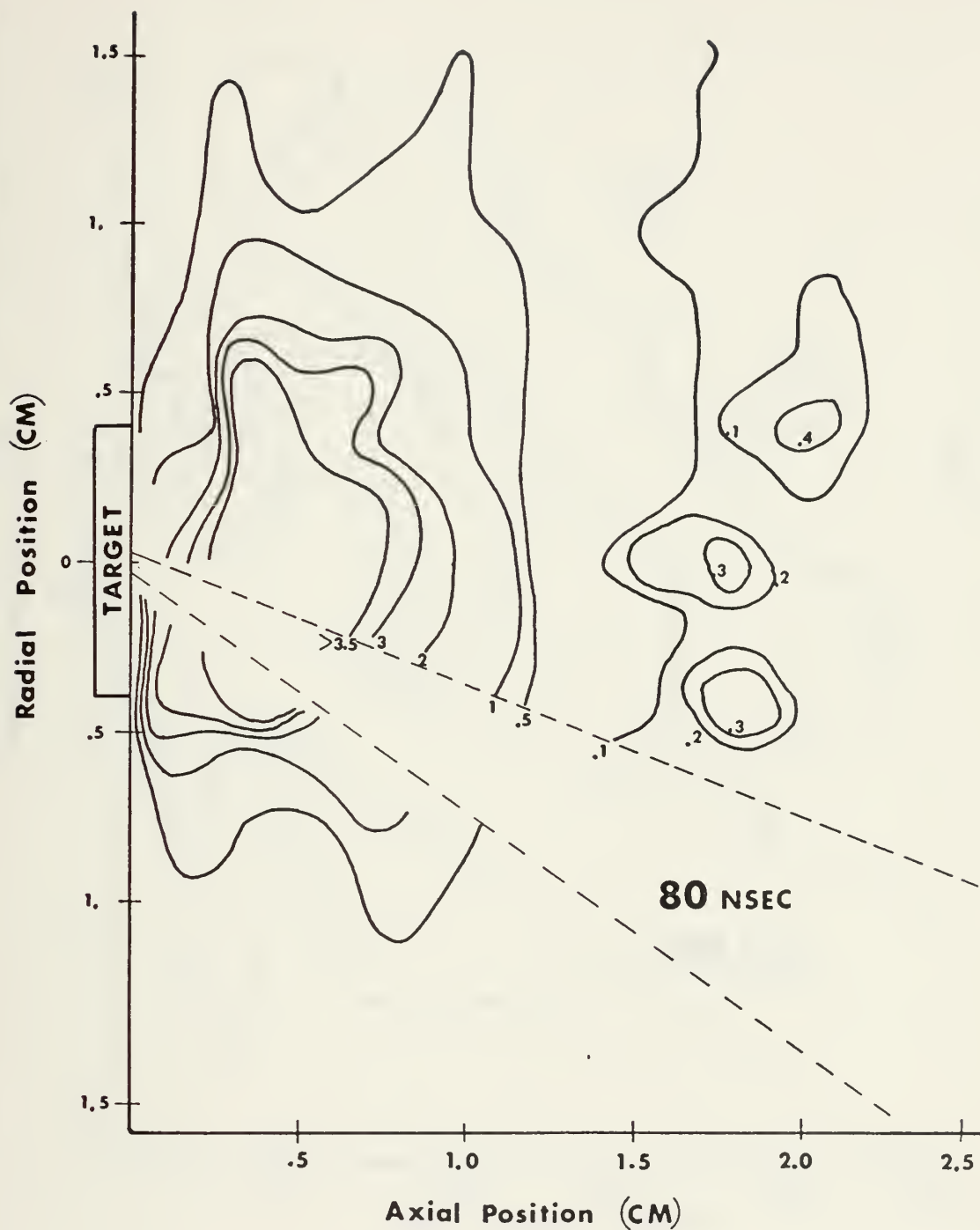
Figure 31. Laser-produced plasma relative density contours at
t = 80 nsec.
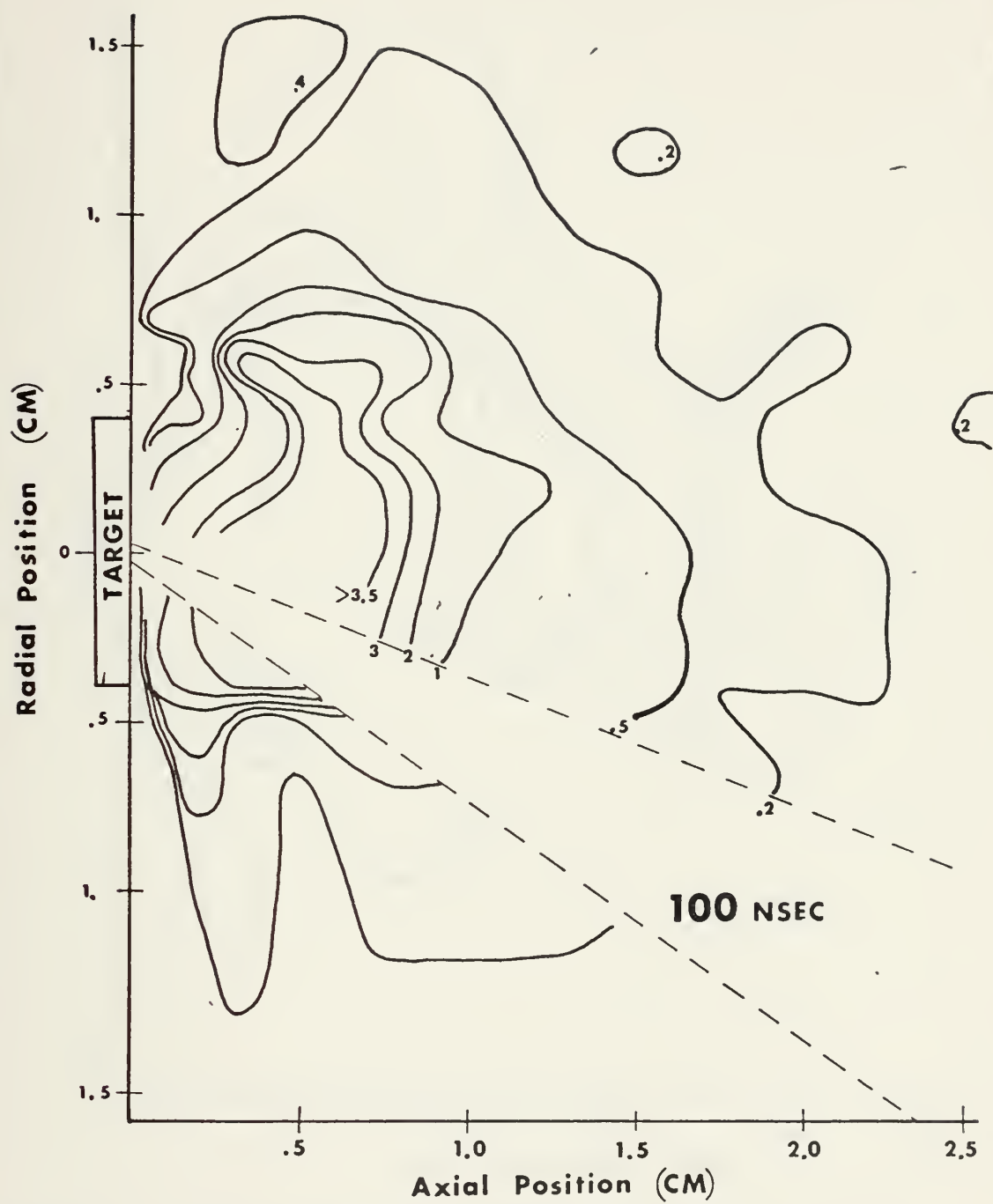
Figure 32.   Laser-produced plasma relative density contours at
t = 100 nsec.
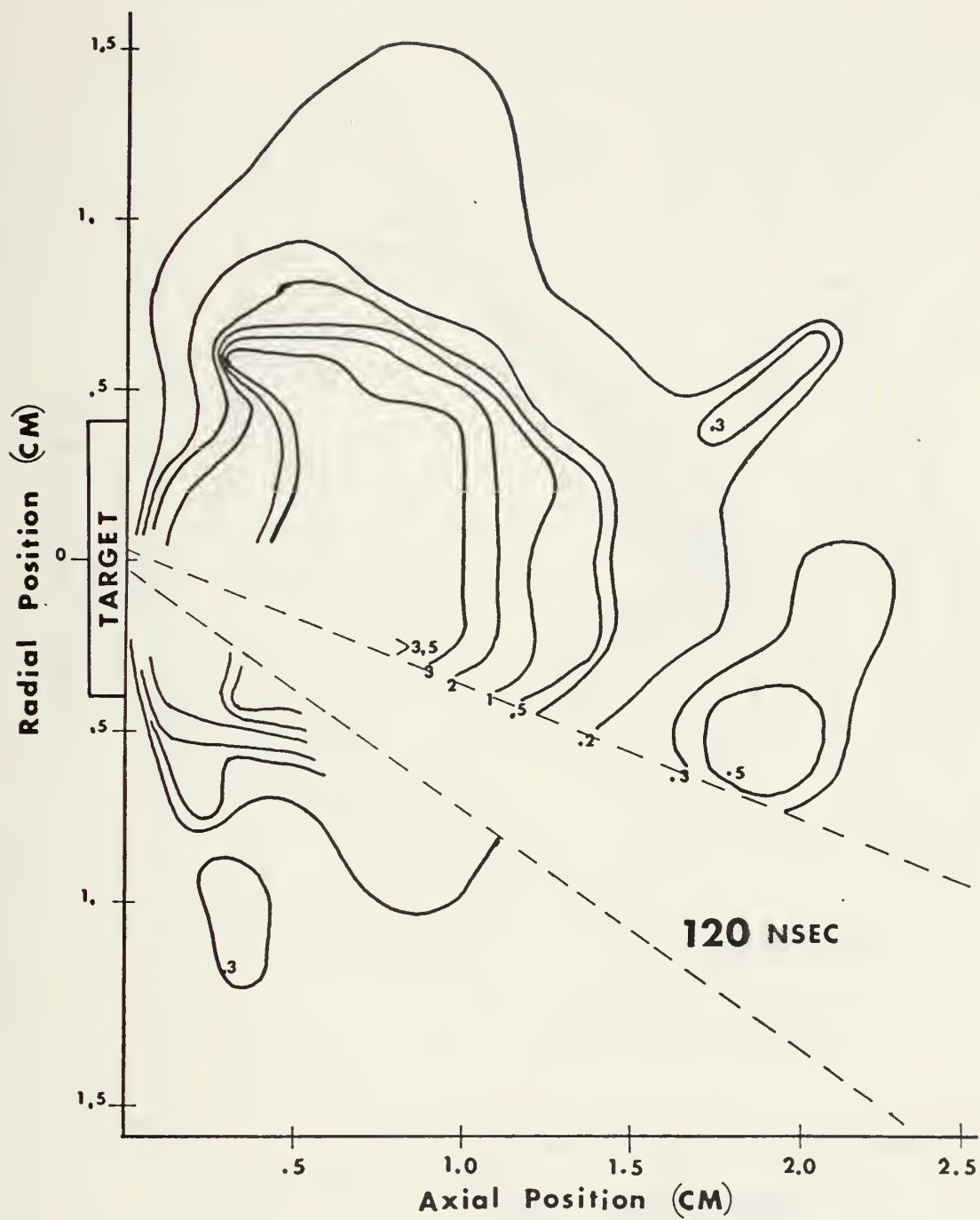
Figure 33. Laser-produced plasma relative density contours at t = 120 nsec.

57

Figure 34. Laser-produced plasma relative density contours at
t = 140 nsec.

58
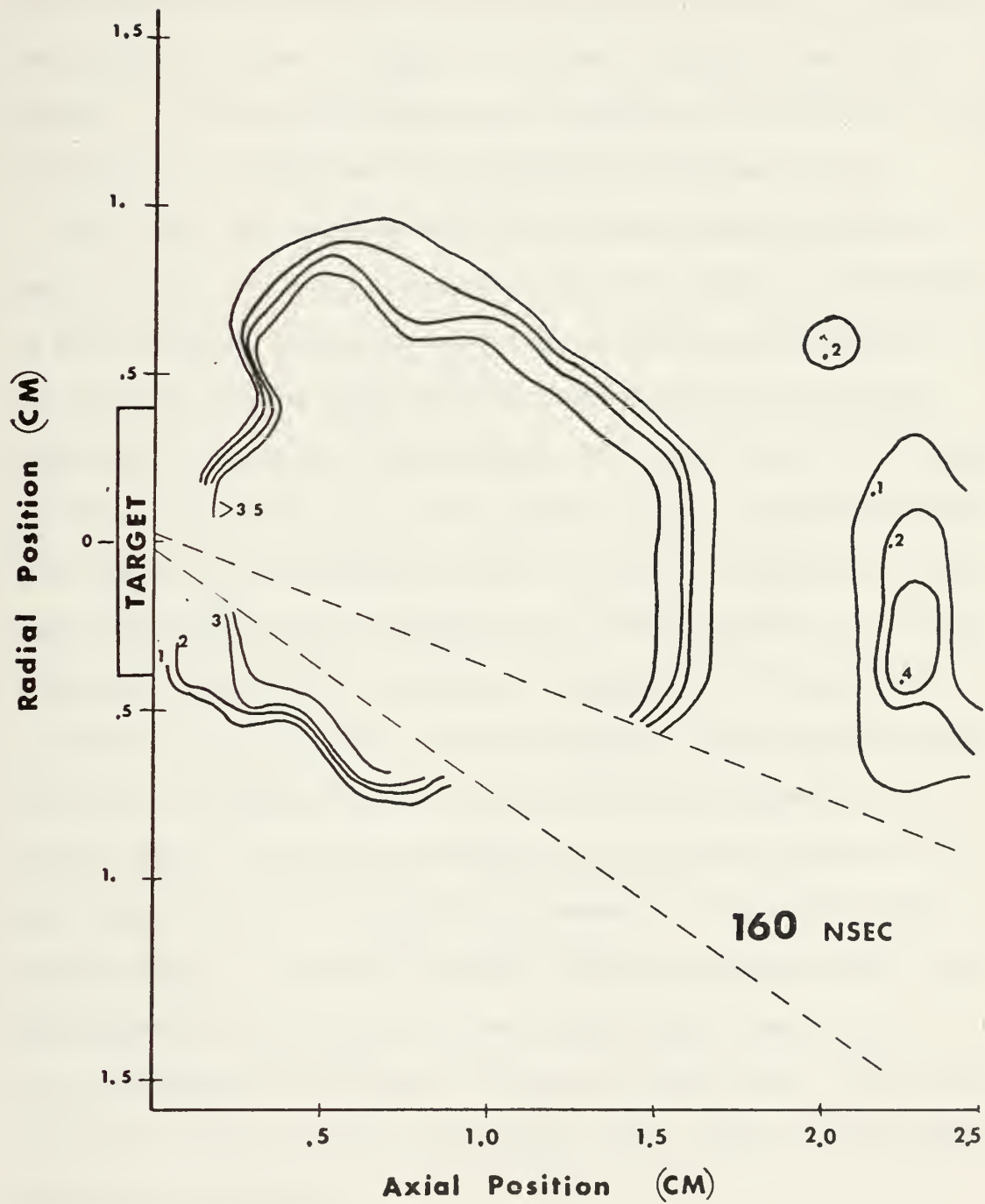
Figure 35. Laser-produced plasma relative density contours at
t = 160 nsec.

59

F. DENSITY MAPPING OF THE MAIN PLASMA

As an extension of section IV. E., relative density contour maps were completed at 100 nsec intervals from 100 to 800 nsec. The same mapping grid as shown in Figure 24 was used to produce these maps. However, the oscilloscope scales were increased to 100 nsec and 2 volts per division. The results are illustrated in Figures 37 to 44.

The first, very obvious feature of the main plasma is noted at 60 nsec in Figure 36. The main plasma body with densities corresponding to probe response voltages greater than 14 volts has been shaded. This map indicates that at early times the main plasma does not expand symmetrically about the target normal. The radial density is strongly skewed to the left between z = 0.2 and z = 0.8 cm. The high density area appears to be centered at (0.6, $\pi/2$, 0.5). Since these contour maps were made for only a single plane, no determination of the three dimensional distribution is possible. Examination of Figures 30 to 34 in section IV. E. indicates that this asymmetry decays rapidly so that by 120 nsec the main plasma has become essentially symmetric about the target normal. To further investigate and hopefully verify the late time symmetry of the main plasma with respect to the target normal, a special target of 1/8 inch thick 6061 aluminum alloy was constructed and mounted onto the face of the half inch target normally used. A 28 cm converging lens was used to focus the laser pulse to the smallest obtainable focal spot size at the target face. This was accomplished with an autocollimator.

Two double probes (numbers one and two) were positioned inside the chamber as depicted in Figure 45.
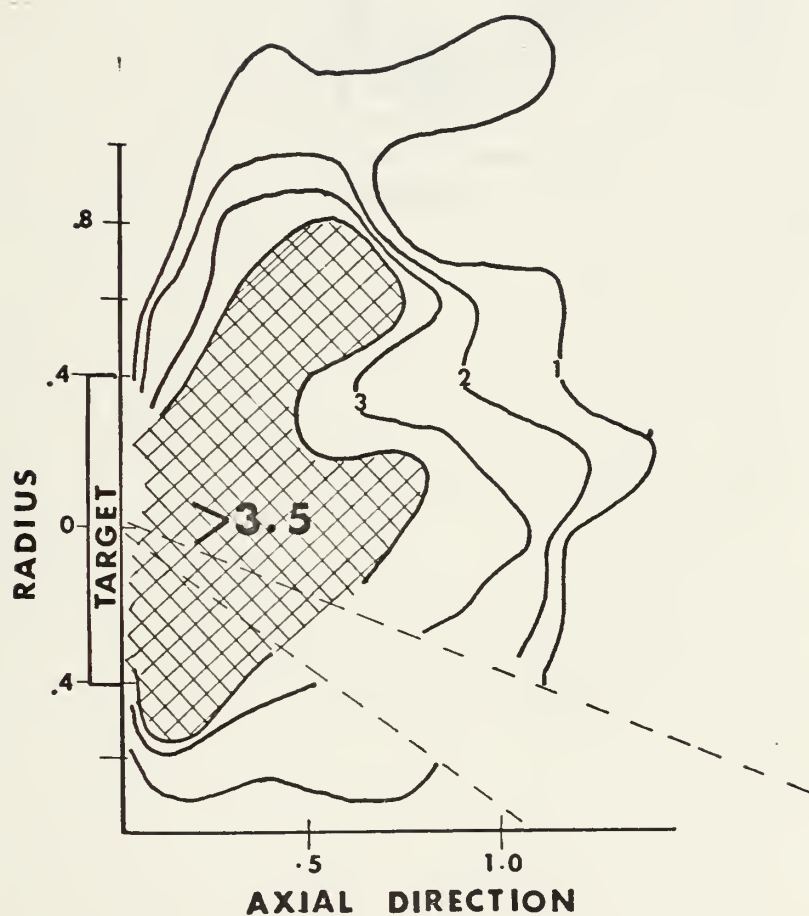
Figure 36. Early time asymmetry of the main plasma with respect to the target normal
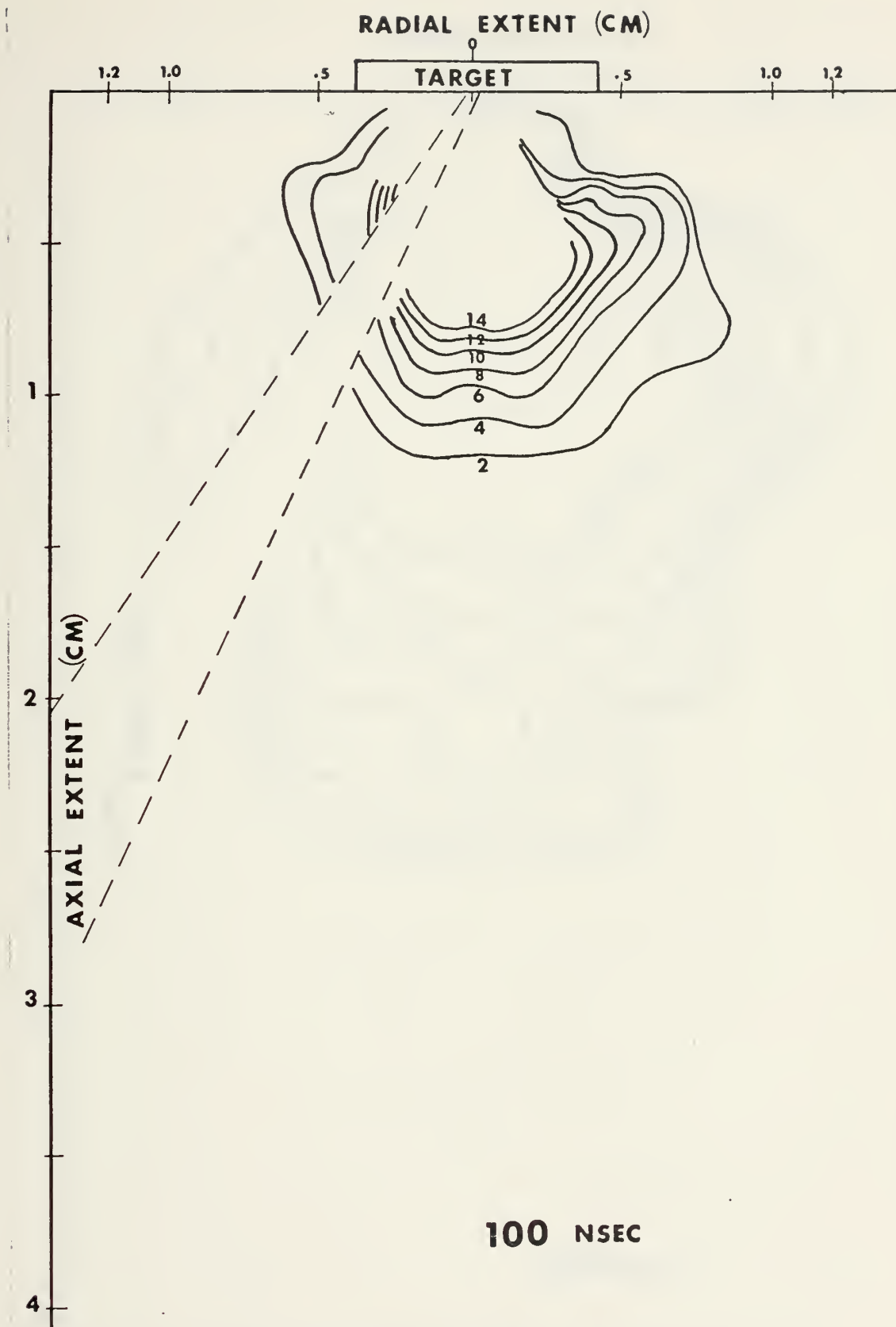
Figure 37. Laser-produced plasma relative density contours at
t = 100 nsec.
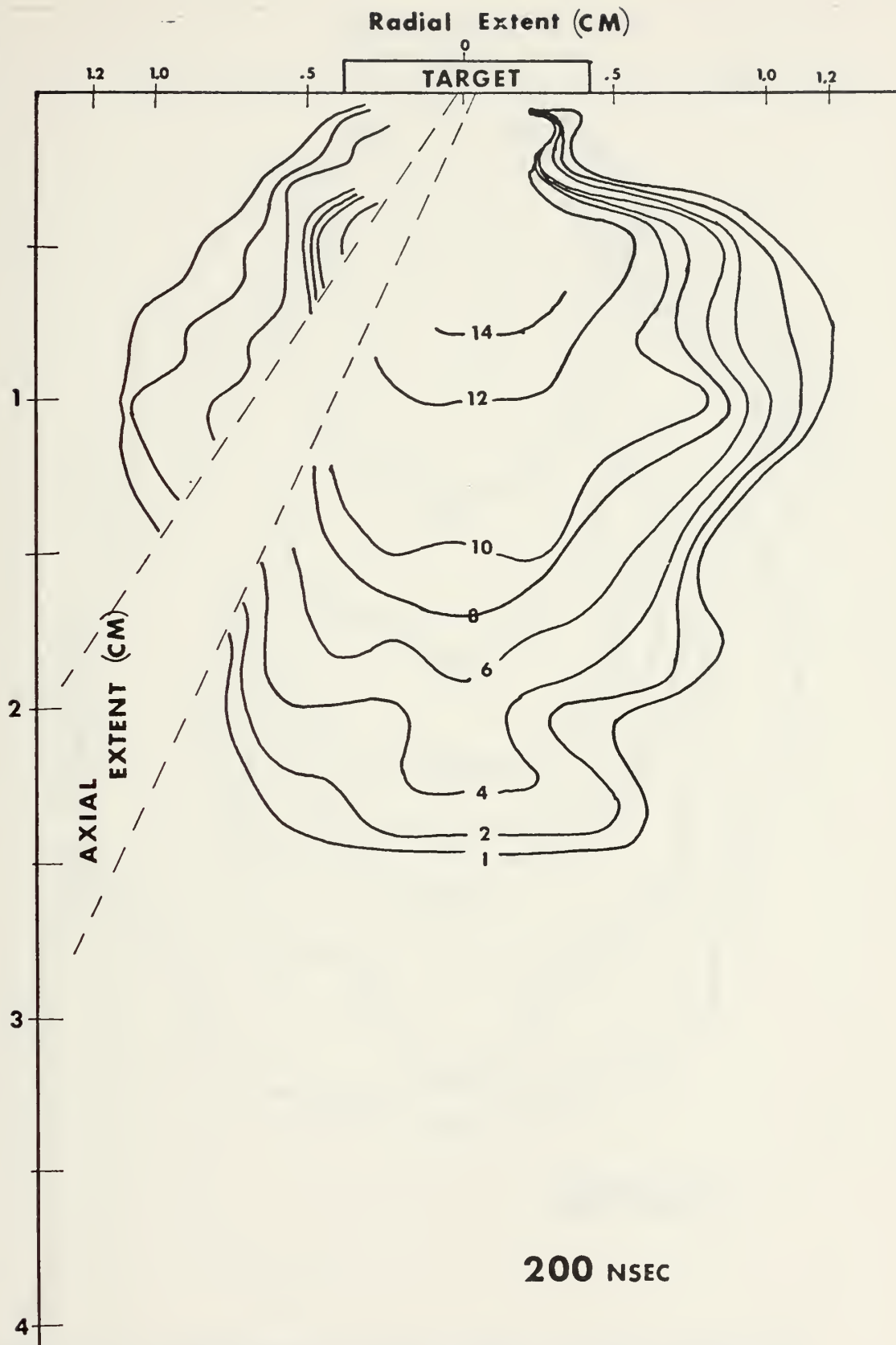
Figure 38. Laser-produced plasma relative density contours at
t = 200 nsec.

63
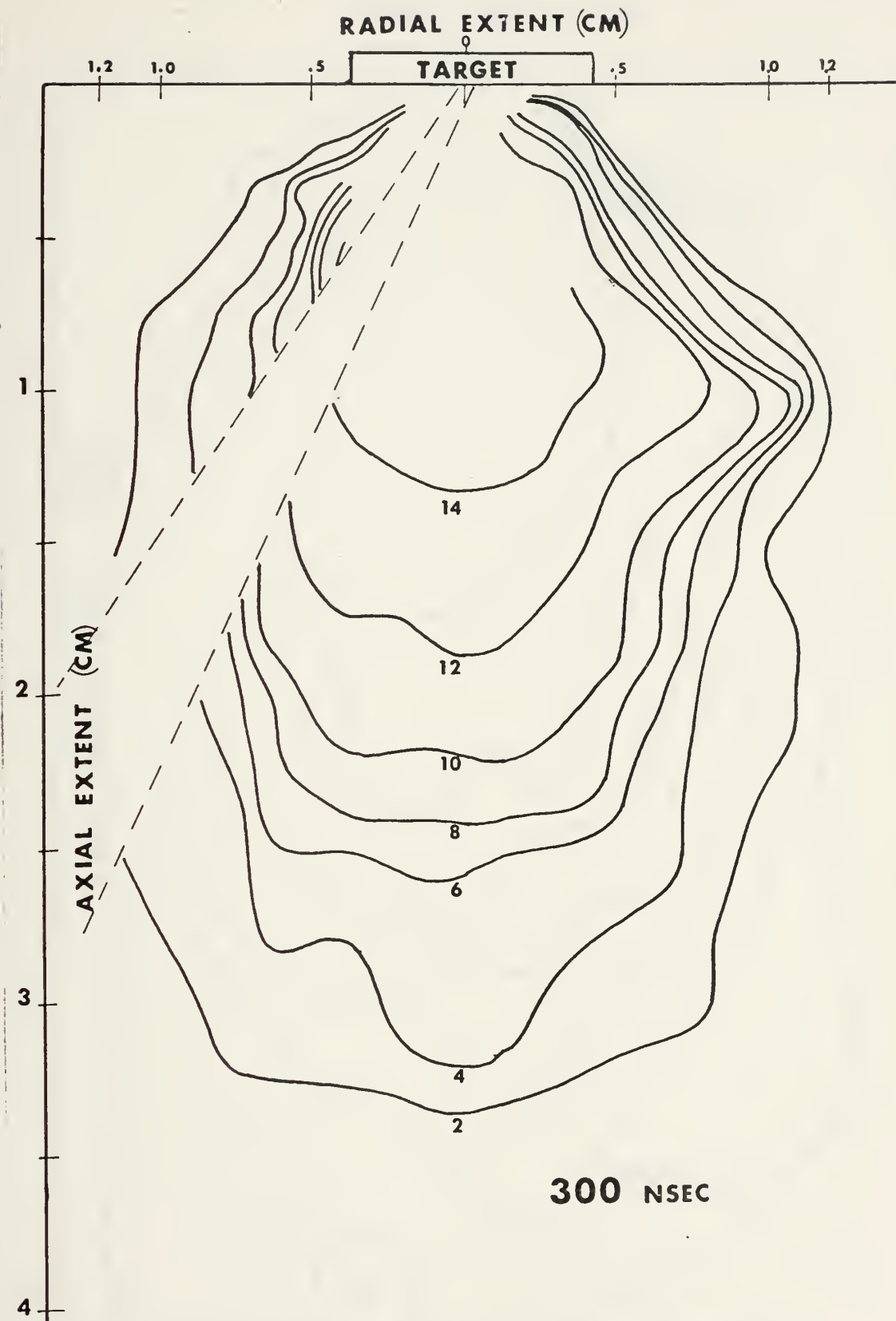
Figure 39. Laser-produced plasma relative density contours at t = 300 nsec.

64
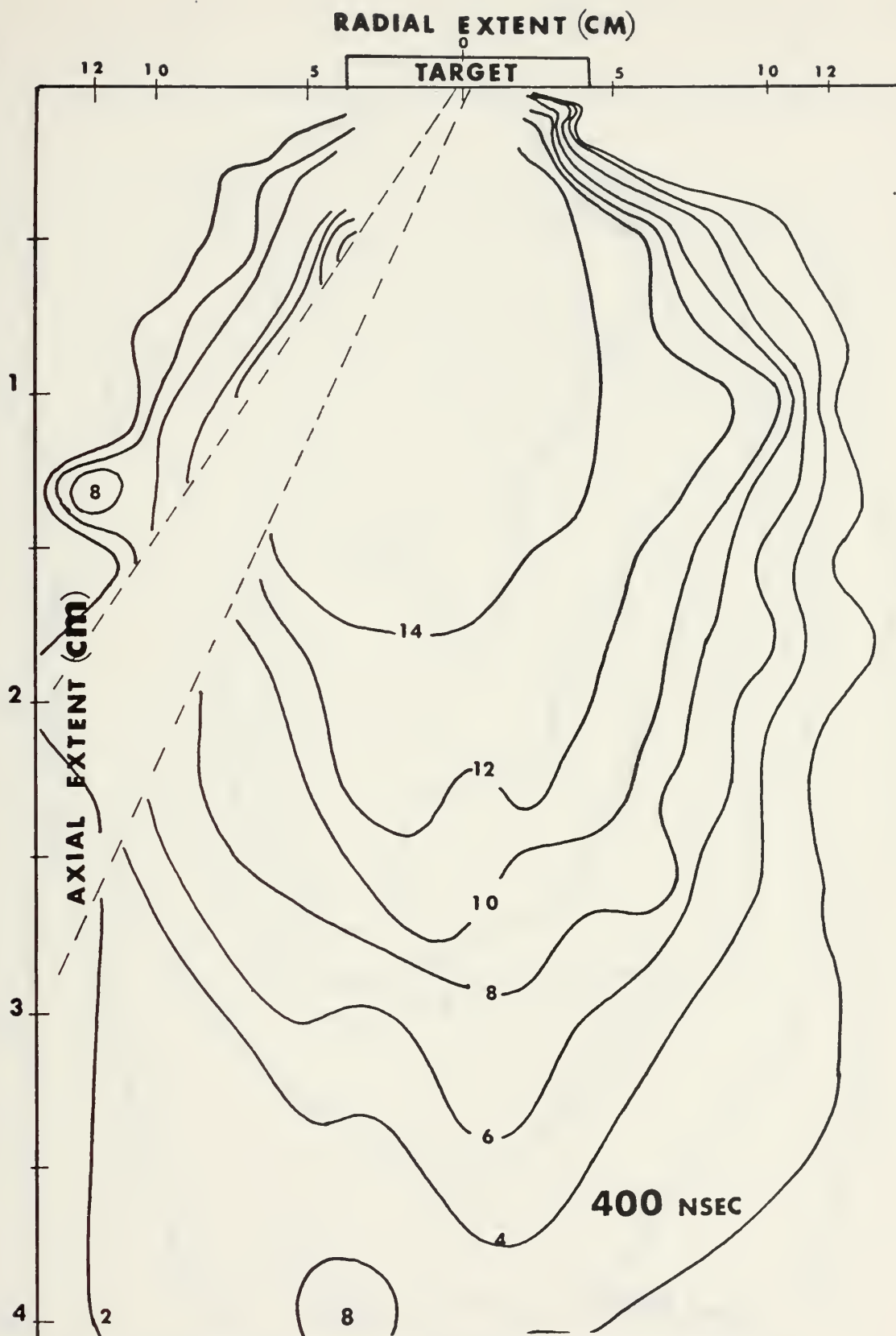
Figure 40.   Laser-produced plasma relative density contours at
t = 400 nsec.
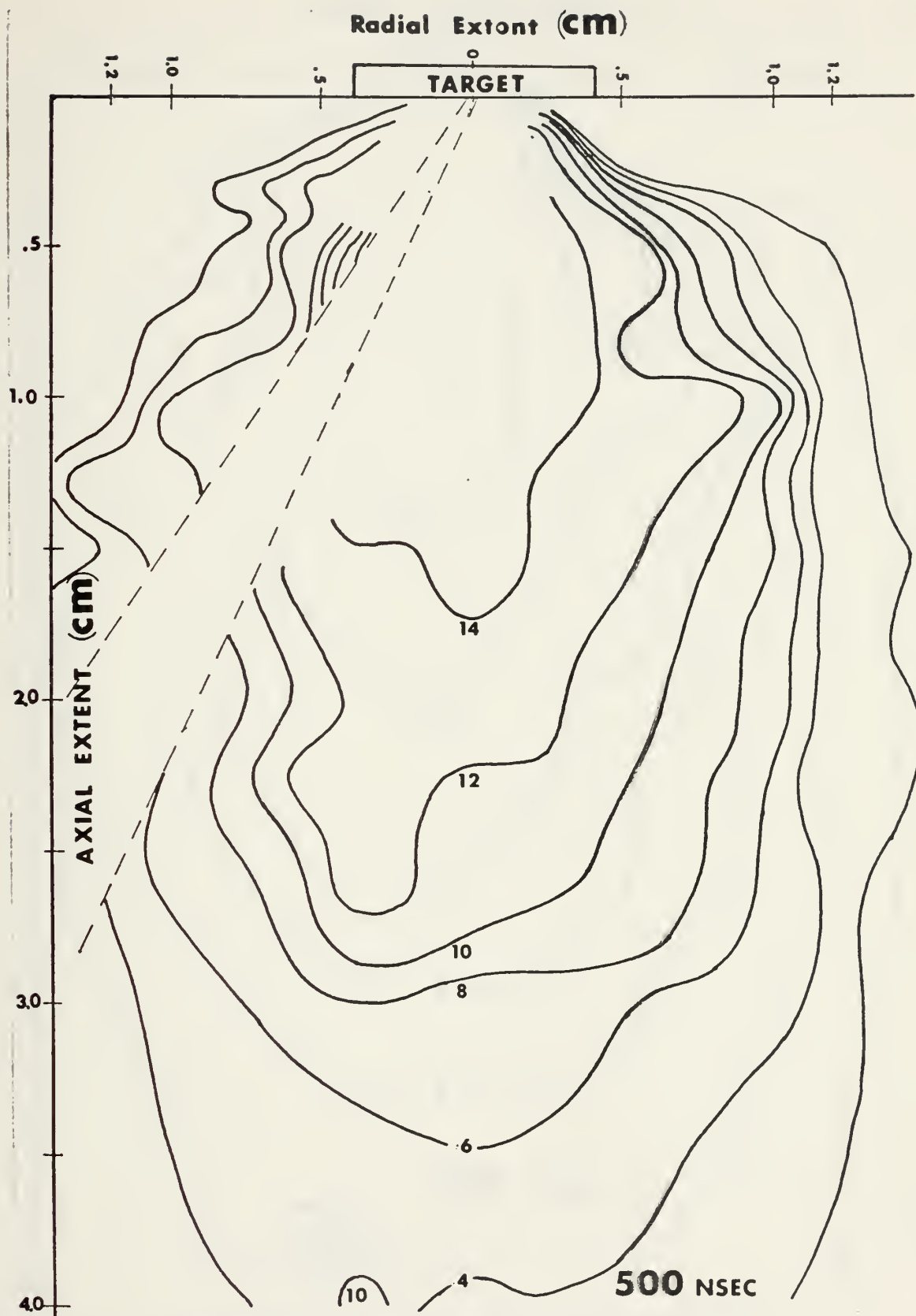
Figure 41. Laser-produced plasma relative density contours at
            t = 500 nsec.
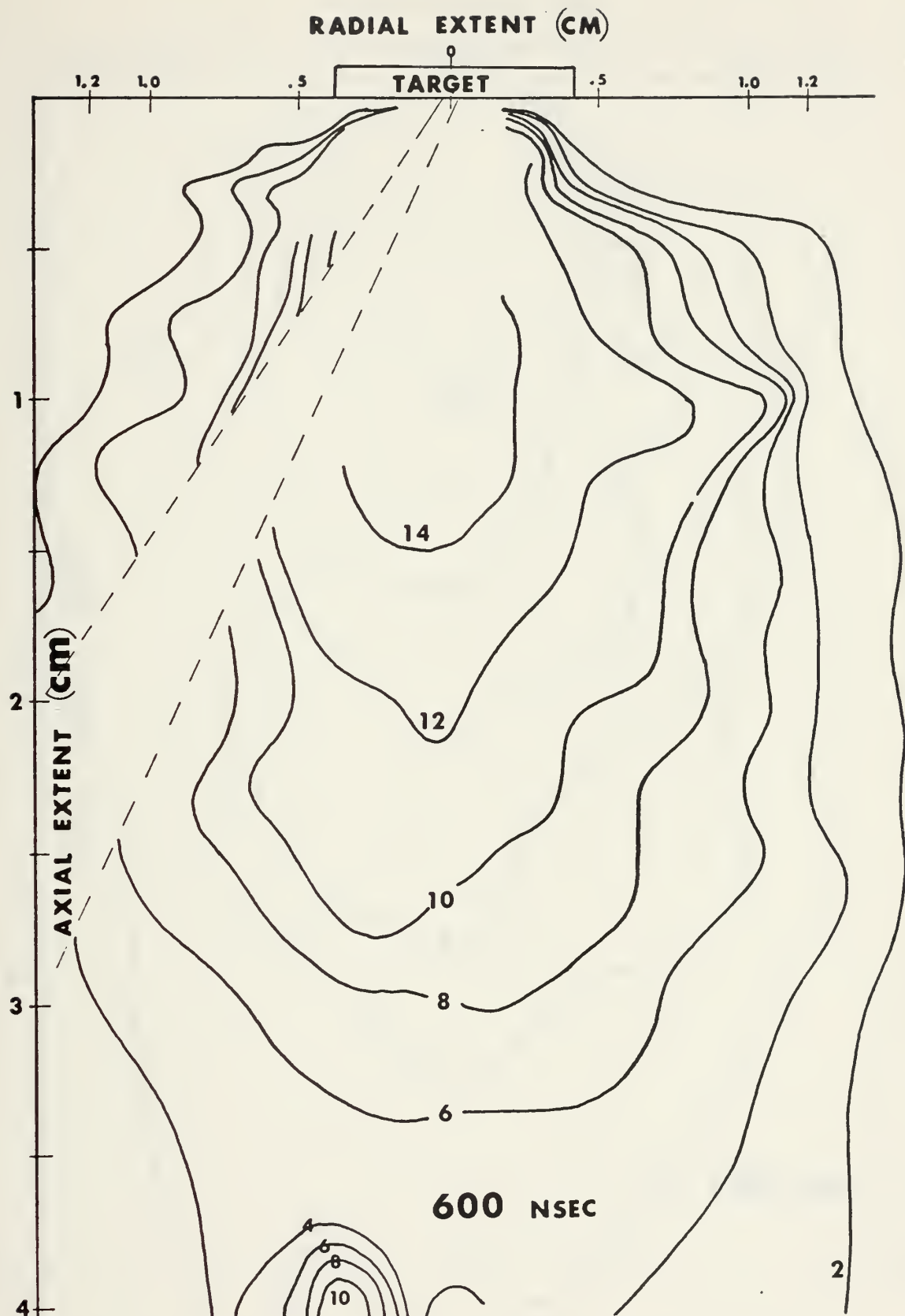
Figure 42. Laser-produced plasma relative density contours at t = 600 nsec.
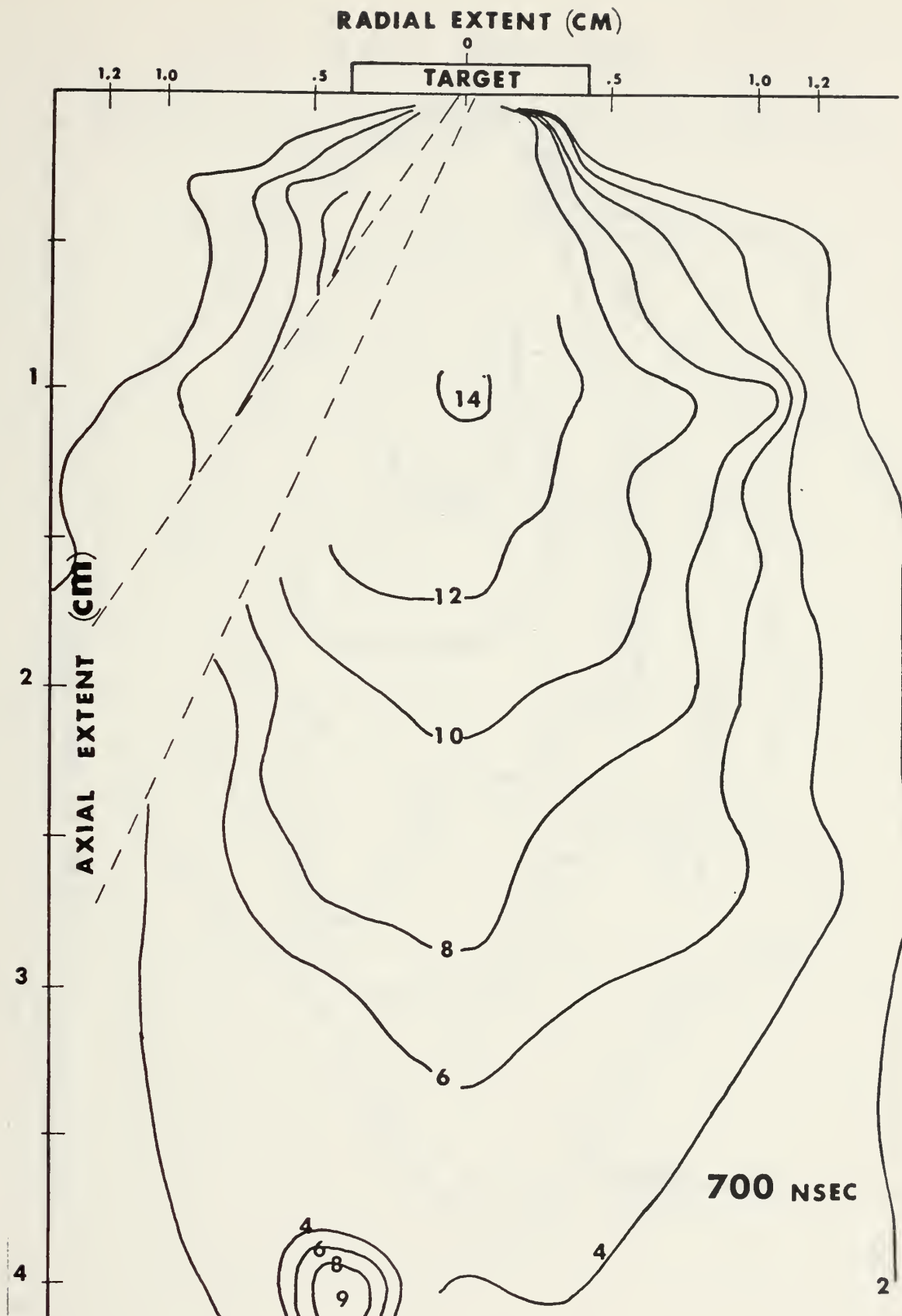
Figure 43. Laser-produced plasma relative density contours at
t = 700 nsec.
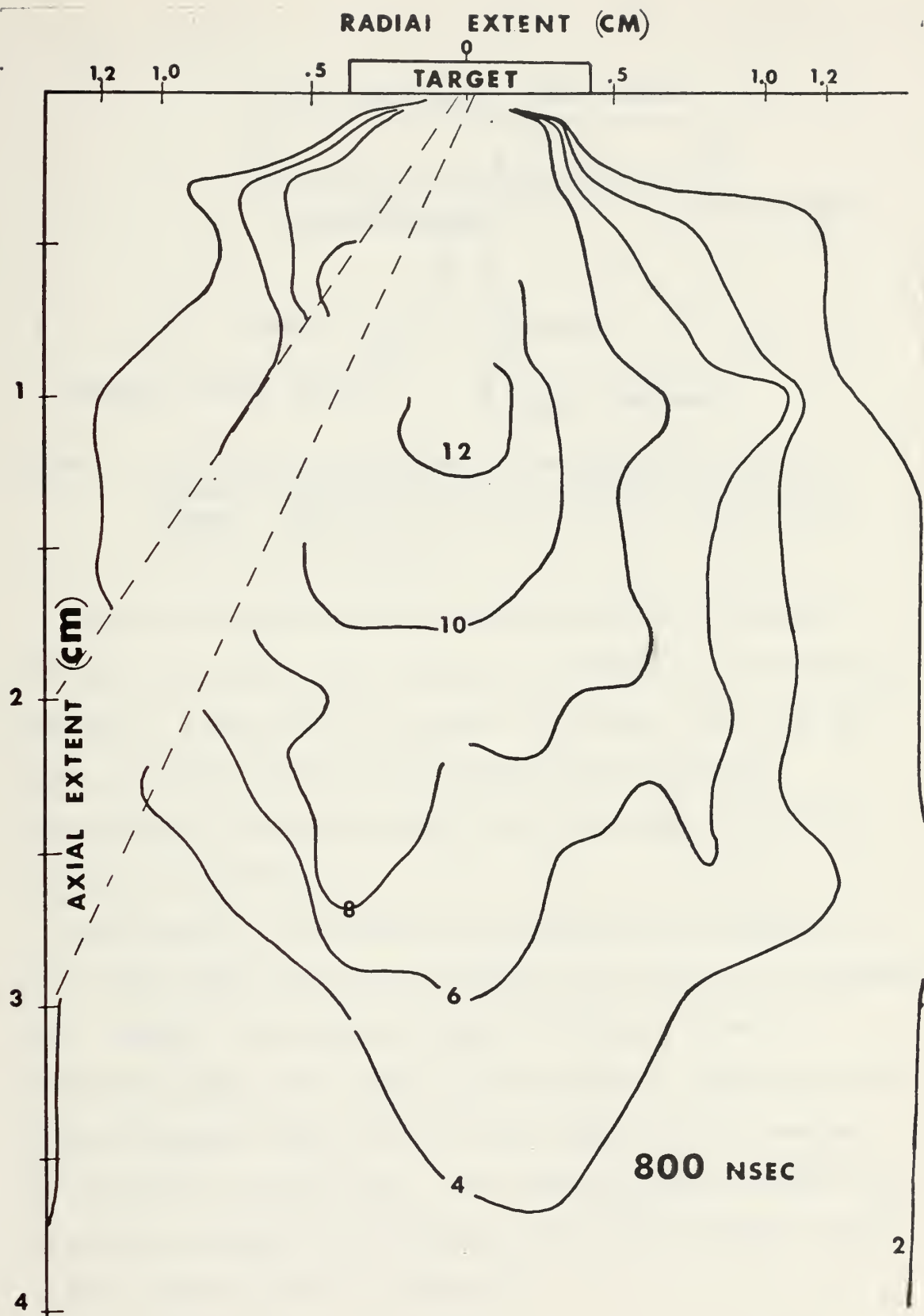
Figure 44. Laser-produced plasma relative density contours at
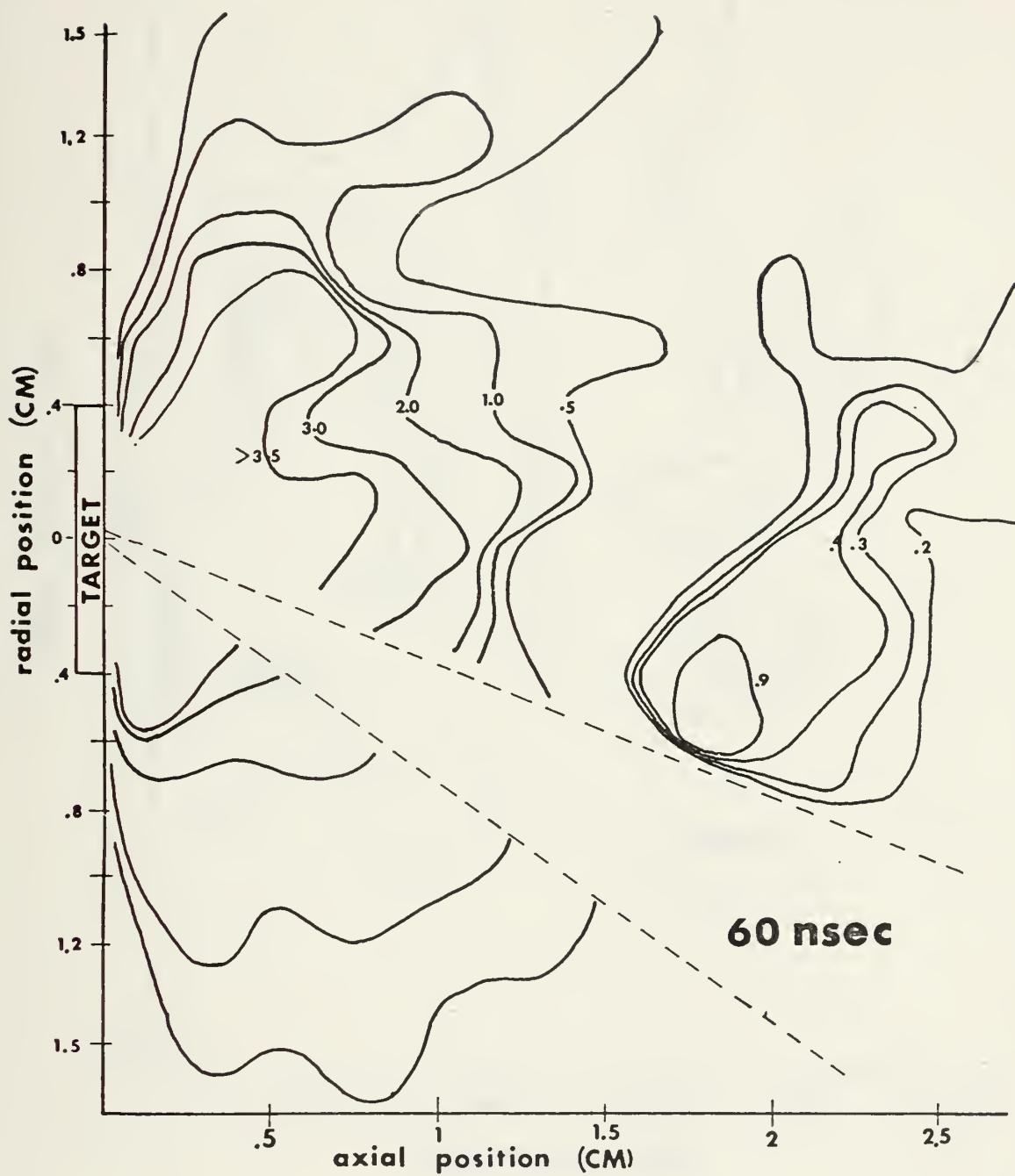t = 800 nsec.

69
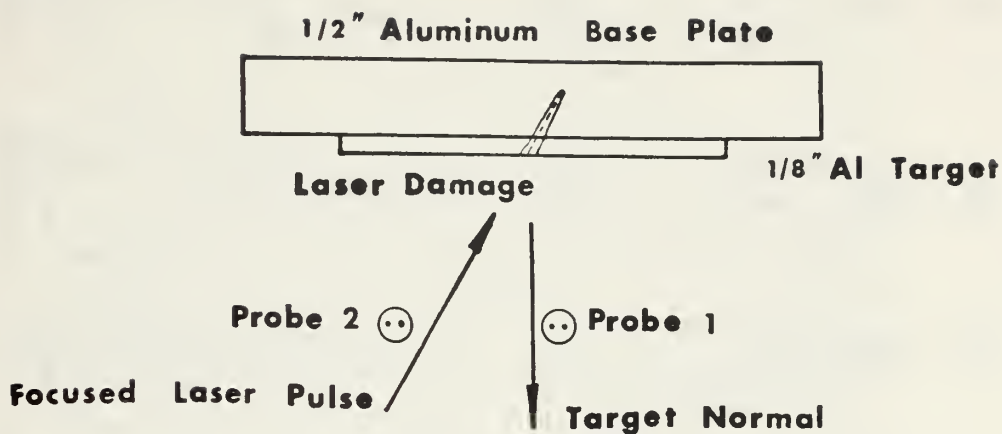
Figure 45. Experimental arrangement for verification of late time plasma expansion symmetry with respect to the target normal. Probe one is at $(0.2, \pi/2, 2.5)$ and probe two at $(2.2, 3\pi/2, 2.5)$.

A total of 50 shots were made without disturbing the target. Pictures of the double probe responses were taken every five shots as displayed on a Tektronix 555 dual beam oscilloscope. The laser had burned a visible hole into the target after the fourth shot. Reproductions of the oscilloscopic traces at ten shot intervals are included as Figure 46.

Some increase in the signal at probe number two was expected due to a shotgun effect as the plasma expands from the base of the deepening hole. However, as the traces in Figure 46 indicate, there is no appreciable change in the plasma density sampled by either probe during the entire sequence except that the early plasma pulse is somewhat attenuated after the fifth shot. This behavior strongly suggests that the expansion dynamics are independent of the plasma behavior prior to its rapid expansion into the background.
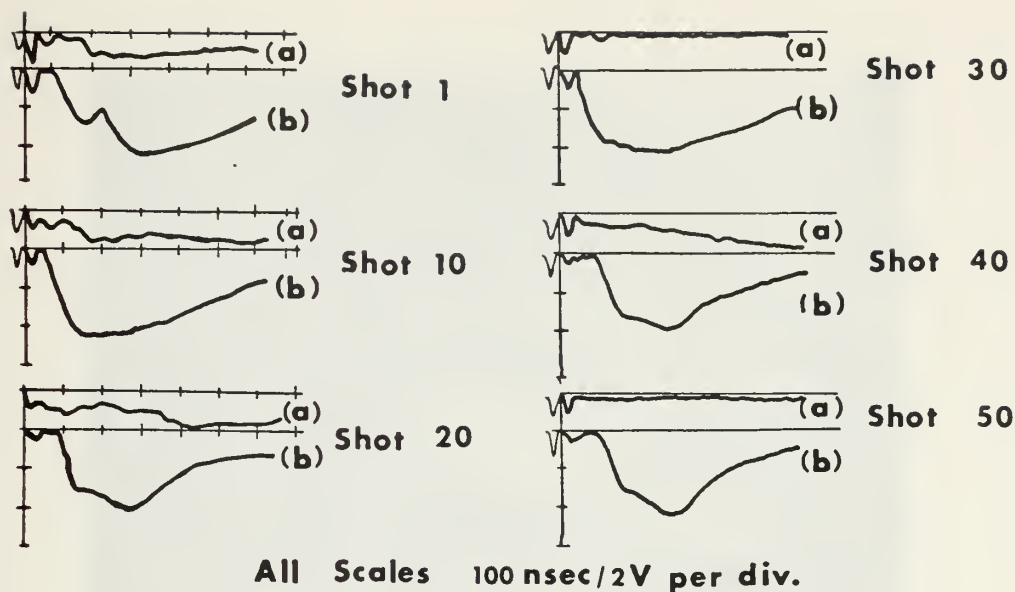
Figure 46. Series of oscilloscopic traces taken on a dual beam
oscilloscope during the burning of a hole 1.029 cm deep
in an aluminum target. (a) probe two and (b) probe one

Following this experiment, a detailed examination of the crater was

undertaken with an electron microscope. Figure 47 is an electron

micrograph of the entry point of the laser pulse, Figure 48 depicts

the exit hole from the 1/8 inch plate, Figure 49 shows a cross section

of the hole in the 1/8 inch plate, Figure 50 is a cross section of the

crater burned into the 1/2 inch back plate, Figure 51 shows a cross

section of the base of the hole excavated into the back plate and

Figure 52 depicts a typical crater wall.

Careful measurement of the volume of the cavity reveals that

approximately 0.014 cm^3 of aluminum were excavated. This represents a

total of 8.44 X 10^{20} aluminum atoms or approximately 1.7 X 10^{19} atoms

per laser pulse. This value is two orders of magnitude larger than

the 10^{17} atoms reported by Honig [Ref. 23]. However, examination of

Figure 47 indicates evidence of splashes of molten material radiating

71
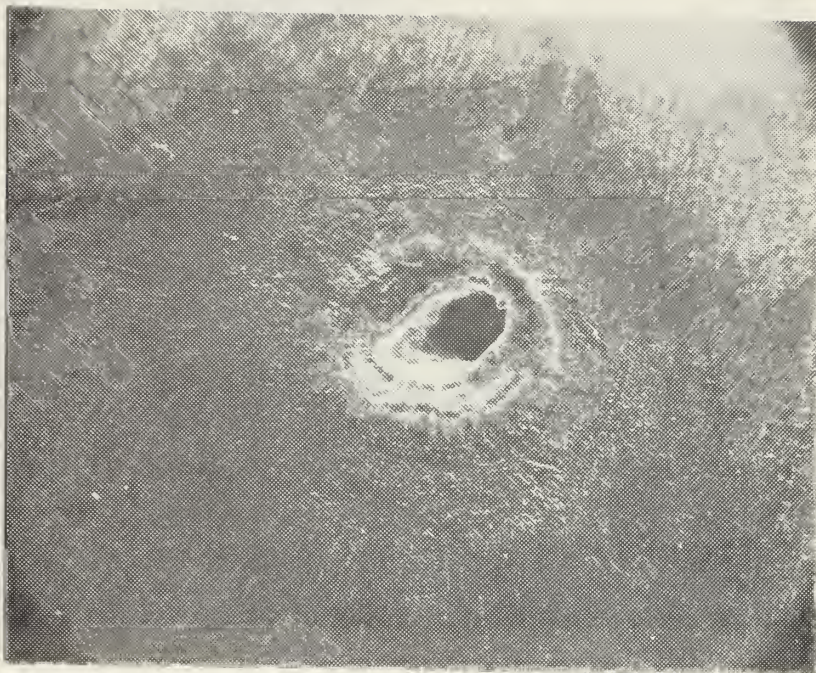
Figure 47. Entry Hole in the 1/8 inch Aluminum Target. Magnification is 18X.
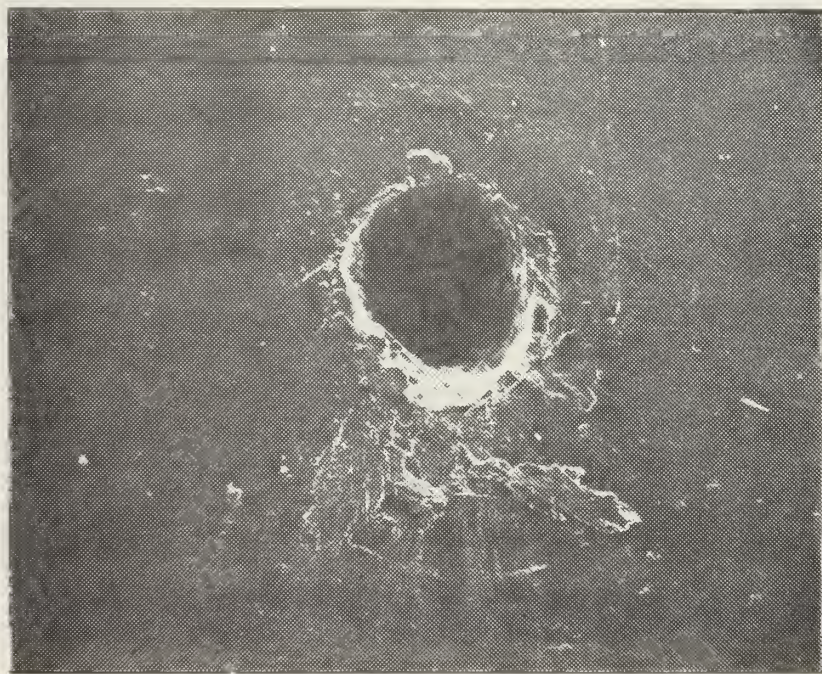
Figure 48. Exit hole as the laser pulse leaves the 1/8 inch target plate. Magnification is 40X.

Figure 49. Cross section of the hole burned through the 1/8 inch aluminum target plate. Magnification is 23X.
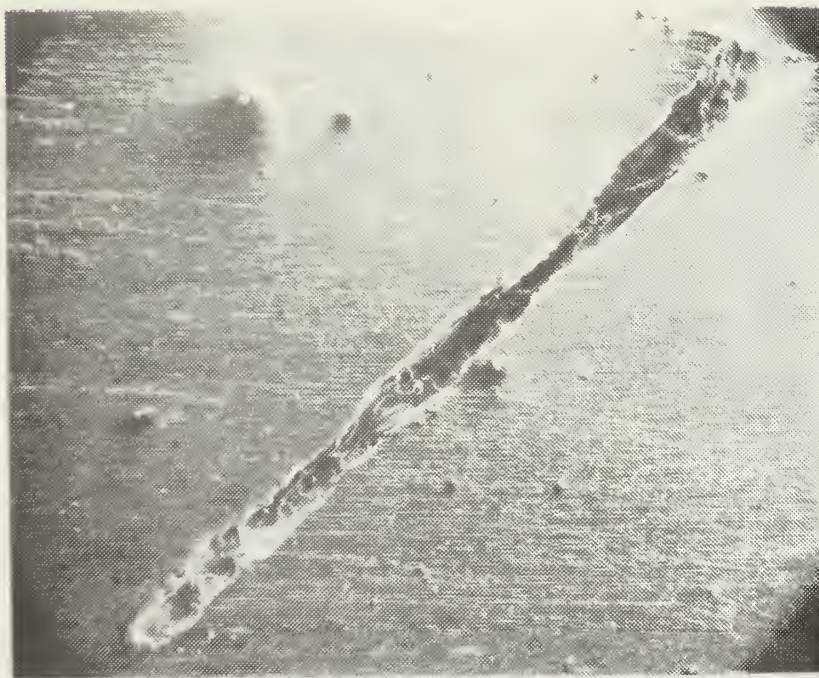
Figure 50. Cross section of the crater burned into the 1/2 inch aluminum back plate. Magnification is 17X.
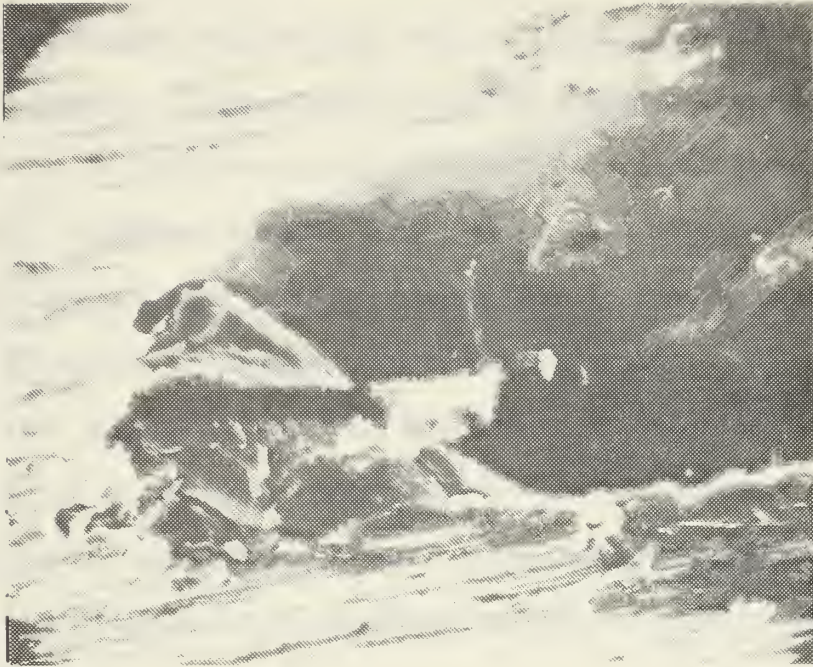
Figure 51. Base of the crater burned into the 1/2 inch aluminum back plate. Magnification is 480X.
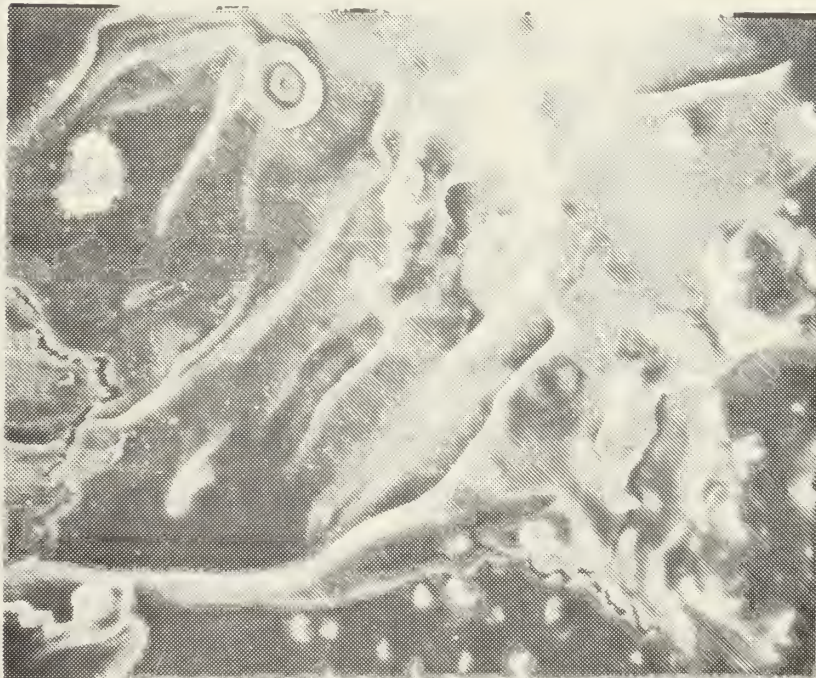
Figure 52. Typical section of the crater wall in the 1/2 inch aluminum back plate. Magnification is 540X.

from the entry point of the laser pulse. Examination of the probes after the experiment reveals that each is heavily coated with a layer of shiny aluminum. These splashes and the aluminum coating have not been observed in previous experiments using the laser in a defocused mode. This evidence indicates that a great deal more material was ejected during the hole burning process than is ejected when the laser pulse is defocused to produce only a shallow crater. Rather than being ionized, this additional material appears to be essentially neutral and may even be in a partially condensed state. This statement is supported by the aluminum coating on probe number two which did not indicate the presence of a significant number of ions at any time during the experiment.

An obvious cause for the increase in ejected material is that the hole tends to contain all of the incident laser energy whereas in the shallow crater produced by the defocused laser, a significant amount of the incident energy may be reflected from the target and expanding plasma. Examination of Figure 51 reveals evidence of dynamic shock processes in the base of the crater. Large pieces of aluminum are apparently being ejected by shock waves. The ragged appearance of the entire surface of the crater suggests that dynamic removal of material may be more important than thermal processes. Inhomogeneities in the aluminum alloy structure may strongly contribute to the appearance. This subject will not receive further consideration in this investigation.

Main plasma density gradients in the radial and axial direction are plotted in Figure 53 for times of 100 nsec, 400 nsec and 800 nsec. The radial density gradient is plotted at z = 1.0 and z = 2.0 cm. The axial density gradients are along the target normal.

75

These main plasma density contours lend further evidence for radial confinement of the plasma. This evidence is seen in the cylindrical shape of the expanding plasma out to 3.0 cm (see Figure 40) and by the initially steep and slowly diffusing radial density gradients seen in Figure 53.

The high density gradients for small z values at long time intervals seen in Figures 43 and 44 must be the result of rapid plasma cooling in contact with the target face since the laser pulse shuts off at $t = 30$ nsec.

To obtain a more detailed picture of the plasma density gradients close to the target under slightly different conditions, data was collected on a one millimeter grid from $z = 0.2$ cm to $z = 1.2$ cm and radially to 1.5 cm. Contour maps were constructed at 100 nsec intervals from 200 nsec to 800 nsec. These maps are included as Figures 55 and 56. The data were obtained with probe number three biased at -15 volts and with the laser energy reduced to 4.0 ± 0.4 J.

The most striking feature of the plasma is that it retains nearly the same density gradients and radial dimension throughout the time scale of this survey. This is most dramatically illustrated in Figure 54 where the one volt contour for 200 nsec is superimposed on the one volt contour for 800 nsec. As can be seen in Figure 54, the radial extent has increased from 0.7 cm to only 1.0 cm during this time interval. This provides further evidence for the presence of a radially confining force. Also note that between 0.5 cm and 1.2 cm the density gradients are almost entirely in the negative radial direction so that any temperature gradient in the negative axial direction would provide the necessary source term for the reversed self-induced magnetic field reported by Bird.

76
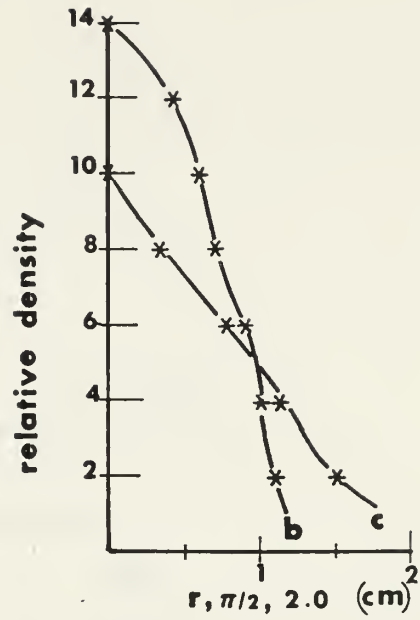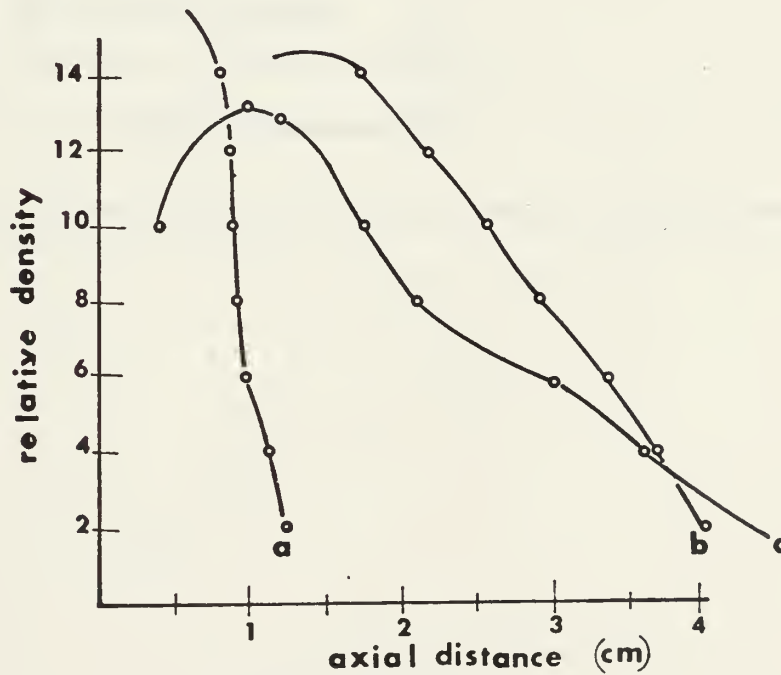
Figure 53. Main plasma density gradients at (a) 100 nsec, (b) 400 nsec and (c) 800 nsec.
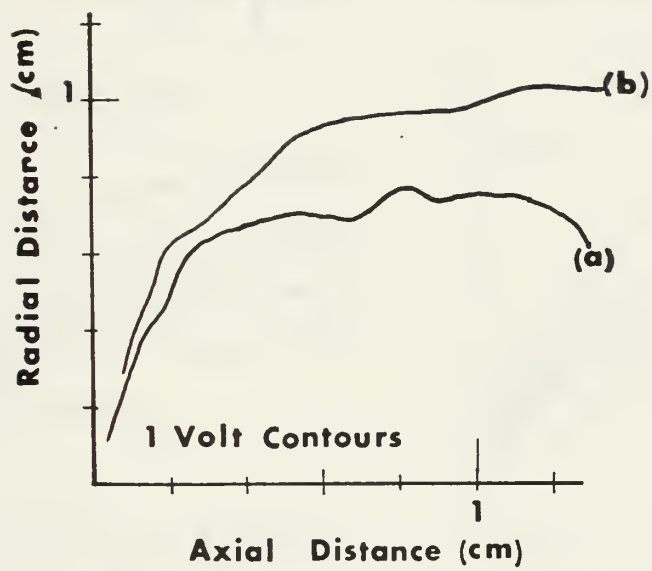
Figure 54. Density contours for (a) 200 nsec and (b) for 800 nsec.
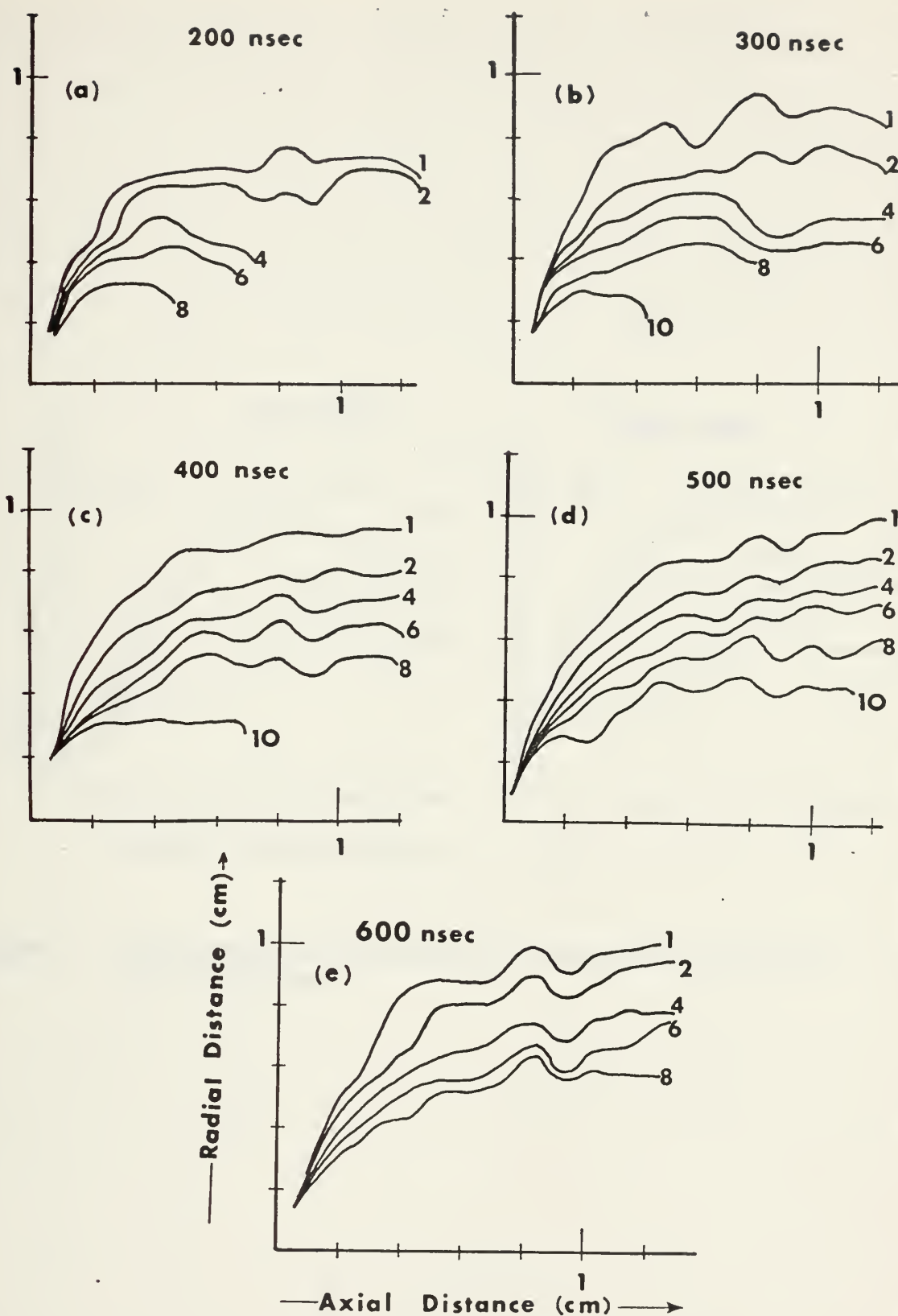
Figure 55. Laser produced plasma density contours at (a) 200 nsec, (b) 300 nsec, (c) 400 nsec, (d) 500 nsec and (e) 600 nsec.
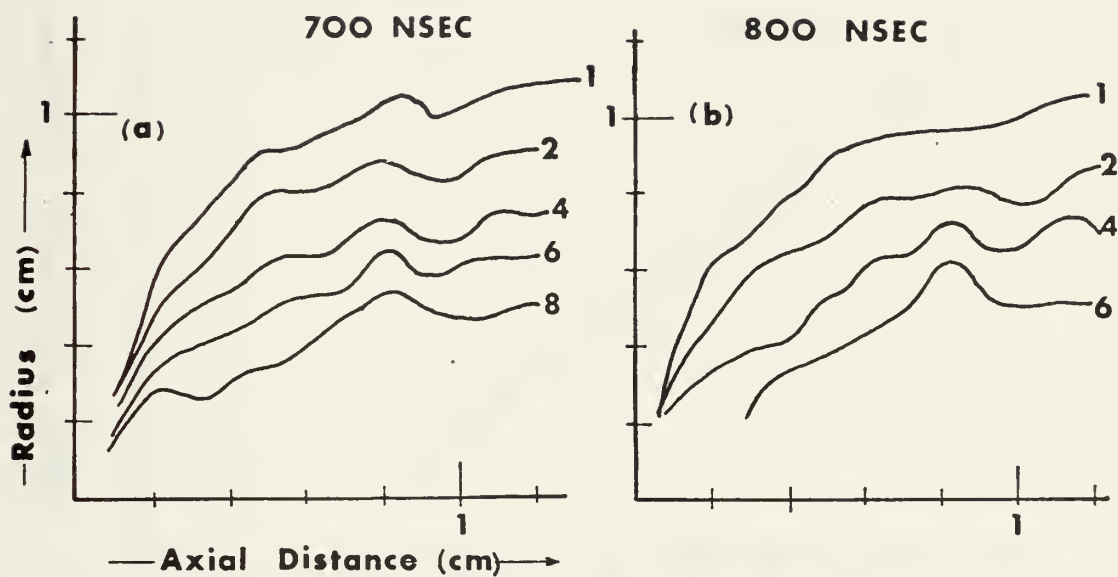
Figure 56. Laser produced plasma density contours at (a) 700 nsec and (b) 800 nsec.

G. DEPENDENCE OF THE EARLY PLASMA ON LASER PULSE ENERGY

The maximum density in the early signal has been found to vary
linearly with the laser pulse energy. A series of oscilloscopic traces
of the double probe response at (0, 0, 1.9) were recorded with the
laser pulse energy varying from 2.9 joules to 9.2 joules. The peak
early probe response versus laser energy is plotted in Figure 57.
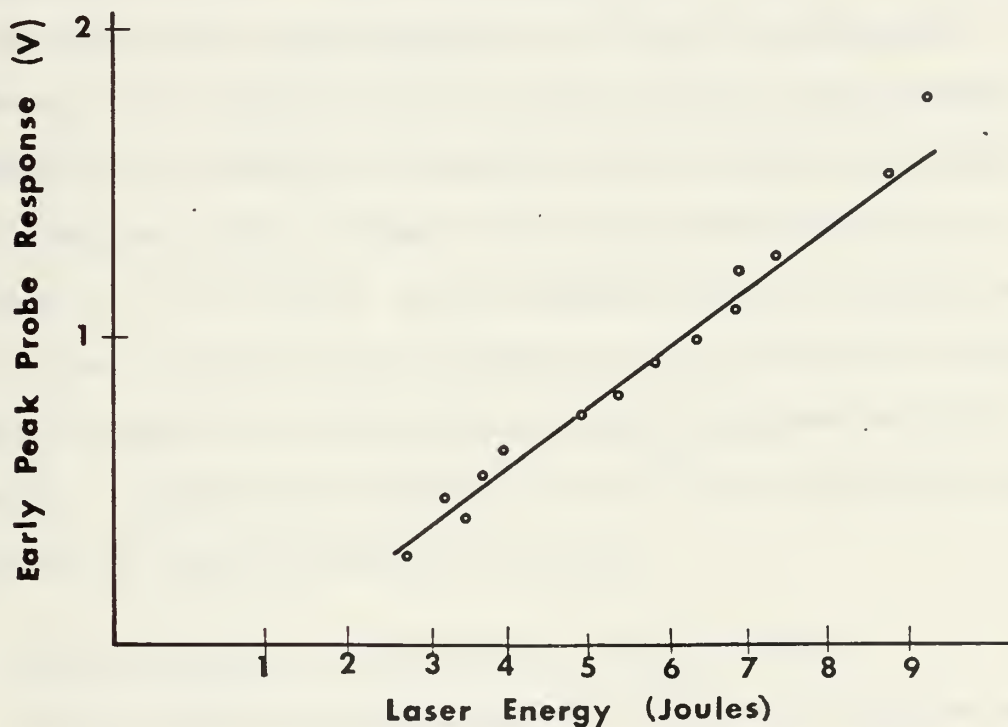
Figure 57. Peak Double Probe Response to the Early Plasma Versus Laser
Pulse Energy

It appears that the early response has a linear dependence on the
laser energy. For this particular probe (probe number three) and
within the energy range plotted, the dependence can be expressed in the
relation:

$$(13) \quad V_{PP} = (1.1E_L - 0.375) \quad \text{volts}$$

Where V_{PP} is the peak probe response to the early plasma pulse and E_L

is the laser pulse energy in joules. It should again be noted that these

81

data and equation (13) are valid only for this experiment. The amplitude of the early pulse is highly dependent on background gas pressure as shown by Arifov [Ref. 5]. These data were collected in near vacuum at 10^{-5} torr. This pressure is at the threshold of the pressure dependent region described by Arifov. There are peak ion densities of 2.5×10^{12} cm $^{-3}$ in the early plasma pulse at this pressure. As the early plasma pulse propagates, it ionizes the background. However, if the background density is less than the ejected plasma density then the additional ionization will be comparatively small. The background density is equal to the early plasma density at a pressure of 7×10^{-5} torr. As the background pressure increases above this value, ionization by the streaming plasma increases the total ion density detected by the probe and the pressure dependent region is reached. The significant boundary at 7×10^{-5} torr is consistent with Arifov's and Isenor's work [Refs. 5 and 25].

H. TIMING SEQUENCE FOR DISTURBANCES LEAVING THE TARGET

An attempt has been made to determine the times at which the various disturbances left the target. This was accomplished by assuming that the speed of the disturbance is constant between the target and the data point. By noting the time at which the disturbance reaches a specific data point and subtracting the transit time using the measured speed of the disturbance an estimate of the time at which the disturbance left the target is obtained. This method appears to give reasonable results for the early disturbance and the photoelectric response due to the constancy of their propagation speeds. Repeated measurements with available data were averaged. The average computed departure time is t = 16 $\pm$ 2 nsec for the photoelectric disturbance and t = 18 $\pm$ 6 nsec

82

for the early plasma disturbance. The average of the times at which
the main plasma left the target is t = 2 $\pm$ 15 nsec assuming a constant
speed of 1.1 X 10^7 cm/sec. This last value does not seem consistent
with any dynamic model for the plasma generation. It is assumed that
the error is introduced because the main plasma speeds are much higher
close to the target. It is not possible to measure the position of
the main plasma front at distances less than 0.6 cm because the early
disturbance is still separating from the main plasma body. This is
illustrated in Figure 58. This problem plus the higher oscilloscope
time scale (100 nsec per division) used to measure the main plasma
account for the high standard deviation in this computation.
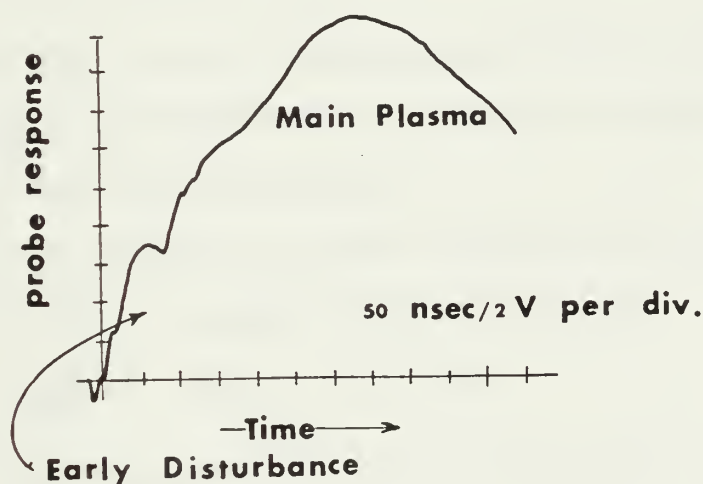
Figure 58. Double probe response at (0, 0, 0.6) showing incomplete
separation of the early disturbance from the main plasma
body.

I. CORRELATION OF THE QUARTZ PRESSURE PROBE AND DOUBLE PROBE RESPONSES

In this experiment a double probe and a quartz pressure probe were
placed side by side at an axial distance of 1.4 cm from the target.
Probe responses were recorded from each diagnostic probe on successive
shots using the same delay cable.

In this investigation, the momentum transport of the plasma provides the strain on the quartz pressure probe. Assuming that plasma particle collisions with the pressure probe are elastic and that the mass of the plasma is much less (6 orders of magnitude at least) than that of the probe and its holder, the force density producing the strain in the gauge is:

$$(13) \quad F = \frac{dP}{dt} = \frac{d}{dt}(m_i v_i n_i + m_e v_e n_e + m_n v_n n_n)$$

Since the electron mass is negligible compared with the atomic mass we have $m_i = m_n \gg m_e$ and equation (13) can be approximated by:

$$(14) \quad F = \frac{d}{dt}(m_n V_{LP}(n_i + n_n))$$

It should be noted that this equation assumes that the plasma flow velocity, V_{LP}, is much larger than the plasma ion thermal speed. This assumption is justified in Appendix A.

Applying the assumption of elastic collisions and doing a simple dimensional anaylsis on equation (14) indicates that:

$$(15) \quad F = \frac{\Delta P}{\Delta t} = 2m V_{LP}(n_i + n_n)/T_{LP}$$

Where T_{LP} is the time for the plasma to travel one cm. Since $T_{LP} = (V_{LP})^{-1}$ equation (15) can be rewritten as:

$$(16) \quad F = 2m(V_{LP})^2(n_i + n_n) \quad \text{newtons/cm}^3$$

This analysis describes the plasma as a square pulse which it is not. However, for the purposes of this discussion the approximation of a square plasma pulse will do. For the main plasma pulse with $m = 27$ AMU, $V_{LP} = 1.1 \times 10^7$ cm/sec and $(n_i + n_n) = 2 \times 10^{15}$ cm^{-3}, the strain producing force density is 0.08 newtons/cm^3.

A similar analysis of the early plasma pulse with $V_{LP} = 1.1 \times 10^8$ cm/sec and $(n_i + n_n) = 2.5 \times 10^{12}$ cm^{-3} yields a strain producing force density of 0.01 newtons/cm^3.

The ratio of these two stress producing force densities is 0.125. This is also the ratio of voltage outputs from the crystal in the presence of each pulse since the probe response is proportional to the stress.

These impulsive forces produce stress waves in the aluminum gauge. These waves propagate with the speed of sound. For aluminum, $U_s = 6,420$ m/sec [Ref. 4]. Therefore it takes 390 nsec for the stress wave to propagate through the 0.25 cm aluminum cover disc and epoxy to the quartz gauge.

Figure 59 depicts the signals produced from the same position by (a) the double probe and (b) the pressure probe. As can be seen, the main plasma front corresponds very well with the large, late response from the pressure probe. However, the early response from the pressure probe occurs approximately 200 nsec before a stress wave generated by the early plasma would arrive at the crystal. No conclusive explanation is offered for this temporal discrepancy in the arrival of the early pressure probe response. Perhaps the speed and sharpness of the early plasma cause the wave to travel through the aluminum at a speed in excess of the speed of sound. The electrodes are well shielded with epoxy and the outer case is isolated from the circuit so that electrostatic pickup is unlikely. However, the early signal does correlate with the time an expected electrostatic pickup would be measured. It is also possible that the obvious early signal is not that associated

85

with the early momentum transfer. The expected amplitude of the early
signal is approximately 4 mV. A signal of this magnitude could easily
be lost in the noise.

The fact that there are two distinct disturbances registered by the
pressure probe indicates the presence of two momentum transporting pulses.
However, the poor temporal correlation of the early signal makes the
results of this experiment somewhat inconclusive.

It should be noted that researchers at the Stanford Research
Institute have fired high power, 30 nsec, laser pulses at the gauge's
aluminum target face. The quartz gauge then measures the momentum
transported to the target by the fast blow off of laser produced plasma.
These investigations have revealed two momentum impulses delivered to
the target as depicted in Figure 60.
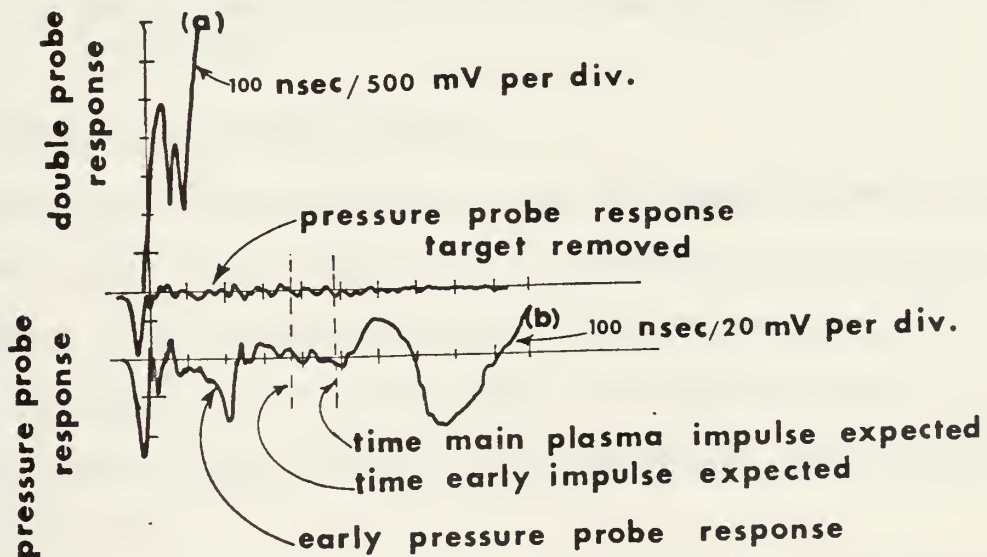
Figure 59.   Correlation of signals received by (a) the double probe
             and (b) the pressure probe at (0, 0, 1.4) in the presence
             of a laser plasma.

86
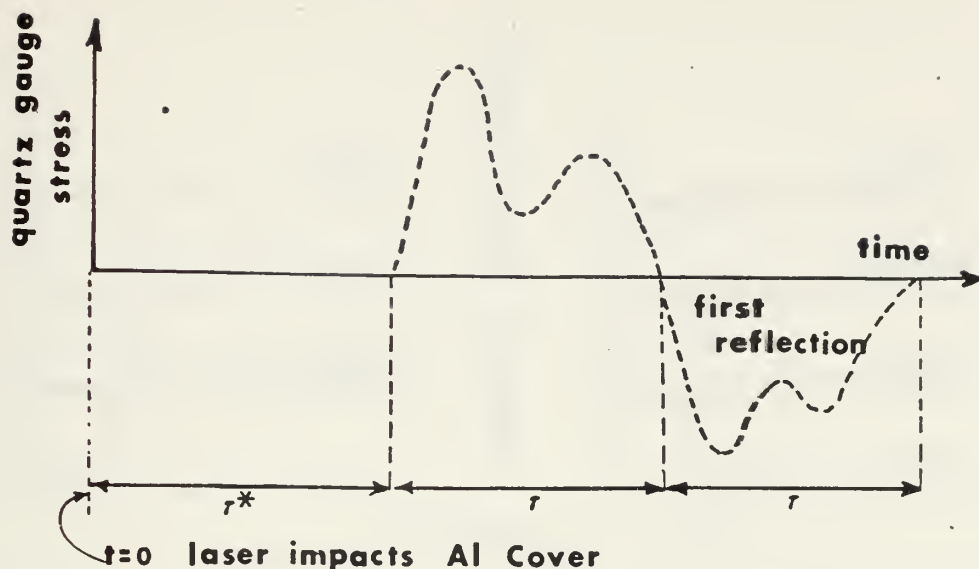
Figure 60. Stress time history in a laser irradiated sample in vacuum. r^* is the propagation time of the stress pulse through the aluminum cover. r is the propagation time of the stress pulse through the quartz guage.

J. AZIMUTHAL MAGNETIC FIELD SYMMETRY

To verify the azimuthal symmetry of the self-induced magnetic field a series of pictures were taken at $\theta = 5^\circ$ intervals at $(1.0, \theta, 1.5)$. The magnetic probe was inserted through a holder in port five of the chamber (See Figure 4). The probe holder is circular and nests in a circular flange allowing rotation of the probe without disturbing the r or z coordinates.

Figure 61 reproduces the probe response at 15 degree intervals from $\theta = \pi$ to $\theta = \pi/2$. The gross aspects of the magnetic probe response are symmetric.
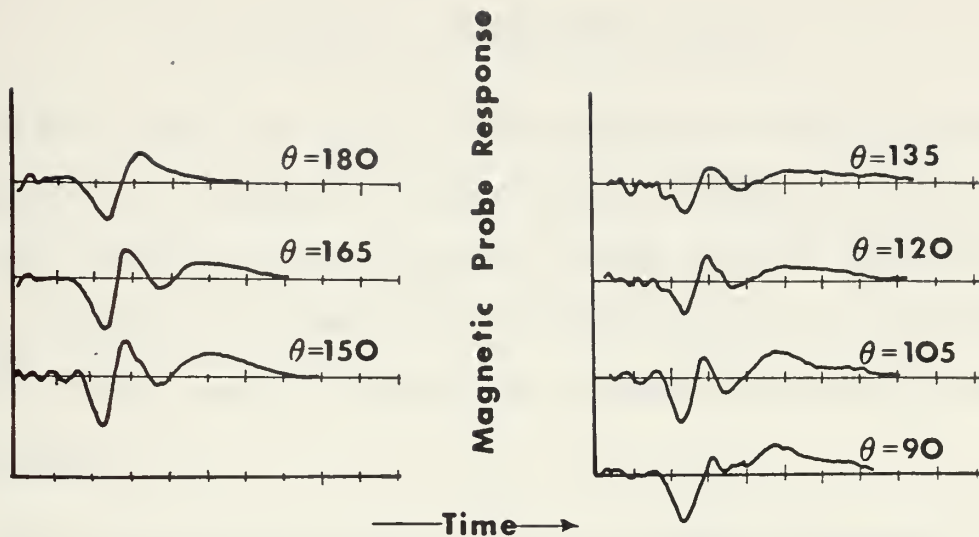
Figure 61. Magnetic Field Symmetry for (1.0, θ, 1.5). Scales are 100 nsec and 100 mV per division.

Unfortunately this experiment was conducted prior to discovery of the plasma expansion asymmetries. Therefore the oscilloscope scales were 100 nsec and 100 mV per cm. These scales and the z coordinate of 1.5 cm do not allow resolution of the early magnetic field asymmetries expected with the plasma density anisotropy. Therefore, this experiment should be repeated with r = 0.5 cm, θ = zero to π and z = 0.5 cm. The oscilloscope scales should be set at 100 mV and 20 nsec per division.

IV. ANALYSIS OF EXPERIMENTAL RESULTS

In this section two facets of the experimental results are examined. In section (A), a comparison is made between the particle content in the early plasma pulse and the number of atoms initially exposed to the laser radiation (to a depth equal to the skin depth). In section (B) the $\vec{J} \times \vec{B}$ force density is analyzed as a possible source for the radial confinement.

A. ORIGIN OF THE EARLY PLASMA PULSE AND ITS PRESSURE DEPENDENCE

Assuming a macroscopically neutral plasma and plasma symmetry about the axis of propagation, the total number of ions involved in the early plasma pulse is approximately 2×10^{13} Al ions. The skin depth for aluminum is 61 angstroms. The laser focal spot size is 0.15 cm. The total volume initially exposed to the laser radiation is 1.08×10^{-8} cm^3. This corresponds to a total of 6.5×10^{14} aluminum atoms. This agrees to within one order of magnitude with the number of observed ions. If the early plasma pulse also has neutrals by the time it reaches the probe grid then this agreement will be even better. Therefore, at least in terms of total numbers, the early blowoff of plasma could be due to those atoms which are directly stimulated by the initial laser radiation. The pressure dependence of the early plasma has been previously described by Arifov [Ref. 5]. Assuming that the early blow off of material is independent of background gas density implies that there are initially 2.4×10^{12} ions/cm^3 in the fast stream. Background pressures reach this density at 7×10^{-5} torr. This pressure is consistent with onset of the pressure dependent region. The fast streaming early plasma

further ionizes this background. However, when the background pressure is low, the additional ions do not add appreciably to the total. As background densities increase above the threshold there are significantly more ions created by the fast streaming plasma. As the background pressure is increased above 250 mtorr the fast streaming early plasma must be stopped in a short distance causing a reduction in early signal strength.

B. ANALYSIS OF THE $\vec{J} \times \vec{B}$ FORCE DENSITY

McKee [Ref. 38] using typical values for plasma expansion into a 250 mtorr background found that the $\vec{J} \times \vec{B}$ force density was much less than the radial pressure gradient force density. McKee also plotted this force density at 120 nsec for 250 mtorr of nitrogen background gas. He found that the magnitude of the largest force at this time is 1.4×10^4 newtons/m^3. A reproduction of his computer produced plot is included as Figure 62.

Bird [Ref. 8] has found magnetic fields of the order of 200 gauss at $(0.4, \pi/2, 0.75)$ for aluminum plasmas. This measurement was made at 200 nsec after arrival of the laser pulse. The pressure was 0.1 microns which is close to the pressure independent region for both the magnetic field magnitude and magnitude of the early disturbance as reported by Arifov [Ref. 5]. The current corresponding to this 200 gauss field is of the order of 400 amps/cm^2. Using maximum current and magnetic field densities indicates the presence of a $\vec{J} \times \vec{B}$ force density of approximately 7×10^4 nt/m^3. This is consistent with McKee's maximum values.

At 500 nsec, the extent of the plasma (2 volt contour) is approximately r = 1.5 cm by z = 4.5 cm. Assuming symmetry with respect
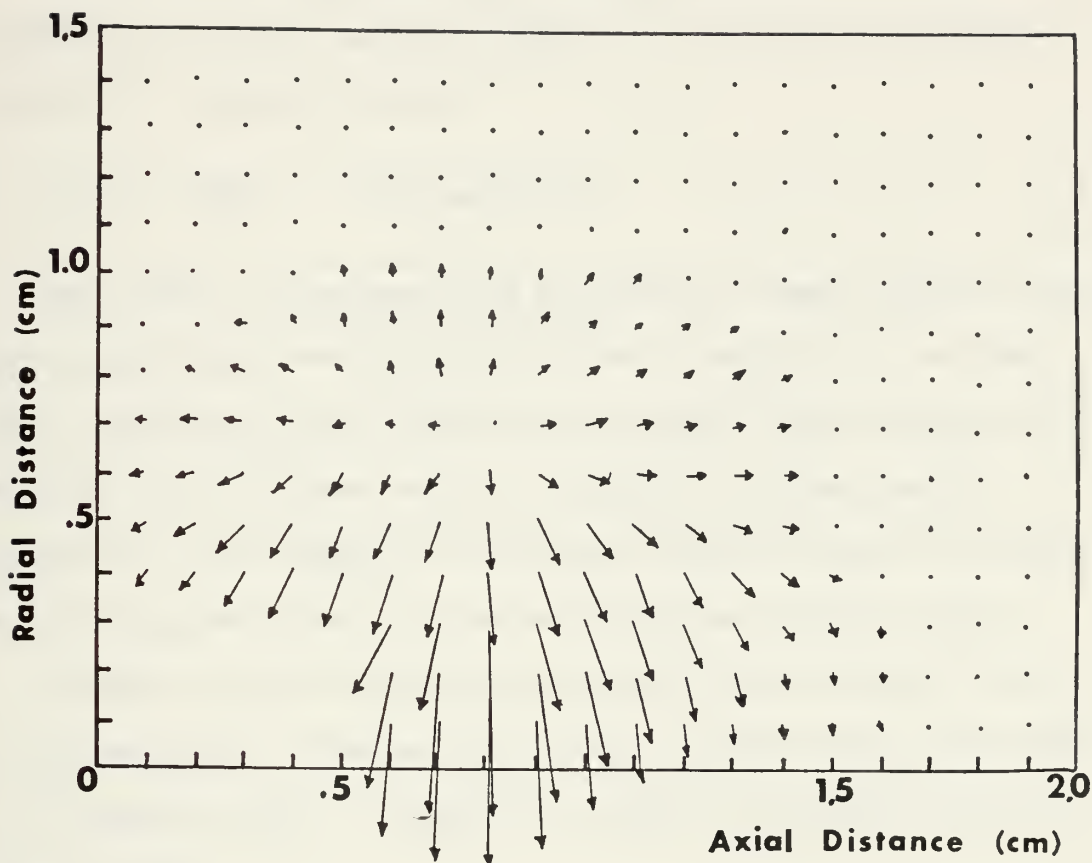
Figure 62. $\vec{J} \times \vec{B}$ force density at 120 nsec for 250 mtorr of nitrogen background gas. The magnitude of the largest force at this time is 1.4×10^4 nt/m^3.

to the target normal this corresponds to a total volume of 32 cm^3. If 10^{17} atoms are ejected and ten percent are ionized, then the ion density would be on the order of 3×10^{14} ions/cm^3.

In section III. F. ion densities for the streaming main plasma of 1.4×10^{13} V_p (V_p is the probe response voltage) were found. Typical probe response voltages are on the order of ten volts for the main plasma. This corresponds to a total ion density of 1.4×10^{14} ions per cm^3. These two results are in good agreement. The total plasma density including neutrals is then taken to be 10^{15} cm^{-3}.

91

Assuming a plasma temperature of three electron volts, and a characteristic density gradient length of $\ell = 0.8$ cm, the pressure gradient force density becomes:

(17) $nkT/\ell = 10^5$ newtons/m^3

Using either the maximum $\vec{J} \times \vec{B}$ force density found by McKee or that found on page 90 we see that the $\vec{J} \times \vec{B}$ force density is of the same order of magnitude as the pressure force density found in equation (17). Therefore the $\vec{J} \times \vec{B}$ force density is capable of at least partial confinement of the plasma and in any case should be taken into account in describing the dynamics of the expanding laser produced plasma.

In order for this confinement to continue for the observed times, the characteristic diffusion times must be at least of the same order as the observed effect. Otherwise the plasma will diffuse through the magnetic field.

The magnetic field diffusion time is given by:

(18) $\tau_m = \mu_o \sigma \ell$

The characteristic length (ℓ) of the magnetic field at 200 nsec is estimated from McKee's data to be 0.8 cm. The D.C. conductivity of the plasma is given by:

(19) $\sigma = n_e e^2 / m_e \nu_e$

where ν_e is the electron collision frequency. For electron-ion and electron-neutron collisions the collision frequencies are given by Tanenbaum [Ref. 46].

(20) $\nu_{ei} = 3.62 \times 10^{-6} n_i T_e^{-3/2} \ln \Lambda \quad sec^{-1}$

(21) $\nu_{en} = 2.60 \times 10^4 n_n T_e^{1/2} \sigma^2 \quad sec^{-1}$

Where T is in °K, n in particles/m^3, $\ln \Lambda$ is typically about ten, σ is of the order 10^{-10}m. Assuming $T_e = 4$ eV, $n_i = 10^{20}$ m^{-3} and $n_n = 10^{21}$ m^{-3} the collision frequencies are found to be $\nu_{ei} = 3.62 \times 10^8$ sec^{-1} and $\nu_{en} = 5.6 \times 10^7$ sec^{-1}. Substituting these values into equation (19) reveals a D.C. conductivity of 7.8×10^3 mho/m. Using this value in equation (18) we find that the magnetic field diffusion time is of the order:

(22) $\tau_m = 626$ nsec

This value appears consistent with McKee's work and explains how the plasma could be radially confined within the time scale surveyed in this investigation ($t < 800$ nsec). While not plotted, an examination of the data indicates that the plasma becomes very diffuse after 900 nsec. This is due in part to diffusion but is more probably due to general cooling and recombination.

V. SUMMARY AND CONCLUSIONS

The early disturbances have been separated into "reverse" photo-
electric response due to photoemission of electrons from the probe and
a series of at least two additional disturbances traveling with constant
speeds of 1.1×10^8 cm/sec and 5.9×10^7 cm/sec. The first of these
disturbances has been analyzed in detail.

The early disturbance is found to propagate along a line describing
the path of the reflected laser pulse. The disturbance is symmetric
about this propagation axis.

After separating the photoelectric response, consideration must be
given to the possibility that the remaining disturbance is created by an
ionizing potential wave or a blast wave. References 2, 9, 22 and 47
provide some insight into the ionizing potential wave phenomenon. In
this experiment, the background gas density is approximately 9×10^{11} cm^{-3}.
Assuming that the temperature of the background is three electron volts
after ionization by the potential wave we can use equation (25) from
Appendix A to obtain an estimate of the quiescent plasma ion density
necessary to generate the observed probe current of 0.66 amperes at
(0, 0, 1.0).

$$(26) \quad n_i = 1.67 \ I_+ (m_i/kT_e)^{1/2}/eA_p \quad (\text{cm}^{-3})$$

The average molecular weight of air is $m = 28.96$ AMU $= m_i$. The surface
area of the electrodes is 0.0146 cm^2. Inserting these values into
equation (25) indicates that the required ion density is 1.5×10^{15} ion
charges/cm^3. This ion density is three orders of magnitude greater than
the background gas density. This argument appears sufficient to exclude

ionization of the background gas by any means as a possible source for the early disturbance.

The higher densities observed can only be supplied from the target in the form of a fast blowoff of material. This possibility has been considered by many researchers [Refs. 10, 15, and 24]. However, a review of the literature indicates that this early blowoff is generally thought to be composed entirely of electrons. The results of the present research in which transverse electric and magnetic fields were introduced indicate that the early disturbance is composed of ions and electrons. Ion densities of 2.4 X 10^{12} cm^{-3} have been measured in this fast streaming plasma. Electron densities may be slightly higher than this creating a macroscopically negative plasma potential. This would explain the previous observations.

The pressure dependence of the early plasma has been previously described by Arifov [Ref. 5]. Assuming that the early blowoff of material is independent of background gas density implies that there are initially 2.4 X 10^{12} ions/cm^3 in the fast stream. Background pressures reach this density at 7 X 10^{-5} torr. This pressure is consistent with onset of the pressure dependent region. The fast streaming early plasma further ionizes the background. However, when the background pressure is low, the additional ions do not add appreciably to the total. As background densities increase above the threshold there are significantly more ions created by the fast streaming plasma. As the background pressure is increased above 250 mtorr, the fast streaming early plasma must be stopped in a short distance causing a reduction in early signal strength. In this investigation the early plasma density is strongly attenuated between 0.8 and 2.0 centimeters. However, a small signal is still

observable out to the limits of this survey (5 cm). Residual
ionization decreases rapidly so that by 100 nsec there is little
remaining evidence of the passage of this early pulse.

The main plasma speed has been measured at 1.1 X 10^7 cm/sec. Early
time anisotropies and asymmetries are observed in the expansion of the
main plasma. This results in an initial high density area on the side
of the target away from the incident laser pulse. This asymmetry is
short lived and for times greater than 120 nsec, the plasma can be
described as symmetric about the target normal. This late time
symmetry in the free expansion is evident even when the plasma is created
in a deep hole and gains momentum in a direction off the target normal
before reaching the surface of the hole. In this investigation a one
centimeter deep hole was excavated into an aluminum alloy target.
Throughout the excavation there was little observed change in the plasma
expansion. This suggests that the expansion dynamics are independent
of the manner in which the plasma reaches the surface of the target.

Previous investigators [Ref. 23] have observed approximately 10^{17}
particles ejected per incident laser pulse under similar conditions.
In this hole drilling exercise approximately 10^{19} atoms were ejected per
incident laser pulse. Most of this material was neutral and completely
coated the exposed probes. The reason for identifying the additional
material as neutral is that little change was observed in the ion
densities at probe one and probe two though heavily coated with aluminum,
never did register a significant ion density.

Examination of the cross sectioned crater indicates that a
significant amount of the target damage is generated by dynamic shock

waves rather than by thermal processes. This is especially true of the base of the crater where whole chunks of material are being ejected, possibly by dynamic shock processes.

The main laser plasma is observed to expand very rapidly in the radial direction to a diameter of approximately 2.4 cm. This maximum radial extent is achieved at an axial distance of 0.3 cm. At this point the plasma plume ceases to grow in the radial direction and expands symmetrically along the target normal with a cylindrical shape. Peak plasma densities in the main plasma pulse are approximately 2.5 X 10^{14} cm^{-3}. Radial density gradients remain high for at least one microsecond while the axial density gradient decreases steadily with increasing time. This behavior is strongly suggestive of the presence of a radial confining force acting on the expanding plasma. The self-induced magnetic fields generate a $\vec{J}$ X $\vec{B}$ force density which is seen to be comparable (within an order of magnitude) with the radial pressure gradient force density. This confining force is postulated as an important element in creating the observed cylindrical shape of the laser produced plasma. This $\vec{J}$ X $\vec{B}$ force must be included in any dynamic model of the expanding plasma.

Table (3) summarizes the properties of the various plasma features.

PLASMA FEATURE	SPEED (cm/sec)	ION CHARGE DENSITY (cm^{-3})	TOTAL NUMBERS	TOTAL ENERGY (joules)
Photons	3.0 X 10^{10}	–	–	8 X 10^{-5}
First Early Plasma	1.1 X 10^{8}	2.4 X 10^{12}	2 X 10^{13}	0.55
Second Early Plasma	5.9 X 10^{7}	3.0 X 10^{12}	1 X 10^{13}	0.079
Main Plasma	1.1 X 10^{7}	2.5 X 10^{14}	1 X 10^{16}	1.1
Target Thermal Energy	–	–	–	1.5

The total energy radiated by photons with wavelengths between
0.12μ and 0.267μ has been previously computed. The energy content in
each of the two early plasmas assumes that each of the plasma particles
has a directed speed equal to the speed of the plasma front. The
ionization energy and assumed early plasma temperature of ten electron
volts contribute a negligible amount of energy.

The energy of the main plasma is much more difficult to compute.
Using the methods outlined by Dawson [Ref. 14] the temperature in the
main plasma body is estimated to be $T_o = M_i V^2_{LP}/5(Z + 1)$. Early in the
expansion, the average ionic charge is assumed to be Z = 3. This gives
a plasma temperature of 170 eV and a total plasma energy of 1.1 joules.

Examination of Figures 37 to 44 indicates that only a small portion
of the particles in the main plasma have the directed velocity seen in
the plasma front. The bulk of the main plasma does not move from the
immediate vicinity of the target. The sum of those energies accounted
for in Table (3) is 3.2 joules or about 65 percent of the energy in the
incident laser beam. The energy absorbed in the target by conduction
and shock wave absorption has been estimated at 20 to 30 percent of the
incident laser pulse energy by Peter Krehl at the Stanford Research
Institute (personal communication).

This account of the incident energy neglects energy contained in the
neutral particles which constitute 90 percent of the ejected material,
reflected laser pulse energy and plasma radiation at frequencies other
than those between 0.12 and 0.267 microns. These mechanisms must
account for the additional 35 percent of the incident energy.

VI. AREAS WARRANTING FURTHER RESEARCH

Because of the early time asymmetry of the expanding laser plasma, a three-dimensional map of both the early and main pulses is necessary to fully understand their extent. In conjunction with this, the data obtained in this investigation should be used to provide a computer generated map of the plasma density.

Development of plasma temperature diagnostic techniques at NPS would allow production of similar maps for the plasma's isotherms. With this information, the school's computer should be used to plot the cross product of density and temperature gradients. This would predict the magnitude and direction of the magnetic field due to the $\dfrac{\vec{\nabla}kT_e}{e} \times \dfrac{\vec{\nabla}n_e}{n_e}$ source term described by McKee and Bird. These results could then be compared with McKee's measurements [Ref. 38] in the pressure independent region described by Bird [Ref. 8].

This investigation has revealed asymmetries in the early expansion of the laser produced plasma from a plane target. The dependence of these asymmetries on the angle of incidence of the laser pulse requires investigation. In conjunction with this, an accurate measure of the reflected laser pulse energy at 1.06 microns should be correlated with the angle of incidence.

The pressure dependence of these early time asymmetries could help explain the pressure dependence of the early plasma density and magnitude of the self-induced magnetic field strength [Refs. 5 and 8].

Measurement of currents in the target generated by the inhomogeneous blowoff of ions and electrons and by the self-induced magnetic fields could help resolve the induced magnetic field and plasma density characteristics at distances too close to the solid target material to be measured with external probes.

APPENDIX A

I. DOUBLE PROBE THEORY

When a potential difference is applied between two electrodes immersed in an ionized but macroscopically neutral plasma, the positive ions are attracted to the negative electrode and the plasma's electrons are attracted to the positive electrode. This action tends to destroy the plasma's neutrality by creating space charge electric fields. The plasma responds to this perturbation by creating a sheath which restricts the charge separation to a short distance from the intruding electrodes. This sheath absorbs the potential difference in a very short distance which is of the order of a few Debye lengths. The Debye length is equal to:

$$(23) \quad \lambda_D = 69 \times (T/n_e)^{1/2} \text{ (meters)}$$

Assuming a temperature of 100 eV and an electron density of 10^{14} cm^{-3}, the Debye length is 7.4×10^{-4} cm. The bulk of the plasma remains charge neutral.

When the surface area of the two electrodes is equal and the entire system (electrodes, biasing power supply, scopes, etc.) is isolated from ground it is said to "float" with the plasma potential.

If the biasing potential is initially zero and the double probe is immersed in a neutral plasma with $T_i = T_e$ then the random electron flux to the probe tips will be larger than the random ion flux due to the higher electronic thermal velocity. This will cause the probe tips to collect a net negative charge until the potential change is just sufficient to allow an equal flux of ions and electrons. The probe tips

will then be at a potential below that of the plasma. This potential is called the floating potential. This is illustrated in Figure 63.
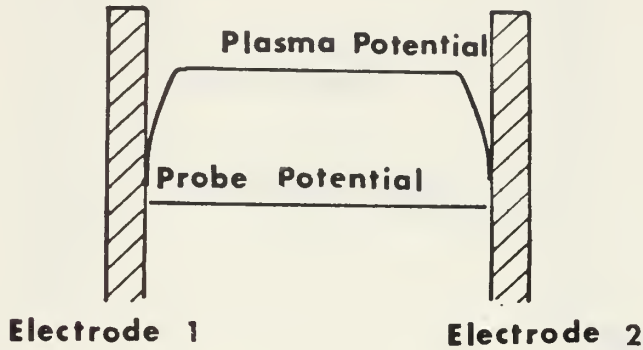
Figure 63. Probe potential with zero bias applied.

If the number two probe is now biased slightly negative, V_2 will become more negative and V_1 will become slightly less negative. Thus more electrons will flow to probe one. This results in a positive current flow to probe two. When the number two probe potential becomes negative enough to exclude electrons and collect the saturation ion current, probe number one will be at a potential just sufficient to allow collection of the net electron flux necessary to cancel the ion current to probe one. This condiction satisfies Kirchoff's Law:

$$(24) \quad \left| I_{+1} \right| - \left| I_{e1} \right| = \left| I_{+2} \right| - \left| I_{e2} \right|$$

The potentials involved in this situation are depicted in Figure 64 and the current flows in Figure 65.

An important advantage of the double probe is that the current in the system is limited by the ion saturation current. In the absence or imbalance of ions, the potential of the entire system changes so that the maximum current drawn is always limited by the ion densities present.
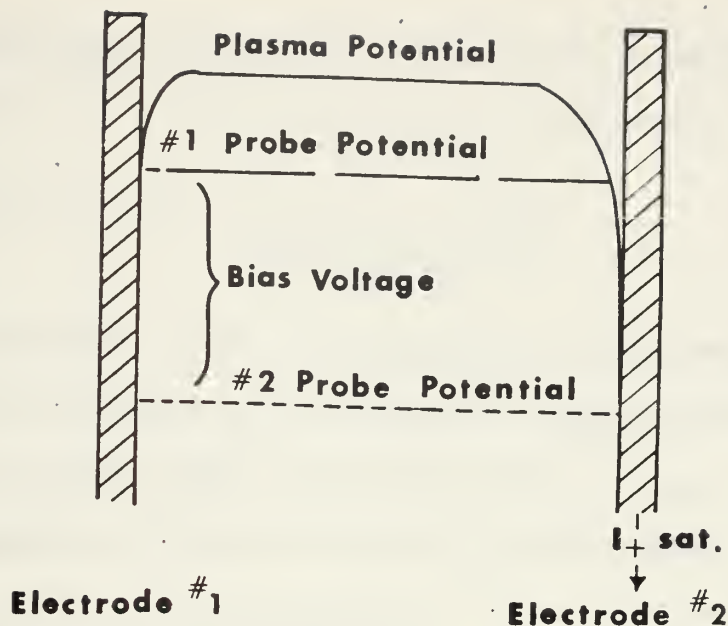
Figure 64. Collection of saturation ion current at probe two.
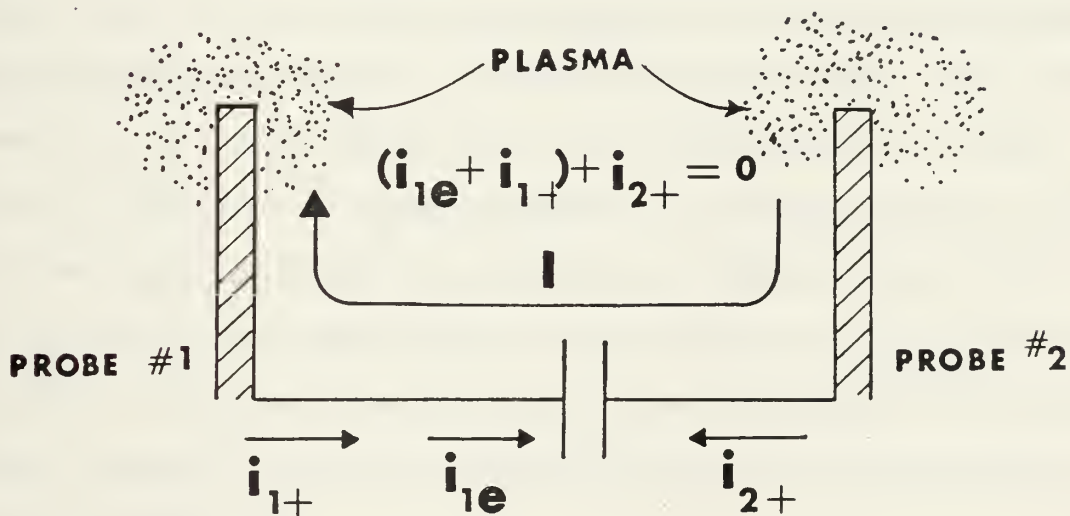
Figure 65. Currents flowing in a double probe collecting saturation ion current at probe number two.

For a macroscopically static plasma, the saturation ion flux to a cylindrical probe of surface area (A) is given by [Ref. 45]:

$$(25) \quad n_i = 1.67 I_+ (m_i/kT_e)^{1/2}/eA_p \quad (cm^{-3})$$

The electron temperature (T_e) can either be estimated or found from the slope of the probe characteristic at the origin [Ref. 11).

$$(26) \quad dI/dV = \frac{e}{kT_e} \cdot \frac{(i_{1+}) \cdot (i_{2+})}{(i_{1+})+(i_{2+})}$$

If the areas of the two electrodes are equal and the product of the probe bias voltage and the average ionic charge is much less than the average thermal energy of the ions, then $i_{1+} = i_{2+}$. Substituting this into equation (26) and solving for T_e we find that:

$$(27) \quad T_e = eI_i(1/dI/dV)/2k$$

It should be remembered that these equations are valid only in a static plasma. In the current investigation, the initial random thermal energy is rapidly converted to ordered flow kinetic energy. This is at least true for plasma expansion into near vacuum conditions. Dawson [Ref. 14] finds that the expansion appears to have taken place by the time the plasma has expanded to dimensions of 0.01 to 0.1 cm. If the flowing plasma is to remain charge neutral, then $n_e = n_i Z_i$ and the flow velocities of ions and electrons must be equal. Therefore, the ordered kinetic energy of the plasma is predominantly due to the ions because of their greater mass.

Assuming that $T_e = T_i = 100$ eV and a flow velocity of 10^7 cm/sec, the ratio of ion thermal to ion directed speed is 2.5×10^{-4} and the ratio of the electron thermal speed to flow speed is approximately 13. Therefore the smaller current will be that of the ions.

Now $I_+ = V/R$ where R is the resistance across which the current is measured. This is also the average number of positive charges collected by the probe per unit time. This can be expressed as:

104

(28) $V/R = \overline{n_i Z_e} A V_{LP}$

Where $\overline{n_i Z_e}$ is the average electronic charge per unit volume and (A) is the cross sectional area of the probe perpendicular to the plasma stream velocity (V_{LP}).

Equation (28) does not include secondary emission at the probe tips due to ion bombardment. Koopman [Ref. 30] has measured this effect and finds that the secondary emission coefficient varies between zero and 0.5 electrons emitted per incident ion. He also found that secondary emission was not strongly dependent on the ion kinetic energy in the range of energies encountered here. Therefore, the secondary emission can be treated as a constant. To include this effect, equation (28) can be rewritten to include an average number of secondary emissions per incident ion:

(29) $V/R = \overline{n_i Z_e} (1 + \epsilon) A V_{LP}$

Since A, V, R and V_{LP} are measured quantities and ϵ is a constant, equation (29) provides a reasonable estimate of the absolute plasma density. For equation (29) to be valid we require that the probe electrodes be of equal area and that the plasma be homogeneous across the probe tips. The probes were carefully constructed to satisfy the first condition. Previous workers at NPS have been careful to keep the plane containing the probe tips perpendicular to the direction of the streaming plasma. However, the probe tips are about one millimeter apart and the characteristic density gradients have lengths of five millimeters. Therefore, it was suspected that this orientation was not critical. To test this hypothesis, the probe was maintained in the

105

same geographical position and rotated through a variety of angles. Figure 60 shows the results as recorded from the oscilloscopic tracings. These reproductions show that the signals are essentially unaffected by rotation of the plane containing the probe tips.

On the basis of this experiment, the plane containing the probe tips was maintained perpendicular to the z-axis throughout the experiments regardless of the expected plasma flow velocity.
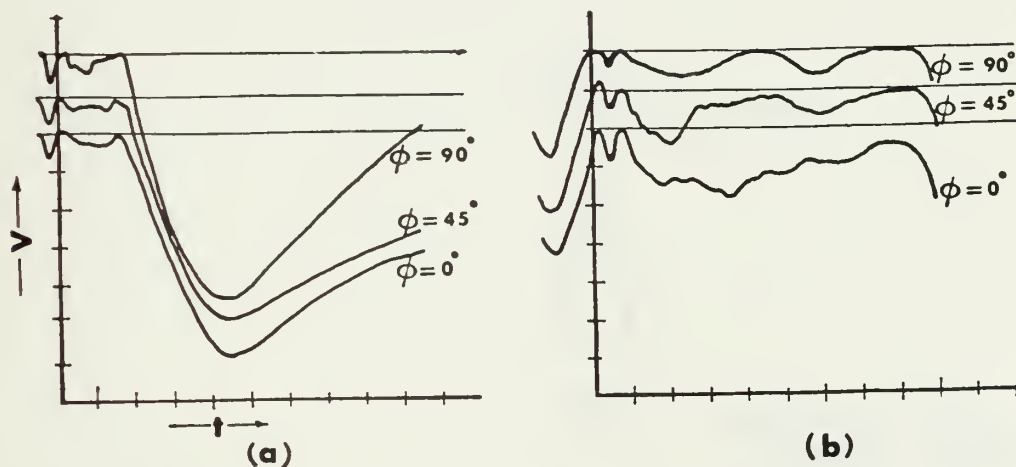
Figure 66. Effect of rotating the plane containing the probe tips with respect to the targets z-axis. The angles (∅) given are the angles between the plane defining the probe tips and the target normal. (a) recorded at two volts and 100 nsec per division and (b) is recorded at 500 mV and 20 nsec per division.

II. DOUBLE PROBE CONSTRUCTION

Figure 67 depicts the probe circuit used throughout this investigation. In one instance the four microfarad capacitor was replaced with a 0.5 microfarad capacitor. No detectable difference in the probe response was noted.
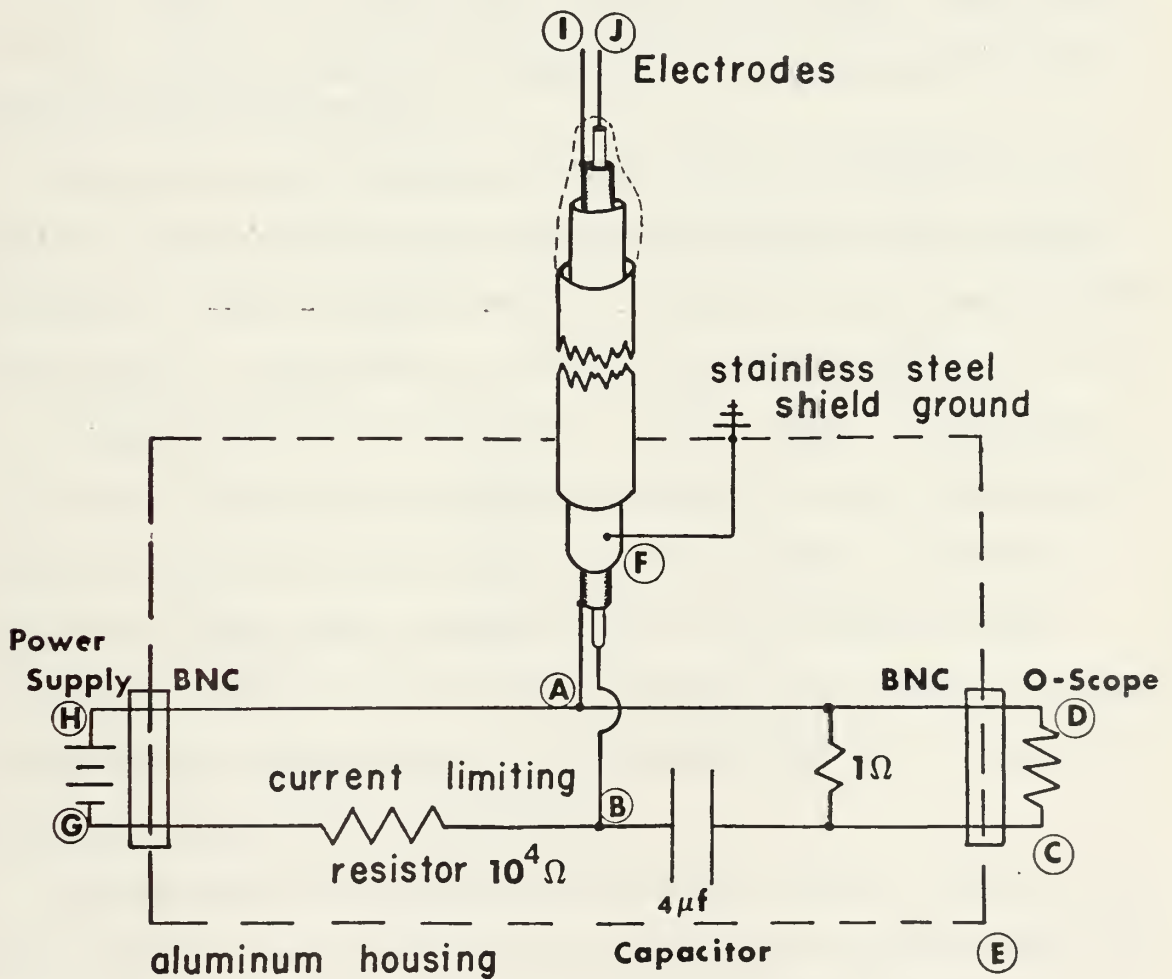
Figure 67. Double Probe Circuit

The following tests have proven effective to insure proper probe operation.

    1. Check each electrode for continuity (no resistance between (A) and (I) and between (B) and (J)).

    2. Insure isolation of the probe circuit from the aluminum housing. (>100 kΩ between (H) and (E) and between (C) and (E)).

    3. Insure adequate grounding of the stainless steel probe shield. (zero resistance (F) to (E)).

    4. Check the current limiting resistor. (>5kΩ (G) to (B))

    5. Check the current viewing resistor for one ohm. ((D) to (C)).

    6. Check the circuit for continuity. (No resistance (H) to (D) and one ohm from (H) to (C)).

Most of the glass enclosed probes were made by a professional glass blower. These probes had very fine tungsten electrodes with a diameter of 0.013 cm. The electrodes were 0.25 cm long and were set approximately 0.08 cm apart. The diameter of the glass tip was approximately 0.1 cm.

At one point in the investigation, a larger signal to noise ratio was desired. This was necessary when examining the early disturbance at distances greater than two centimeters from the target. In order to achieve this higher ratio a double probe was constructed with large electrodes. Production of this probe required little technical expertise and the method is repeated here as it requires a minimum of equipment and could be duplicated in any laboratory.

The electrodes were constructed from 0.05 cm diameter tungsten rods. These rods were cut to approximately four centimeter lengths and one end of each rod was spot welded to a 0.05 by 0.3 cm nickel interface. A solid copper lead was spot welded to the other end of the nickel interface. This is depicted in Figure 68.

108
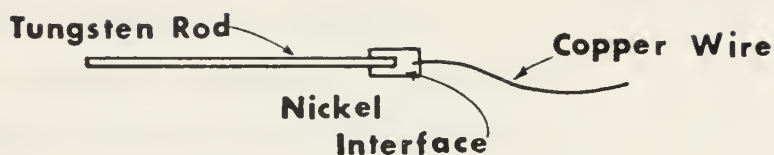
Figure 68.   Tungsten electrode connection to the copper lead through
a nickel interface.

Two of these electrodes were then cut to lengths differing by one cm
(2.5 cm and 3.5 cm). It should be noted that tungsten has a tendency to
split when snipped. The most successful cutting method involves notching
the tungsten rod with a file and then breaking it over a sharp corner
much as glass rod or tubing is cut. The tips were then etched in a
saturated solution of sodium hydroxide at the same time. The etching
process is depicted in Figure 69.
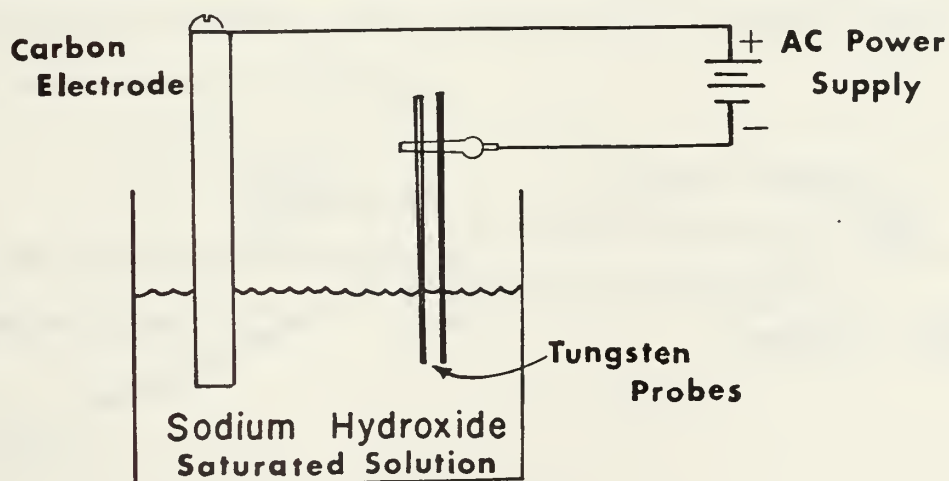
Figure 69.   Etching the tungsten electrode tips.

The etching time was ten minutes and produced identical tips as depicted
in Figure 70.
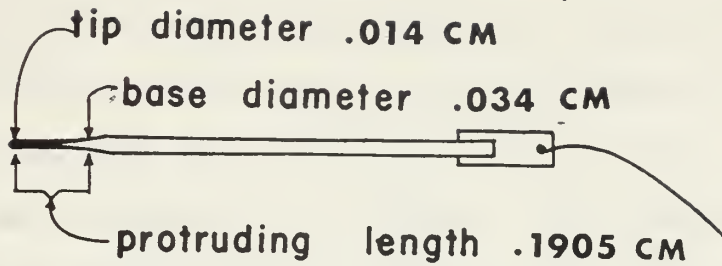
Figure 70. Etched Tungsten Electrode

In the next step, a five millimeter diameter pyrex tube was cut to
a length of 20 cm. Two 0.75 mm outside diameter, 0.60 mm inside
diameter alumina tubes were cut to lengths of 1.5 and 2.5 cm and a piece
of RG-174/U microcoaxial cable was cut to a length of 30 cm. One end
of the coax was stripped and inserted inside the stainless steel shield
which is then inserted inside the pyrex tube. At this point the
electrodes are soldered to the microaxial cable. Figure 71 depicts the
probe in this state of completion.
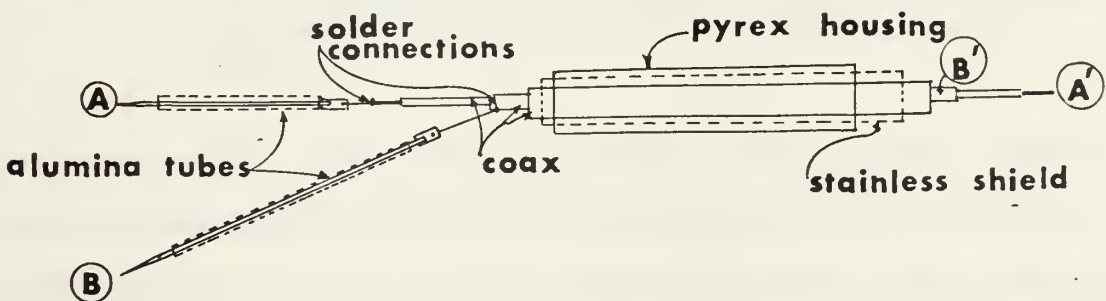
Figure 71. Nearly Completed Double Probe

To insure proper insulation, all exposed leads in the two electrode
circuits are covered with a thin coat of "RTV." When this is dry the
probe should be checked for circuit continuity. (zero ohms (B) to B')
and between (A) and (A').

110

The supporting structure for the electrode tips is made of liquid procelain. The exposed electrode tips are lightly tied together with thread and the entire circuit is stretched between two clamps. A thin coat of procelain is then applied. After the first coat is dry, the probe may be removed from the clamps. Several additional thin coats should be applied until the desired strength is achieved. Figure 72 depicts the finished probe.
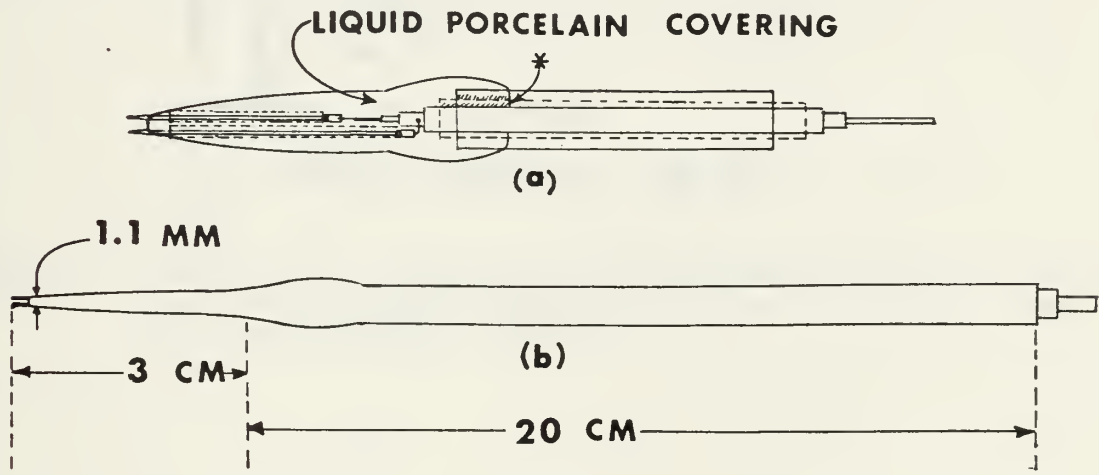
Figure 72. Finished Double Probe (a) internal configuration (b) external dimensions.. * Insure that the liquid procelain is drawn into the aparatus here to provide adequate strength.

Because of the larger size of this probe, there was some concern that the plasma might be perturbed sufficiently to distort the data. To determine what effect this larger probe had on the plasma features a comparison was made between the probe response of the finest probe available and this slightly larger probe. The comparison is duplicated as Figure 73. As can be seen, all features are clearly retained, the primary difference being a larger signal from the probe with the larger electrodes. Because of the additional size of this probe it was not

used in any experiments where additional diagnostic information was
taken downstream.
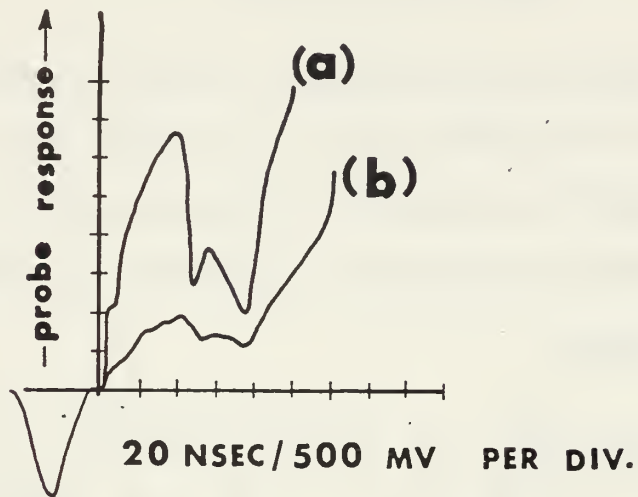
Figure 73. Comparison of the density profile sampled at (0, 0, 1.0) by
(a) the large probe biased at -20 volts and (b) by a very
fine probe biased at -15 volts.

APPENDIX B

I. PRESSURE PROBE THEORY

When a force is exerted on a piezoelectric crystal such as quartz,
it results in the formation of a stress within the crystal. This stress
distorts the ionic structure of the crystal resulting in an increase in
the polarization of the sample. This process is depicted in Figure 74.

(a)   (b)
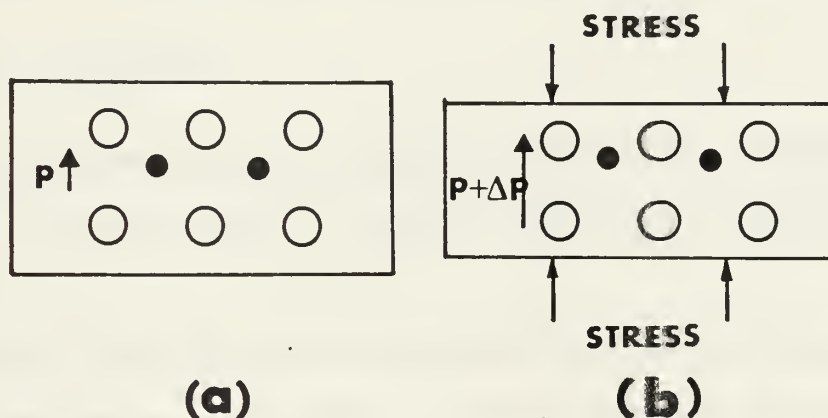
Figure 74. (a) Unstressed Piezoelectric Crystal
           (b) Stressed Piezoelectric Crystal
           The stress changes the polarization by ΔP, the induced
           piezoelectric polarization.

Recall that the electric displacement vector is given by:

$$(30) \quad \vec{D}_x = \epsilon \vec{E}_x + \vec{P}_x$$

For a one dimensional strain, the piezoelectric equation is:

$$(31) \quad D_x = Td_{21} + \epsilon E$$

When D_x = electric displacement vector, T = stress, d_{21} is the
Piezoelectric Strain Constant, E = electric field and ϵ is the
permittivity.

113

For an X-cut quartz crystal [Ref. 18]

    (a) d_{21} = 2.25 X 10^{-12} coulombs/newton

    (b) ϵ = 4.06 X 10^{-11} farad/meter

In the static case the open-circuit voltage is given by [Ref. 4]:

    (32) $g = d_{21}/\epsilon$ = 0.055 ℓF/tw volt-meters/newton

and the short-circuited charge for a given applied force is:

    (33) $Q = d_{21}F\ell/t$

where F is the force which is considered positive for an extensional stress, ℓ = crystal length, w = crystal width and t = the crystal thickness.

    The material presented above is satisfactory for low frequency impulses. In this investigation, the anlysis is further complicated because the plasma produces a stress wave with a short wave length. Graham, et al., [Ref. 18] have analyzed the short-circuit piezoelectric current induced by the application of a rapidly changing impulsive load. The load propagates as a stress wave along the x-axis of a quartz disk. The displacement current generated by this stress wave will be:

    (34) i_D = A dD/dt

Where (A) is the electroded area and D is the displacement vector. Substituting equation (31) for (D) we find that:

    (35) $\int_0^\ell \vec{D}(x)dx = \int_0^\ell \vec{P}(x)\,dx + \epsilon\int_0^\ell \vec{E}(x)\,dx$

114

Where ℓ is the thickness of the quartz disk. By assuming that a short circuit exists between the electrodes and that the crystal has constant permitivity the last integral in equation (35) becomes zero [Ref. 18].

$$(36) \qquad \int_0^\ell \epsilon \vec{E}(x)dx \ = \ 0$$

The conductivity of the crystal is essentially zero so that equation (35) becomes:

$$(37) \qquad \frac{1}{\ell} \cdot \int_0^\ell \vec{P}(x)dx \ = \ \vec{D}$$

At this point it is assumed that the piezoelectric polarization, $P(x)$, is proportional to the x-component of the stress by a coefficient (f). This coefficient is independent of time and stress for a given stress range. Therefore:

$$(38) \qquad P(X) \ = \ f \, \sigma(x)$$

Where $\sigma(x)$ is the x-component of the stress. This assumption is verified by Graham [Ref. 19]. With the assumption that the quartz is linearly elastic we can write:

$$(39) \qquad \sigma(x,t) \ = \ \sigma(x - U_s t)$$

Where U_s is the wave propagation speed in the crystal.

The solution for the current from equations (34) and (37) is therefore found to be:

$$(40) \qquad i = AdD/dt = -\frac{fAU_s}{\ell} \int_0^\ell \frac{\partial \sigma(x)}{\partial x}dx \ = \ \frac{fAU_s}{\ell}(\sigma_0 - \sigma_\ell)$$

Where σ_0 is the x-component of stress at the stress input electrode and σ_l is the x-component of stress at the rear electrode.

For early times in the wave transit, $\sigma_l = 0$ and equation (40) becomes:

$$(41) \quad i_D = \frac{fAU_s\sigma_0}{l}$$

Equation (41) predicts that for times less than the wave transit time, the current is proportional to the stress which is proportional to the force applied to the crystal which in the present investigation equals the momentum transported to the crystal by the plasma. Therefore in this investigation the pressure probe response is directly proportional to the momentum transport in the plasma.

II.   PRESSURE PROBE CONSTRUCTION

Stanford Research Institute provided the pressure probe used in this investigation. It is a Sandia Quartz Gauge. The time resolution of this type gauge is on the order of a few nanoseconds [Ref. 18]. Figure 75 depicts the construction of the gauge.
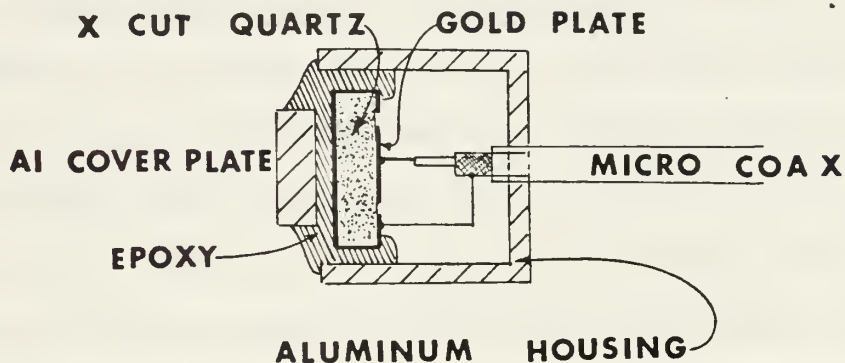

Figure 75.   Sandia Quartz Gauge.

This gauge used a guard ring configuration described in detail by Graham [Ref. 18]. The configuration is pictured in Figure 76.
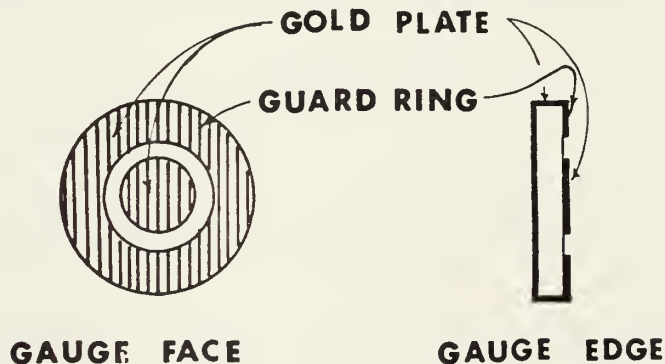
Figure 76.   Guard Ring Electrode Configuration

The inner portion of the quartz disc is isolated electrically from the outer portion by separating the vapor coated electrode into two regions as shown above.

117

This configuration helps to eliminate field distortions. At the outer edge of the disk, the discontinuity in electric potential and dielectric permittivity causes electric field fringing similar to that found in parallel plate capacitors. The guard ring eliminates this distortion by restricting observation to the central region of the disk where there is negligible fringing.

The guard ring also helps to eliminate distortions due to the generation of unloading waves. As the stress pulse moves through the disk in the axial direction, boundary conditions generate shear and dilatational waves immediately behind the wavefront at the lateral edge of the disk. These unloading waves then propagate laterally inward from the lateral boundary and the crystal is no longer in a state of one dimensional strain. The central region of the disk will be in one dimensional strain only for the first wave transit time if the width of the outer electrode is such that an unloading wave does not reach the central region during the first wave transit time.

BIBLIOGRAPHY

1. Afanasyev, Yu. V., Krohkin, O. N. and Sklizkov, G. V., "Evaporation and Heating of a Substance Due to Laser Radiation," *IEEE Journal of Quantum Elect*, v. QE-2, no. 9, p. 483, 1966.

2. Albright, N. W. and Tidman, D. A., "Ionizing Potential Waves and High-Voltage Breakdown Streamers," *Phy. Fluids*, v. 15, no. 1, p. 86, January 1972.

3. Ambartsumyan, R. V., Basov, N. G., Boiko, V. A., Zuev, V. S., Krokhin, O. N., Kryukov, P. G., Senat-Skii, Yu. V. and Stoilov, Yu. Yu., "Heating of Matter by Focused Laser Radiation." *Soviet Phys. JETP*, v. 21, no. 6, p. 1061, 1965.

4. *American Institute of Physics Handbook*, 3rd ed., McGraw-Hill, 1972.

5. Arifov, T. V., et al., "Laser-Induced Current Pulses From a Target in a Gas," *Sov. Phys. JETP*, v. 28, no. 2, p. 201, February 1969.

6. Basov, N. G., Boiko, V. A., Dement'ev, B. A., Kronkhin, O. N., and Sklizkov, G. V., "Heating and Decay of Plasma Produced by a Giant Laser Pulse Focused on a Solid Target, " *Soviet Phys. JETP*, v. 24, no. 4, p. 659, 1967.

7. Bernal, E., Ready, J. F. and Levine, L, P., "Ion Emission from Laser Irradiation of Tungsten," *IEEE Journal of Quantum Elect.*, v. QE-2, no. 9, p. 480, 1966.

8. Bird, R. S., *The Pressure Dependence of Spontaneous Magnetic Fields in Laser Produced Plasmas*, Ph.D. Thesis, Naval Postgraduate School, 1973.

9. Bobin, J. L., et al., "Shockwave Generation in Rarefied Gases by Laser Impact on Berryllium Targets," *J. Appl. Phys.*, v. 39, no. 9, p. 4184, August 1968.

10. Chang T. Y. and Birdsall, C. K., "Laser-Induced Emission of Electrons, Ions, and Neutrals from Ti and Ti-D Surfaces," *Applied Phys. Ltrs.*, v. 5, no. 9, p. 171, 1964.

11. Chen, F. F., *Chapter in Plasma Diagnostics Techniques*, Huddlestone, R. H. and Leonard, S. L., eds., p. 178, Academic Press, New York, 1965.

12. Cobb, J. K., and Muray, J. J., "Laser Beam-Induced Electron and Ion Emission From Metal Foils," *Brit. J. Appl. Phys.*, v. 16, p. 271, 1965.

13. Davis, L. J., _Self-Generated Magnetic Fields Produced by Laser Bombardment of a Solid Target_, MS Thesis, Naval Postgraduate School, 1972.

14. Dawson, J. M., "On the Production of Plasma by Giant Pulse Laser," _Phys. Fluids_, v. 7, no. 7, p. 981, 1964.

15. DeMichelis, C., "Laser-Interaction with Solids--A Bibliographical Review," _IEEE Journal of Quantum Electronics_, v. 6, no. 10, p. 630, October 1970.

16. Ehler, A. W. and Weissler, G. L., "Vacuum Ultraviolet Radiation from Plasmas Formed by a Laser on Metal Surfaces," _Appl. Phys. Ltrs._, v. 8, no. 4, p. 89, 1966.

17. Giori, F., Mackenzie, L. A. and McKinney, E. J., "Laser-Induced Thermionic Emission," _Appl. Phys. Ltrs._, v. 3, no. 2, p. 25, 1963.

18. Graham, R. A., et al., "Piezoelectric Current from Shock-Loaded Quartz - A Submicrosecond Stress Guage," _J. Appl. Phys._, v. 36, no. 5, p. 1775, May 1965.

19. Graham, R. A., "Strain Dependence of Longitudinal Piezoelectric Elastic and Dielectric Constants of X-cut Quartz," _Phy. Rev. B._, v. 6, no. 12, p. 4779, December 1972.

20. Gregg, D. W. and Thomas, S. J., "Momentum Transfer Produced by Focused Laser Giant Pulses," _J. Appl. Phys._, v. 37, no. 7, p. 2787, 1966.

21. Gregg, D. W. and Thomas, S. J., "Kinetic Energies of Ions Produced by Laser Giant Pulses," _J. Appl. Phys._, v. 37, no. 12, p. 4313, 1966.

22. Hall, R. B., "Laser Production of Blast Waves in Low Pressure Gases," _J. Appl. Phys._, v. 50, no. 4, p. 1941, March 1969.

23. Honig, R. E., and Woolston, J. R., "Laser-Induced Emission of Electrons, Ions, and Neutral Atoms from Solid Surfaces," _Appl. Phys. Ltrs._, v. 2, no. 7, p. 138, 1963.

24. Honig, R. E., "Laser-Induced Emission of Electrons and Positive Ions from Metals and Simiconductors," _Appl. Phys. Ltrs._, v. 3, no. 1, p. 8, 1963.

25. Isenor, N. R., "Effect of Background Gas on Laser Induced Electron Emission from Metal Targets," _J. Appl. Phys._, v. 36, no. 1, p. 316, January 1965.

26. Keilhacker, M., et al., "Preionization for Collisionless Shock Wave Experiments by Means of Photoionization," _Phys. Fluids_, v. 13, no. 9, September 1970.

120

27. Kittel, C., Introduction to Solid State Physics, 4th ed., p. 492, Wiley and Sons, 1971.

28. Knecht, W. L., "Initial Energies of Laser-Induced Electron Emission from W," Appl. Phys. Lett., v. 6, no. 6, p. 99, March 1965.

29. Koopman, D. W., University of Maryland Technical Note BN-658, Experimental Study of Streaming Laser-Produced Plasmas, June 1970.

30. Koopman, D. W., "Langmuir Probe and Microwave Measurements of the Properties of Streaming Plasmas Generated by Focused Laser Pulses," Phys. Fluids, v. 14, no. 8, p. 1707, August 1971.

31. Koopman, D. W., "Precursor Ionization Fronts Ahead of Expanding Laser-Plasmas," Phy. Fluids, v. 15, no. 1, p. 56, January 1972.

32. Koopman, D. W., "Momentum Transfer Interaction of a Laser Produced Plasma with a Low-Pressure Background," Phys. Fluids, v. 15, no. 11, p. 1959, November 1972.

33. Langer, P., Tonon, G., Floux, F., and Ducauze, A., "Laser Induced Emission of Electrons, Ions, and X-rays from Solid Targets," IEEE Journal of Quantum Elect., v. QE-2, no. 9, p. 499, 1966.

34. Lichtman, D., and Ready, J. F., "Laser Beam Induced Electron Emission," Phy. Rev. Ltrs., v. 10, no. 8, p. 342, 1963.

35. Lichtman D. and Ready, J. F., "Reverse Photoelectric Effect and Positive Ion Emission Caused by Nd-In-Glass Laser Radiation," Appl. Phys. Ltrs., v. 3, no. 7, p. 115, 1963.

36. Linlor, W. I., "Ion Energies Produced by Laser Giant Pulse," Appl. Phys. Ltrs., v. 3, no. 11, p. 210, 1963.

37. Linlor, W. I., "Some Properties of Plasma Produced by Laser Giant Pulse," Phys. Rev. Ltrs., v. 12, no. 14, p. 383, 1964.

38. McKee, L. L., An Investigation of the Self-Generated Magnetic Fields Associated with a Laser Produced Plasma, Ph.D. Thesis, Naval Postgraduate School, 1972.

39. McLaughlin, T. A., Inductive Magnetic Probe Diagnostics in a Plasma, MS Thesis, Naval Postgraduate School, 1970.

40. Ready, J. F., "Development of Plume of Material Vaporized By a Giant-Pulse Laser," Appl. Phys. Ltrs., v. 3, no. 1, p. 11, 1963.

41. Ready, J. F., "Mechanism of Electron Emission Produced By a Giant-Pulse Laser," Phys. Rev., v. 137-2A, p. A620, 1965.

42. Segall, S. B. and Koopman, D. W., "Application of Cylindrical
     Langmuir Probes to Streaming Plasma Diagnostics," _Phys. Fluids_,
     v. 16, no. 7, p. 1149, July 1973.

43. Stamper, J. A., et al., "Spontaneous Magnetic Fields in Laser-
     Produced Plasmas," _Phy. Rev. Ltr._, v. 26, no. 17, p. 1012,
     April 1971.

44. Sucov, E. W., et al., "Plasma Production by a High-Power Q-Switched
     Laser," _Phys. Fluids_, v. 10, no. 9, p. 2035, September 1967.

45. Swift, J. D. and Schwar, M. J. R., _Electrical Probes for Plasma
     Diagnostics_, p. 148, American Elsevier, 1969.

46. Tanenbaum, B. S., _Plasma Physics_, p. 348, McGraw-Hill, 1967.

47. Turcotte, D. L., and Ong, R. S. B., "The Structure and Propagation
     of Ionizing Wave Fronts," _J. Plasma Phy._, v. 2, no. 2, p. 145.

48. Yamamoto, K., and Takayoshi, O., "On the Floating Probe Method for
     the Measurement of Ionized Gas," _J. Phy. Soc, Japan_, v. 11, no. 1,
     p. 57, January 1956.

49. Wright, T. P., "Early-Time Model of Laser Plasma Expansion," _Phys.
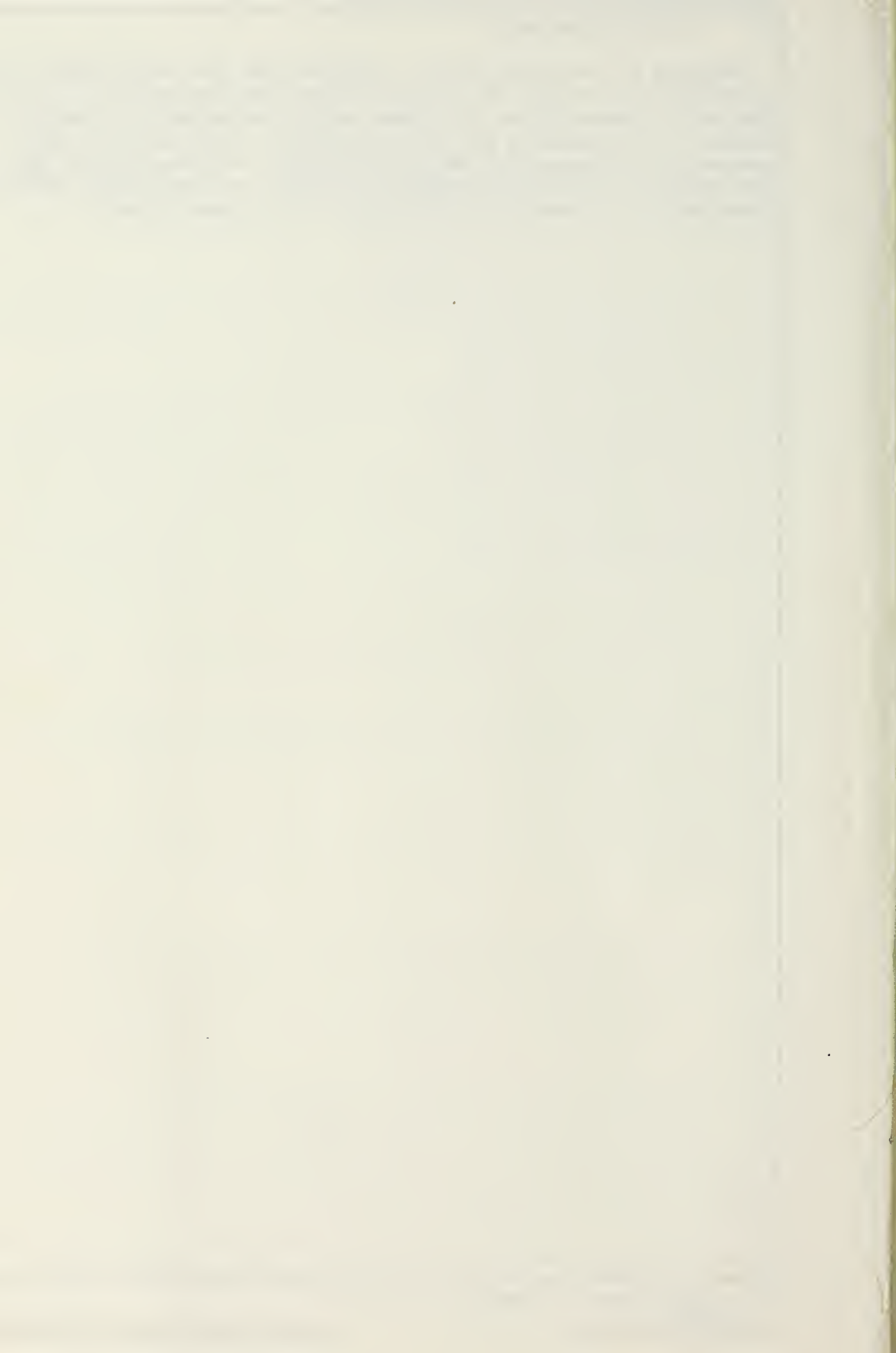   Fluids_, v. 14, no. 9, p. 1905, September 1971.

INITIAL DISTRIBUTION LIST

		No. Copies
1.	Defense Documentation Center Cameron Station Alexandria, Virginia 22314	2
2.	Library, Code 0212 Naval Postgraduate School Monterey, California 93940	2
3.	Professor A. W. Cooper, Code 61 Cr (Thesis Advisor) Department of Physics Naval Postgraduate School Monterey, California 93940	10
4.	Professor F. Schwirzke, Code 61 Sw (Thesis Advisor) Department of Physics Naval Postgraduate School Monterey, California 93940	4
5.	Captain R. S. Case Jr., USAF AFWL/DYS Kirtland AFB, New Mexico 87117	1
6.	Lieutenant Commander K. M. Brooks Sr., USN (Student) USS Coral Sea Care-of Fleet Post Office San Francisco, California 96601	1

REPORT DOCUMENTATION PAGE		READ INSTRUCTIONS BEFORE COMPLETING FORM
1. REPORT NUMBER	2. GOVT ACCESSION NO.	3. RECIPIENT'S CATALOG NUMBER
4. TITLE (and Subtitle) An Investigation of Early Disturbances Found in Association with Laser-Produced Plasmas		5. TYPE OF REPORT & PERIOD COVERED Master's Thesis: December 1973
		6. PERFORMING ORG. REPORT NUMBER
7. AUTHOR(s) Lieutenant Commander K. M. Brooks, Sr., USN		8. CONTRACT OR GRANT NUMBER(s)
9. PERFORMING ORGANIZATION NAME AND ADDRESS Naval Postgraduate School Monterey, California 93940		10. PROGRAM ELEMENT, PROJECT, TASK AREA & WORK UNIT NUMBERS
11. CONTROLLING OFFICE NAME AND ADDRESS Naval Postgraduate School Monterey, California 93940		12. REPORT DATE December 1973
		13. NUMBER OF PAGES 125
14. MONITORING AGENCY NAME & ADDRESS(If different from Controlling Office) Naval Postgraduate School Monterey, California 93940		15. SECURITY CLASS. (of this report) Unclassified
		15a. DECLASSIFICATION/DOWNGRADING SCHEDULE

16. DISTRIBUTION STATEMENT (of this Report)

Approved for public release; distribution unlimited.

17. DISTRIBUTION STATEMENT (of the abstract entered in Block 20, If different from Report)

18. SUPPLEMENTARY NOTES

19. KEY WORDS (Continue on reverse side if necessary and identify by block number)

20. ABSTRACT (Continue on reverse side if necessary and identify by block number)

A plasma was produced by the interaction of a 300 MW, 25 nsec, Nd laser pulse with an aluminum target. The resulting plasma expanded into an ambient background of 2.5×10^{-5} torr and was analyzed using floating double probes, magnetic probes and a quartz pressure probe. An early disturbance was noted before arrival of the main plasma.

Further experiments separate this early signal into photoelectric response and two fast plasma pulses traveling with constant speeds of 1.1×10^8 cm/sec and 5.9×10^7 cm/sec.

DD FORM 1473 EDITION OF 1 NOV 65 IS OBSOLETE
1 JAN 73
(Page 1)   S/N 0102-014-6601 |

20. ABSTRACT (Continued).

Mapping of the plasma density indicates that the early plasma pulse is not symmetric with respect to the target normal but expands along a line defining the reflect laser pulse. This same mapping indicates that the main plasma expands anisotropically for the first 60 nsec resulting in an early time asymmetry with respect to the target normal. At times greater than 120 nsec, the asymmetry of the main plasma is no longer evident and its density distribution is symmetric with respect to the target normal.